Interface Effects and Deposition Process of Ionically Self-Assembled Monolayer Films: In Situ and Ex Situ Second Harmonic Generation Measurements.

by

Charles Brands

Dissertation submitted to the Faculty of
Virginia Polytechnic Institute and State University
In partial fulfillment of the requirements for the degree of
DOCTOR OF PHILOSOPHY
in Physics

J.R. Heflin, Chairman
R. Davis
G. Indebetouw
U. Täuber
T. Takeuchi

August 24, 2003
Blacksburg, Virginia

Keywords: Nonlinear Optics, Second Harmonic Generation, Thin Films, In Situ Measurements, Interface Effects, Ionically Self Assembled Monolayers

Interface Effects and Deposition Process of Ionically Self-Assembled Monolayer Films: In Situ and Ex Situ Second Harmonic Generation Measurements.

Charles Brands

Committee Chairman: Prof. J.R. Heflin

Department of Physics

Abstract

In this thesis, detailed studies are presented into self-assembled, noncentrosymmetric, optically active films. Second harmonic generation (SHG) is used to measure the second order nonlinear optical susceptibility ($\chi^{(2)}$) of ionically self-assembled monolayer (ISAM) thin films.

Conventional ISAM films are fabricated by alternately immersing a substrate into oppositely-charged polyelectrolyte solutions. The polyelectrolytes bind electrostatically to the oppositely-charged substrate, and thus reverse the charge of the substrate. The charge reversal limits the amount of adsorbed material and primes the substrate for the next layer. During the deposition of the nonlinear optical (NLO) active layer, the chromophores are attracted to the oppositely-charged surface, which results in net orientation of the chromophores. Some of the net orientation is lost during the deposition of the next NLO-inactive layer as this layer orients some of the chromophores away from the substrate.

A disadvantage of the polymer ISAM deposition method is that although there is a net orientation toward the substrate, a large number of chromophores are randomly or oppositely oriented. This reduces the nonlinear optical response. To overcome this problem, two alternative methods with a better net orientation are discussed: hybrid covalent / ionic deposition and multivalent monomer deposition. In both deposition methods, the NLO-active material is a monomer instead of a polymer. In hybrid covalent / ionic deposition, the NLO-inactive polymer is deposited using electrostatic attraction while the NLO-active monomer is deposited covalently. This forces alignment of the chromophores. The multivalent method uses chromophores with multiple charges on one side of the molecule and one charge (same sign) on the other. The difference in electrostatic attraction causes a preferential orientation of the chromophores during deposition. Attempts have been made to further improve the net orientation by complexation of the monomers with cyclodextrins (cone shaped organic molecules), so far with only limited success.

The SHG response of NLO-active layers near the glass and air interfaces is much stronger than the SHG response of layers in the bulk of the film for all deposition methods and NLO-active materials investigated in this thesis. For larger number of bilayers (the bulk regime), the square root of the SHG signal increases linearly with the number of bilayers as expected for a uniform chromophore orientation. We isolated the interface effects through use of buffer layers of NLO-inactive polymers. The glass interface effect extends roughly one bilayer deep for all investigated materials. The air interface effect is different for polymers and monomers. For monomers, this effect extends only one bilayer deep, while it extends multiple layers deep for polymers.

Using glass cells to contain the polyelectrolyte solutions, we were able to measure the SHG signal *in situ*, which proved to be a powerful tool to monitor the deposition rate as a function of chosen parameters. All depositions were rapid, on the order of one minute or less. Provided that a minimum concentration is met, the deposition rate and final SHG values are independent of concentration. Bulk layers deposit at the same rate as layers near the interface. For polymer NLO-active layers a secondary, slower growth of SHG is observed that is presumably due to reorganization of the adsorbed polymer layer. This secondary growth is not observed in the deposition of NLO-active monomers.

To my parents and my sister and her family.

Acknowledgements

I would like to express my gratitude to my advisor, Dr. Randy Heflin, for his guidance in my research and many interesting conversations. I would also like to thank the members of my committee, Dr. Guy Indebetouw, Dr. Richey Davis, Dr. Uwe Täuber, and Dr. Tatsu Takeuchi, for reviewing this thesis.

The technical support from the Electronics Shop (Fred Mahone) and Machine Shop (Melvin Shaver, Scott Allen, John Miller, and B.J. Evans) was essential in my research. Thank you all for turning my sketches into professional real world devices.

Many thanks to Chris Thomas, without whom I would be walking aimlessly through Robeson Hall mangled by the mills of bureaucracy.

For computer related issues, I could always count on Roger Link and Travis Heath. My thanks to you both.

I would like to thank my fellow students and coworkers over the years. My predecessors Daniela Marciu and Charles Figura eased me into this lab. I would especially like to thank Pat Neyman for his help and many interesting conversations inside and outside the field of physics. The topics covered in our conversations over the years seem endless. Seldom did we agree, but it was fun anyway.

Finally, I like to thank my family. I thank my parents for their love and support. They always encouraged my curiosity, and encouraged me to explore opportunities they never had. I thank my sister Yolanda Tiggeman for love, friendship and companionship throughout the years. To Dennis Tiggeman, thank you my friend, we will build another wall some time. On second thought, let's give someone else the opportunity. Thanks to my niece and Princess Melissa for making me an uncle and to Lindsey (also Princess) for doing that again.

Table of Contents

List of Figures

List of Tables

Chapter One: An Introduction to Nonlinear Optical Processes and Materials.

This thesis presents studies into the use of the ionically self-assembled monolayer (ISAM) technique and some variations on the ISAM technique, for second-order nonlinear optical (NLO) materials. The goal is to establish how deposition parameters affect the speed of the deposition process and the magnitude of the NLO response for both polymeric and monomeric NLO chromophores. Also, we compare the NLO response from bilayers near an interface with the response from bilayers in the bulk. We will show that the SHG response due to bilayers near an interface is much stronger than the contribution from the bilayers in the bulk. Finally, time dependent studies into the ISAM process are presented. Provided that a minimum concentration is met, both deposition time and final NLO response are independent of concentration. Interesting differences between polymers and monomers are observed for both the interface effect and the *in situ* growth of the NLO response.

Nonlinear optical (NLO) phenomena are second order or higher electric field effects and therefore require high electromagnetic field intensities to produce a signal of significant strength. The intense optical fields needed for observation of nonlinear optical effects were made possible with the invention of the laser. In 1961, second harmonic generation (SHG) was first observed from a quartz crystal using a ruby laser.[1] This was shortly followed by observation of SHG from a non-centrosymmetric calcite crystal.[2] Since then, nonlinear materials have been the subjects of extensive research. The promise for commercial applications ranges from frequency mixing to optical switches and modulators. Although some NLO devices have been on the market for some time now, the impact of many of these devices on society has been limited by their cost. Commercial products use noncentrosymmetric inorganic crystals as nonlinear optical materials, which are complicated, time-consuming, and expensive to produce. Organic chromophores have been investigated as a possible replacement for these inorganic crystals. Unfortunately, organic chromophores tend to organize in random or centrosymmetric manners, which results in zero second order susceptibility ($\chi^{(2)}$). To produce significant $\chi^{(2)}$, these chromophores need to be arranged with noncentrosymmetric order. The most common method to achieve noncentrosymmetry is to pole the chromophores with an external field at a temperature above the glass transition temperature (T_g) and then decrease the temperature to freeze the chromophores in place[3,4]. This results in strong nonlinear susceptibilities competing with, and sometimes surpassing, inorganic crystals. Unfortunately, these electro-optic poled polymers tend to exhibit insufficient temporal and thermal stability, returning to random orientation. The stability of these devices has been improved through use of high T_g polymers and crosslinking. This is discussed in Chapter 2.

An alternative approach to the poled polymer technique is to fabricate the films into polar order through some form of self-assembly process. Many schemes for self-assembly have been tried. One of these approaches is the ISAM technique where thin polymer films are created using electrostatic interaction between oppositely charged electrolytes. The films are created by alternately immersing the sample in cationic and anionic polyelectrolyte solutions. This simple process results in high quality films with thickness control on the order of a nanometer.

In this thesis, we have developed an increased understanding of the ISAM deposition process as it relates to the NLO response of the resulting film. Special attention has been given to time dependent studies, interface effects, and novel methods to increase the SHG response of the bulk effect.

1.1 A Brief Introduction to Nonlinear Optics.

The basic laws governing electromagnetic radiation can be summarized in differential form by the Maxwell equations

$$\begin{aligned} &\vec{\nabla} \cdot \vec{D} = 4\pi\rho \\ &\vec{\nabla} \cdot \vec{B} = 0 \\ &\vec{\nabla} \times \vec{H} - \frac{1}{c}\frac{\partial \vec{D}}{\partial t} = \frac{4\pi}{c}\vec{J} \\ &\vec{\nabla} \times \vec{E} + \frac{1}{c}\frac{\partial \vec{B}}{\partial t} = 0 \end{aligned} \tag{1.1.1}$$

The various fields are related by

$$\begin{aligned} &\vec{D} = \vec{E} + 4\pi\vec{P} \\ &\vec{B} = \vec{H} + 4\pi\vec{M} \end{aligned} \tag{1.1.2}$$

where $\vec{P}$ is the electric dipole moment per unit volume and $\vec{M}$ is the magnetic dipole moment per unit volume. In the experiments described in this thesis, no free charges and currents are present, so $\rho = J = 0$, and only nonmagnetic media are considered, so $\vec{M} = 0$. Therefore, the Maxwell equations become

$$\begin{gathered}\vec{\nabla}\cdot\vec{E}-4\pi\vec{\nabla}\cdot\vec{P}=0\\ \vec{\nabla}^{2}\vec{E}-\vec{\nabla}(\vec{\nabla}\cdot\vec{E})-\frac{1}{c^{2}}\frac{\partial^{2}E}{\partial t^{2}}-\frac{4\pi}{c^{2}}\frac{\partial^{2}P}{\partial t^{2}}=0\end{gathered}\tag{1.1.3}$$

In most cases of interest, the $\vec{\nabla}\cdot\vec{E}$ term can be shown to be small[5] which leads to the wave equation,

$$-\nabla^{2}\vec{E}+\frac{1}{c^{2}}\frac{\partial^{2}\vec{E}}{\partial t^{2}}=-\frac{4\pi}{c}\frac{\partial^{2}\vec{P}}{\partial t^{2}}.\tag{1.1.4}$$

Usually, the polarization field is considered to be linearly related to the incident electric field

$$\vec{P}=\chi\vec{E}\tag{1.1.5}$$

where χ is the electric susceptibility. This first order approximation is sufficient when the intensity of the incident field is low. With the advent of lasers, high intensities can be reached. To describe the effect of a high intensity field incident on an isotropic material, the polarization can be expanded in a Taylor series

$$\vec{P}=\chi^{(1)}\vec{E}+\chi^{(2)}\vec{E}^{2}+\chi^{(3)}\vec{E}^{3}+\cdots\tag{1.1.6a}$$

or more completely, for anisotropic media,

$$P_{i}=\chi_{ij}^{(1)}E_{j}+\chi_{ijk}^{(2)}E_{j}E_{k}+\chi_{ijkl}^{(3)}E_{j}E_{k}E_{l}+\cdots\tag{1.1.6b}$$

The first coefficient $\chi_{ij}^{(1)}$ is the linear electric susceptibility from equation 1.1.5 and the $\chi_{ij\ldots}^{(n)}$ coefficients are the n^th^ order nonlinear electric susceptibilities. In this thesis, we will only consider the second order electric susceptibility $\chi^{(2)}$ for nonlinear, anisotropic, noncentrosymmetric materials containing no free charges and no free currents.

Consider the interaction of an optical electric field at frequency ω and amplitude E_{ω}

$$E_{\omega}(t)=\frac{1}{2}E_{\omega}(e^{+i\omega t}+e^{-i\omega t}).\tag{1.1.7}$$

When a static electric field E_0 is also present in a medium with a nonzero $\chi^{(2)}$, the second order polarization field becomes

$$\begin{aligned}\vec{P}^{(2)}(t) &= \chi^{(2)}\vec{E}^{2}(t)\\ &= \chi^{(2)}\left[\frac{1}{2}E_{\omega}\left(e^{i\omega t}+e^{-i\omega t}\right)+E_{0}\right]^{2}\\ &= \chi^{(2)}\left[\frac{1}{4}E_{\omega}^{2}\left(e^{+2i\omega t}+e^{-2i\omega t}\right)+E_{\omega}E_{0}\left(e^{i\omega t}+e^{-i\omega t}\right)+\frac{1}{2}E_{\omega}^{2}+E_{0}^{2}\right]\end{aligned} \tag{1.1.8}$$

This equation shows that the polarization field contains components oscillating at various frequencies. The first term in equation 1.1.8 oscillates at frequency 2ω and depends only on the optical electric field and not the static field. This effect is referred to as second harmonic generation (SHG) and is the NLO effect employed of this thesis. The second term oscillates at frequency and causes a variation in the refractive index n in the medium that is linearly proportional to E_0. This effect is known as the linear electro-optic effect. The third term is time independent and is referred to as optical rectification. This is a conversion of an oscillating electric field to a static DC field in the NLO material.

1.2 Applications of Second Order Nonlinear Optical Materials

The generation of second harmonic radiation is one of the most important applications for nonlinear media. Radiation at frequency ω is converted into radiation at frequency 2ω within the nonlinear medium. In this single quantum mechanical process, two photons at frequency ω are simultaneously destroyed while a single photon at frequency 2ω is created. This process is used to change the frequency of an otherwise fixed-wavelength laser source.

There also exist numerous electro-optic waveguide applications (using $LiNbO_3$, for example) such as Mach-Zehnder modulators and directional couplers.

Figure 1.2.1 shows a Mach-Zehnder interferometer with the shaded area representing electrodes of length L above and below the waveguide. A Mach-Zehnder interferometer is a device usable for light modulation. The input beam I_{in} is split in two parts which travel in arms A and B of the interferometer. Assume arm A is the arm sandwiched by the electrodes. The phase shift introduced in A can be varied by an applied voltage. When the two beams are recombined the output intensity I_{out} is modulated due to interference between them. If $\Delta\phi$ represents the difference in phase shift introduced in arms A and B, then the output intensity is given by

$$I_{out} = I_{in}(1 + M\cos\Delta\varphi) \qquad (1.2.1)$$

where M is the modulation factor. The phase difference is given by

$$\Delta\varphi = \frac{2\pi L\Delta n}{\lambda} \qquad (1.2.2)$$

where Δn is the difference in refractive indices between and A and B.

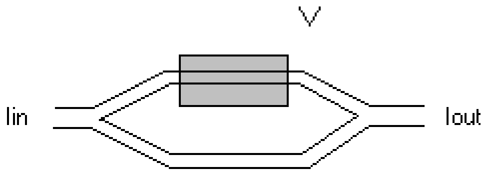

Figure 1.2.1: A Mach-Zehnder electro-optic modulator. The incoming beam is split in two arms and recombined at the end of the two arms. The refractive index of the NLO material in the top arm can be manipulated by adjusting the voltage. A change in refractive index leads to a change in output intensity.

Consider a linear medium where $\overset{\omega}{\mathrm{P}} = \chi^{(1)}\overset{\omega}{\mathrm{E}}$. From equations 1.1.2 and 1.1.3 we get the displacement field

$$\overset{\omega}{D} = \varepsilon\overset{\omega}{E} = \overset{\omega}{E} + 4\pi\chi^{(1)}\overset{\omega}{P} = (1 + 4\pi\chi^{(1)})\overset{\omega}{E} \qquad (1.2.3)$$

Where ε is the electric permittivity of the material. Since the index of refraction n_0 of a material is related to the electric permitivity by $n_0 = \sqrt{\varepsilon}$, the relationship between the index of refraction and the electrical susceptibility is given by

$$\mathrm{n}_0 = \sqrt{1 + 4\pi\chi^{(1)}} \qquad (1.2.4)$$

Thus, the refractive index is independent of the applied field and depends only on the second rank tensor $\chi^{(1)}$ which is a material property.

From the second term of equation 1.1.7 comes the polarization field at frequency ω (first and second order) for a non-centrosymmetric medium.

$$\mathrm{P}_\omega = \chi^{(1)}\mathrm{E}_\omega + \chi^{(2)}\left[2\mathrm{E}_0\mathrm{E}_\omega\right] \qquad (1.2.5)$$

where the propagation terms are omitted for ease of calculation. The magnitude of displacement field is then given by

$$\begin{aligned} D_\omega &= E_\omega + 4\pi P_\omega = E_\omega + 4\pi\left[\chi^{(1)}E_\omega + \chi^{(2)}\left(2E_0E_\omega\right)\right] \\ &= \left[1 + 4\pi\chi^{(1)} + 8\pi\chi^{(2)}E_0\right]E_\omega \\ &= \left[\varepsilon^{(1)} + 8\pi\chi^{(2)}E_0\right]E_\omega = \varepsilon E_\omega = n_\omega^2 E_\omega \end{aligned} \qquad (1.2.6)$$

Thus, the refractive index is

$$\mathrm{n}_\omega = \sqrt{\mathrm{n}_0^2 + 8\pi\chi^{(2)}\mathrm{E}_0} \qquad (1.2.7)$$

So the refractive index of a second-order nonlinear optical material at frequency ω dependents on the applied DC field and can be controlled by altering the magnitude of the field. This is known as the linear electro-optic effect (LEO) or as the Pockels effect.

If a voltage is applied on the electrodes, the electro-optic effect causes a phase shift of

$$\Delta\varphi = \pi \frac{V}{V_\pi} + \Delta\varphi_0 \qquad (1.2.3)$$

where V is the applied voltage, V_π is the voltage needed for a phase shift equal to π, and $\Delta\varphi_0$ is the phase shift difference when no voltage is applied. Thus, by adjusting the voltage, the phase difference between the two beams (and therefore the intensity of the out-coming beam) can be finely controlled. This is of great interest to the optical communications industry where fast optical modulators can be used for encoding information an optical beam.

Because of applications such as those described above, the optoelectronics industry has great interest in the development of improved $\chi^{(2)}$ materials. Unfortunately, present materials that have sufficient lifetime are both difficult and expensive to manufacture. This is the driving force behind research and development in nonlinear organic materials.

1.3 Noncentrosymmetry requirement

To generate a second-order nonlinear optical response, the material structure has to be asymmetric along the direction of the electric field both at the microscopic and at the macroscopic level. If an electric field

$$\mathrm{E(t)} = \mathrm{E}_{\omega} \cos \omega \mathrm{t} \tag{1.3.1}$$

is incident on a material, the resultant second order polarization is

$$\mathrm{P(t)} = \chi^{(2)} \mathrm{E}^{2}(\mathrm{t})\,. \tag{1.3.2}$$

But if the medium is centrosymmetric and thus possesses inversion symmetry, we can write

$$\begin{aligned} -P(t) &= \chi^{(2)}[-E(t)]^{2} \\ -P(t) &= \chi^{(2)}E^{2}(t) \end{aligned} \tag{1.3.3}$$

Equations 1.3.2 and 1.3.3 can only be simultaneously true if the polarization field is zero. Therefore, the $\chi^{(2)}$ is zero for a centrosymmetric medium and no SHG will occur.

This requirement can be visualized by considering the induced dipole moment of a molecule in a sinusoidal electric field (Figure 1.3.1a). The polarization field in linear media (Figure 1.3.1.b) and nonlinear centrosymmetric media (Figure 1.3.1c) exhibit a zero time-averaged response. A noncentrosymmetric nonlinear medium (Figure 1.3.1d) exhibits a nonzero time-averaged field, which can only occur if there is a lack of symmetry between the positive and negative directions.

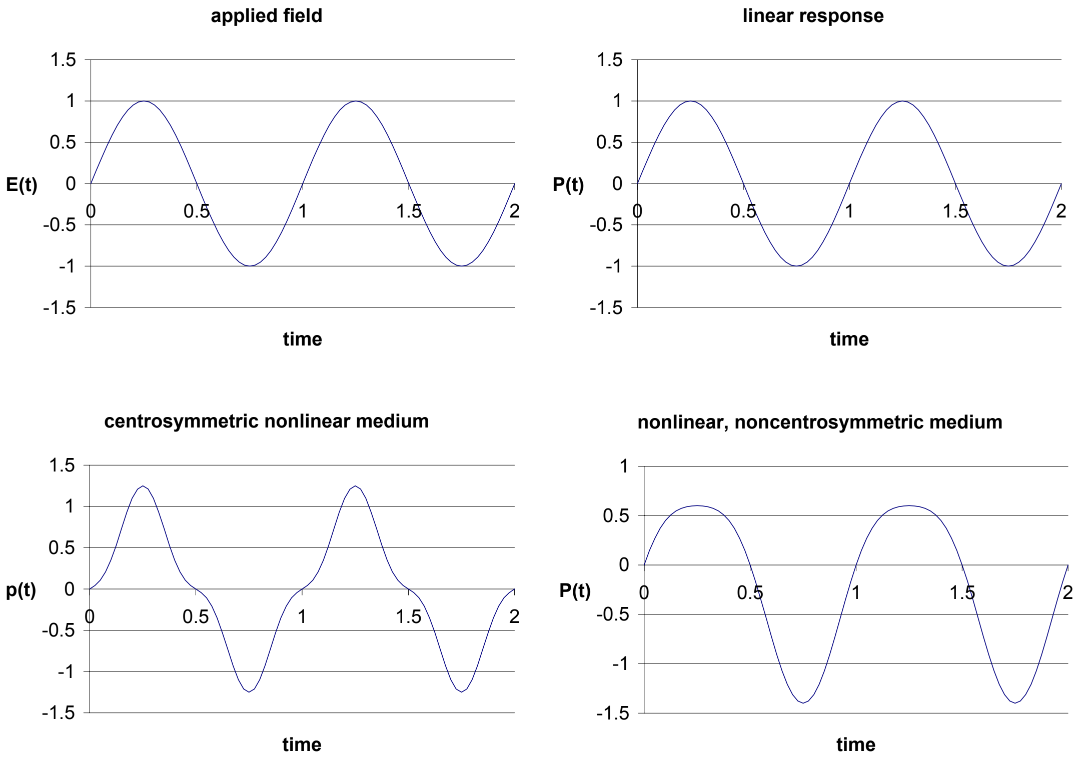
applied field

linear response

centrosymmetric nonlinear medium

nonlinear, noncentrosymmetric medium

Figure 1.3.1. Response of different media to a varying E field. Depicted are: a) the driving E field, b) response of a linear medium, c) response of a nonlinear centrosymmetric medium, and d) response of a nonlinear noncentrosymmetric medium.

Such noncentrosymmetric media have generally been fabricated using inorganic crystals such as potassium dihydrogen phosphate (KDP), β-barium borate (BBO), and lithium niobate (LNB). These crystals exhibit $\chi^{(2)}$ values on the order of 10^{-9} to 10^{-7} esu arising from the electron polarizability due to the crystal's band structure and the asymmetry of the crystal structure. The procedures to grow these crystals are both complex and time consuming, requiring precise variational control of temperatures ranging from 600-1000 ºC at pressures ranging from high vacuum to 1700 atmosphere.[6] Growth times range from 10 days to 8 weeks to produce crystals of dimension 20mm x 30mm x 60 mm. Many of the inorganic crystals show moderate to poor environmental stability, with a particular vulnerability to humidity.

1.4 Microscopic Second Order Hyperpolarizability in Organic Chromophores

Organic molecules and polymers have become an important class of nonlinear optical materials. They form an interesting alternative to inorganic crystals due to their large optical nonlinearities and feasibility of molecular engineering, i.e. creating new materials with appropriate optical properties. The polarization of a molecule induced by an external field can be expanded as a Taylor series and described as (Einstein summation convention).

$$\begin{aligned} p_i &= \mu_i + \alpha_{ij}(-\omega)E_j(\omega) + \beta_{ijk}(-\omega;\omega_1,\omega_2)E_j(\omega_1)E_k(\omega_2) \\ &\quad + \gamma_{ijkl}(-\omega;\omega_1,\omega_2,\omega_3)E_j(\omega_1)E_k(\omega_2)E_1(\omega_3) + \cdots \end{aligned} \qquad (1.4.1)$$

where μ_i is the inherent dipole moment of the material, α_{ij} is the polarizability associated with the linear optical effects, and β_{ijk} and γ_{ijkl} are the first- and second-order molecular hyperpolarizabilities associated with the second- and third-order nonlinear optical effects, respectively. For a number density N of molecules, the second order nonlinear susceptibility $\chi^{(2)}$ can be expressed as an orientational average over the molecules and their hyperpolarizability β_{ijk}

$$\chi^{(2)}_{IJK}(-\omega;\omega_1,\omega_2) = N\sum \beta_{ijk} f(\omega) f(\omega_1) f(\omega_2) \cos(\theta_{iI})\cos(\theta_{jJ})\cos(\theta_{kK}) \qquad (1.4.2)$$

where the f's are the local field factors representing corrections to the electric field experienced by each molecule due to electric fields from its neighbors.

In order to find a chromophore with optimal hyperpolarizability, the origin of hyperpolarizability and the influence of the chemical structure on the hyperpolarizability must be understood. A carbon atom can form up to four covalent bonds in a tetrahedral geometry involving 2s and 2p orbitals. Each bond involves the overlap of a sp^3 hybrid orbital of carbon and an orbital of the bonded atom along the internuclear axis. Such bonds are called σ bonds and electrons involved in these bonds are referred to as σ electrons. Additionally, carbon atoms can form double and triple bonds with each other and other atoms. These other bonds, consisting of unhybridized 2p orbitals, are called π bonds and the electrons involved in π bonds are called π electrons. Because of geometrical restrictions, π bonds can not overlap at the internuclear axis but they can overlap laterally. The π bonds are weaker than σ bonds and therefore σ bonds are chemically more favorable than π bonds. A chain or ring of carbon atoms is said to be conjugated if alternant single and double bonds bind the carbon atoms. Figure 1.4.1 shows two examples of a conjugated molecule. In conjugated structures, the π electrons are delocalized over many atoms. The mobility of π electrons in conjugated systems makes the π electron distribution highly polarizable, which in turn gives rise to large optical nonlinearities. Since $\chi^{(2)}$ also requires noncentrosymmetry, one would expect that the prerequisites for large β molecular hyperpolarizabilities are a large π electron bridge and a pair of strong electron acceptor and donor pair as depicted in Figure 1.4.2.

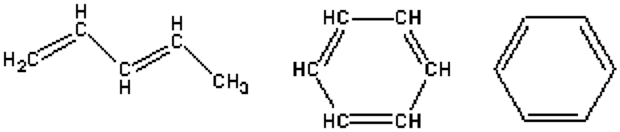

Figure 1.4.1 Two examples of conjugated systems. The structure on the right is a common shorthand notation for the phenyl ring in the middle. The important point is that alternant single and double bonds are needed for a system to be called conjugated.

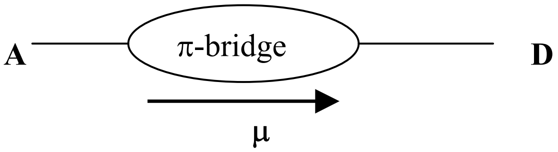

Figure 1.4.2. Schematic structure of an intermolecular charge-transfer molecule (push-pull molecule) known for showing strong second order nonlinear optical properties.

The first thing to consider in choosing a suitable chromophore is the strength of the donor and acceptor groups. Levine *et al.* measured the molecular second order polarizabilties for various para-disubstituted benzenes with electric-field induced second harmonic generation (EFISH).[7] The results are displayed in Table 1.4.1. The strengths of the most common donors and acceptors can be ranked as follows

donor: $N(CH_3)_2 > NH_2 > OCH_3 > OH$

acceptor $NO > NO_2 > CHO > CN$.[7,8]

Acceptor	Donor	β[10^{-40} m^4 / V]	Acceptor	Donor	β[10^{-40} m^4 / V]
CN	CH_3	12	NO_2	CH_3	35
CN	OCH_3	20	NO_2	OCH_3	67
CN	NH_2	56	NO_2	NH_2	197
CN	$N(CH_3)_2$	60	NO_2	$N(CH_3)_2$	218

Table 1.4.1 Molecular second-order polarizabilities for various para-disubstituted benzenes.[7]

A long conjugated chromophore is also desired for a high molecular polarizability. Huijts *et al.* studied the length dependence of the second order polarizability in conjugated organic molecules.[10] They used α-p-methoxyphenyl-ω-p-nitrophenyl polyene (MPNPn with n = 1, 2, 3, 4, 5, see figure 1.4.3). After correction for resonance enhancement, they found a cubic dependence of the molecular polarizability on the length of the π-electron system. Ledoux *et al.* studied the effect of conjugation length on the second order molecular polarizability for polyphenyls.[9] They synthesized polyphenyl molecules with one to four rings per molecule and measured the polarizability (Figure 1.4.4). They found that the polarizability increases with the number of phenyl rings but that the polarizability per unit length reaches a maximum at three rings. This suggests that molecules with more than three rings may not be optimal for macroscopic samples as the loss in the nonlinear susceptibilities, which are proportional to the number of molecules per unit cell, would be too large.

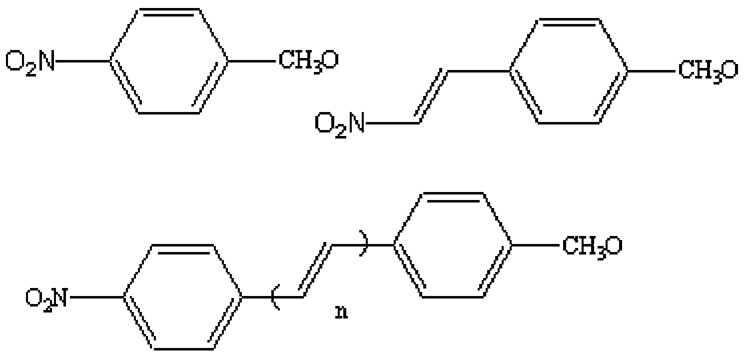

Figure 1.4.3. The para-substituted conjugated organic molecules used by Huijts *et al.*[9]

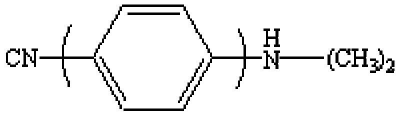

Figure 1.4.4. The Polyphenyls used by Ledoux *et al.*[10]

Besides donor-acceptor groups and conjugation length, the planarity of the molecules is an important aspect to consider, especially for molecules with two or more phenyl rings. The planarity influences the extent of the π-electron system as well as the mobility of the electrons. Leslie *et al.* investigated the value of β for the two molecules of Figure 1.4.5.[11] The addition of the OH group forces the molecule to be planar and hence increases the value of β. In short, to produce chromophores with optimal $\chi^{(2)}$, strong donor-acceptor groups are needed with large conjugation length, and preferably all phenyl rings should be coplanar. Using these simple guidelines, materials with large $\chi^{(2)}$ have been produced. Films made with a technique called poled polymers (discussed in Chapter 2) typically yield $\chi^{(2)}$ values of 10^{-8} to 10^{-7} esu.[12] For comparison, one of the commonly used $\chi^{(2)}$ crystal materials is lithium niobate which has a $\chi^{(2)}$ value of 196 x 10^{-9} esu.

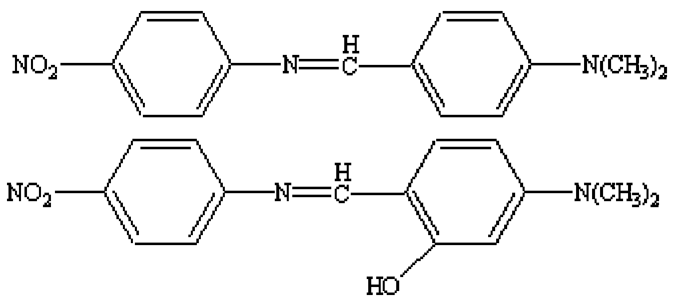

Figure 1.4.5. The influence of planarity on the second order polarizability. The polarizabilities are: $\beta = 98*10^{-40}$ m^4 / V and $\beta = 258*10^{-40}$ m^4 / V for the top molecule and the bottom molecule, respectively.

1.5 Layout for SHG experiments

Figure 1.5.1 shows the layout of the experimental setup used for the SHG experiments. A Q-switched Nd:YAG laser provides a fundamental wavelength of 1064 nm and a 10-nanosecond pulsewidth at 10 Hz. Polarizers control the polarization direction and intensity of the laser beam. The beam is focused on the sample to a spot-size of about 25 μm. The sample is typically varied at an angle between 30 to 60 degrees with respect to the incident beam. The sample is moved and rotated by Aerotech motorized translation and rotation stages controlled by a Joerger SMC-R motor controller. Finally, the fundamental laser beam is filtered out and the remaining SHG signal is detected with a photomultiplier tube (PMT). Data is collected by a CAMAC crate gated off the ND:YAG laser. The signals from the reference photodiode and PMT are digitized by a LeCroy 2249W ADC Analog to Digital Converter. A Kinetic Systems 3922 parallel bus Crate Controller passes the data to a standard PC.

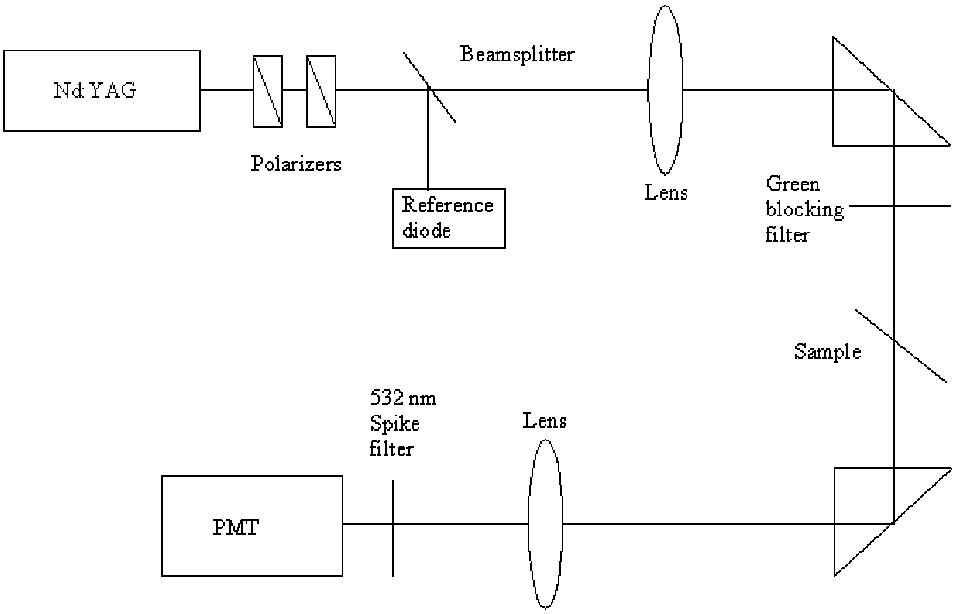

Figure 1.5.1. The setup used for most experiments.

For a well-collimated pump beam, the relationship between the SHG intensity and the pathlength through a single slab of continuous $\chi^{(2)}$ material rotated an angle θ with respect to the beam can be expressed as[13]

$$I^{2\omega}(\theta) = I_{ENV}(\theta)\sin^2\left(\frac{\pi L}{2l_c(\theta)}\right) \qquad (1.5.1)$$

where l_c is the coherence length, $I^{2\omega}$ is the second harmonic intensity, L(θ) is the pathlength, and I_{ENV} is the envelope function discussed in the next paragraph. The coherence length l_c is given by

$$l_c = \frac{\lambda}{4\left(n^{2\omega} - n^{\omega}\right)} \qquad (1.5.2)$$

where n^{ω} and $n^{2\omega}$ are the refractive index values at the fundamental and second harmonic frequencies. The sine squared dependence on L results in oscillations in the second harmonic intensity called Maker fringes. These are due to the phase mismatch between the second harmonic generated at a particular point in the sample and that generated at earlier points, because the fundamental and second harmonic light propagate at different velocities. The maximum intensities occur when the argument of the sine function is

$$\frac{\pi L(\theta)}{2l_c} = \frac{2n+1}{2}\pi , \qquad (1.5.3)$$

or

$$L(\theta) = (2n+1)l_c \qquad (1.5.4)$$

where n is an integer.

The shape of the envelope function is mainly formed by two effects. At an angle of 0 degrees, there is no SHG as there is no coupling between the polarization of the beam and the chromophore orientation if the preferred chromophore orientation is perpendicular to the substrate. As the angle increases, the coupling increases and therefore the SHG increases. However, as the angle increases, the percentage reflection also increases which causes the envelope function to drop at larger angles. These two effects are responsible for an initial rise of the envelope function and a decrease at higher angles. The shape of the envelope is further modified by beam and transmission factors. The height of the envelope function is determined by the square of the fundamental intensity and $\chi^{(2)}$. Herman and Hayden have published a complete derivation.[14] The square root of the envelope function is proportional to the fundamental intensity, the coherence length, and $\chi^{(2)}$

$$I_{ENV}(\theta) \propto \left(l_c \chi^{(2)} I^{\omega}\right)^2 \qquad (1.5.5)$$

where I^{ω} is the fundamental intensity.

Figure 1.5.2 shows the result of a typical scan for a fixed intensity, p-polarized incident beam in our measurements for a glass slide, the same slide after depositing a monolayer of a polycation, and after depositing a monolayer of a polyanion. The polycation is an NLO-inactive polymer and the polyanion is an NLO-active polymer, as will be explained in the next chapter. The data for the glass slide and the polycation layer are multiplied by 10 to make all results clear in one picture. The graphs in the figure are composed of fast oscillating fringes and an envelope function. In our case, the origin of the oscillatory fringes is somewhat different than described above for a continuous $\chi^{(2)}$ medium. We have two thin (<100 nm) $\chi^{(2)}$ films on either side of a glass substrate which has a zero $\chi^{(2)}$. Since each film is much thinner than the coherence length l_c (typically 10 μm), the second harmonic throughout one film can be considered to be generated in phase. That is, from equation 1.5.1 with $L(\theta) << l_c$, we obtain $I^{2\omega} \propto L^2(\theta)$ so that we expect the second harmonic intensity to grow quadratically with the film thickness. The fringes in our data are created by interference between SHG created on one side of the slide and SHG created on the other side. The refractive index of glass is dependent on the wavelength. Since the fundamental beam and the second harmonic beam generated by the first side propagate with different velocities, there is a phase difference between the SHG signals generated on the opposite sides of the glass slide. This phase difference is dependent on the pathlength, which is

$$L_g(\theta) = L_0 / \cos\theta' \qquad (1.5.5)$$

where L_g is the pathlength through the glass, L_0 is the thickness of the glass slide and θ' is the refracted angle in the glass. The phase difference between the second harmonic from the front side film and the back side film caused by the difference in the glass reactive index values n_g^{ω} and $n_g^{2\omega}$ at the fundamental and second harmonic frequencies, respectively, yields a second harmonic intensity given by

$$I^{2\omega}(\theta) = I_{ENV}(\theta)\cos^2\left[\frac{\pi L_g(\theta)}{2l_{c,g}}\right] \tag{1.5.6}$$

where

$$l_{c,g} = \frac{\lambda}{4\left(n_g^{2\omega} - n_g^{\omega}\right)} \tag{1.5.7}$$

and, in this case,

$$I_{ENV} \propto \left(l\chi^{(2)} I^{\omega}\right)^2, \tag{1.5.8}$$

where l is the thickness of the ISAM $\chi^{(2)}$ films. I_{ENV} is dependent on l rather than l_c here because $l \ll l_c$ for the films, as described above. It is important to note that $I^{2\omega}(\theta)$ is thus dependent on $l_{c,g}$ of the glass slide and not on the l_c of the ISAM films for our experimental geometry.

The angular position of the peaks depends on the thickness of the glass slide. Figure 1.5.2 shows that the position of the peaks does not change with deposition of additional layers. It is also important to note that, while quite a bit smaller than the SHG from a single layer of the polar ISAM film, even a glass slide produces some SHG due to the inherent noncentrosymmetric nature of any interface.

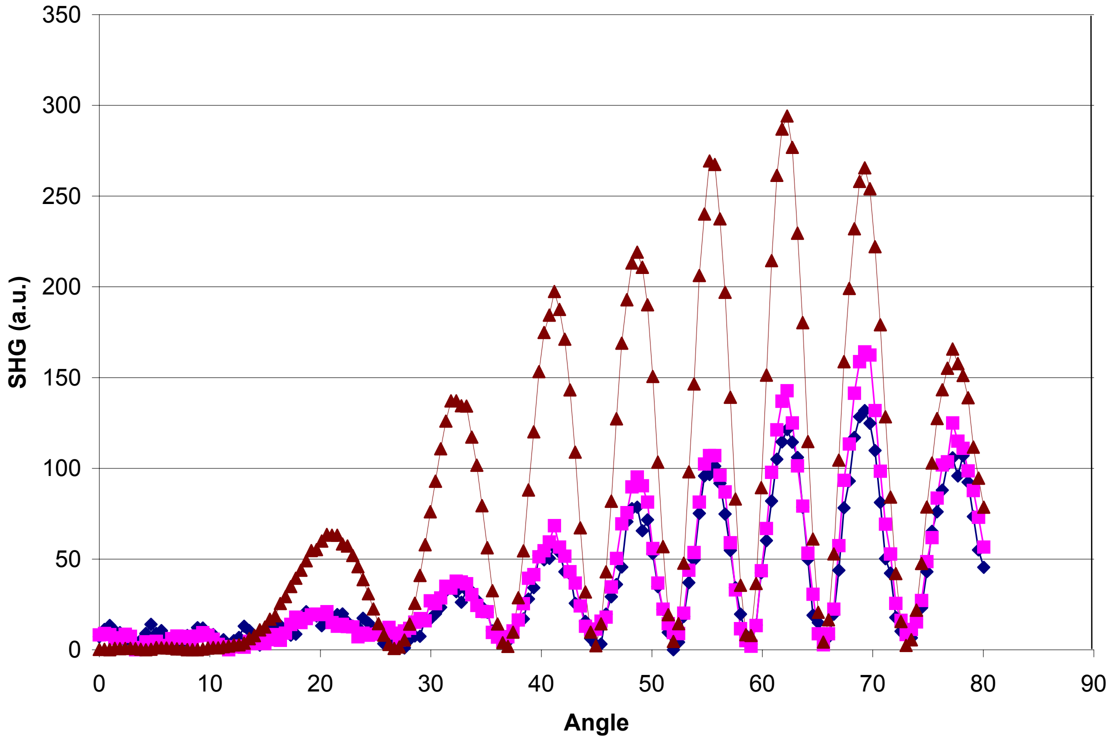

Figure 1.5.2. The SHG as a function of incident angle for a glass slide (diamonds), the same slide after depositing one monolayer of a polycation (squares), and after depositing an additional monolayer of a polyanion (triangles). The data of the glass slide and the polycation monolayer were multiplied by ten for clarity. Note that deposition of additional layers does not influence the position of the peaks and throughs.

1.6 Units

Papers cited in this thesis often express their data in a mixture of electrostatic units (esu) and the international standard of units (SI). For $\chi^{(2)}$, multiply the esu units (cm^2/esu) with 4.19 x 10^{-4} to convert to SI units (m / V). For the molecular hyperpolarizability β, multiply with 4.19 x 10^{-10} to convert from esu units (cm^5/esu) to SI (m^4/V).

1.7 Overview of this thesis

In Chapter 2, we discuss the ionically self-assembled monolayer technique as a method of producing thin polymer films with high directionally ordered chromophores. This method is compared to more conventional methods such as poled polymers and Langmuir-Blodgett films. Also we discuss two variations on the ISAM process, covalent/ionic and multivalent monomer deposition, both developed at Virginia Tech.

To overcome limitations of the polymeric ISAM deposition process we study a variation of the ISAM process in Chapter 3. In the multivalent monomer deposition process, the NLO-active polymer is replaced by an NLO-active monomer. The monomer has one charge on one side of the molecule and multiple charges on the other. All charges have the same sign. The side with the multiple charges experiences a larger attractive force from the oppositely-charged substrate than the singly charged side. Hence, the monomer will be oriented during deposition. This method works very well for films with small numbers of bilayers. With increasing number of bilayers, the chromophores tend to lose orientation. Some initial experiments are shown where we attempt to retain the net orientation with increasing number of bilayers by complexing the chromophores with cyclodextrins. Thus far, the inclusion of cyclodextrins has resulted in only marginal improvements.

In chapter 4 we compare the second harmonic response of NLO-active layers in the bulk to those near the glass and air interfaces. The second harmonic response is much larger near the interfaces than in the bulk. Therefore we attempted to recreate the interface effect by including colloidal silica, colloidal gold, and clay particles in the ISAM films. So far these attempts have proved to be unsuccessful.

Time dependent studies are presented in chapter 5. Using transparent cells, we measured the SHG signal *in situ* during the deposition process. This proved to be an excellent tool for monitoring the ISAM film formation. The time dependent experiments include variations on the ISAM deposition process and concentration dependencies. Most of the ISAM film deposition takes place in less than a minute. The deposition time is essentially independent of previously deposited layers.

Finally, chapter 6 consists of conclusions and recommendations for further studies.

References

[1] P.A. Franken, A.E. Hill, C.W. Peters, G. Weinreich, *Phys. Rev. Lett*. **7** (1961) 118.

[2] R.W. Terhune, P.D. Maker, C.M. Savage, *Phys. Rev. Lett*. **8** (1962) 404.

[3] K.D.Singer, J.E. Sohn, S.J. Lalama, *Appl. Phys. Lett.* **49** (1986) 248.

[4] K.D. Singer, M.G. Kuzyk, J.E. Sohn, *J. Opt. Soc. Am. B* **4** (1987) 968.

[5] R.W. Boyd, *Nonlinear Optics, Academic Press, Inc.* (1992) 57.

[6] J.D. Bierlein, H. Vanherzeele, *J. Opt. Soc. Am. B* **6** (1989) 622.

[7] B.F. Levine, C.G. Bethea, *J. Chem. Phys*. **63** (1975) 2666.

[8] A. Dulcic, C. Sauteret, *J. Chem. Phys* **69** (1978) 495.

[9] R.A. Huijts, R.A. Hesselink, *J. Chem. Phys. Lett*. **156** (1989) 209.

[10] I. Ledoux, J.Zyss, A. Jutland, C. Amatore, *Chem. Phys*. **150** (1991) 177.

[11] T.M. Leslie, R.N. De Martino, E.W. Choe, G. Khanarian, D. Hass, G.Nelson, J.B. Stamotoff, D.E. Stuetz, C.C. Teng, Y.N. Yoon, *Mol. Cryst. Liq, Cryst* **153** (1987) 451.

[12] L. Cheng, R. Foss, G. Meredith, W. Tam, F. Zumsteg, *Mat. Res. Soc. Symp. Proc.* **247** (1992) 111.

[13] W.N. Herman, L.M. Hayden, *J. Opt. Soc. Am. B* **12** (1995) 416.

[14] W.N. Herman, L.M. Hayden, *Polymers for Second-Order Nonlinear Optics, Am. Chem. Symp.* **601** (1995) 275.

Chapter Two: Ionically Self-Assembled Monolayer (ISAM) Film Deposition.

This chapter introduces the ISAM film deposition technique. It starts with an overview of more conventional methods for producing thin organic films with large $\chi^{(2)}$. The ISAM deposition process is then presented with a discussion of its strengths and weaknesses. Lastly, two variations on the "classic" ISAM process developed at Virginia Tech are discussed. These are hybrid covalent / ionic deposition and multivalent deposition.

2.1 Conventional deposition methods

Poled Polymers

The method most extensively used to create organic thin films for $\chi^{(2)}$ applications is the method of poled polymers.[1,2] In this technique, the polymer is first deposited on the substrate by spin casting. The chromophore can be a molecular species dissolved in the polymeric host or the chromophore can be a side group of the polymer chain. Spin casting leaves the chromophores randomly oriented. To achieve non-centrosymmetric ordering of the chromophores, the bulk medium is subjected to electric field poling. Conceptually the process is simple, but it can be quite complex in practice. The film is heated above the glass transition temperature to give the chromophores rotational mobility. A strong electric field (10^5-10^6 V/m) is applied to align, or "pole", the chromophores. The sample is then cooled to freeze the chromophore orientation in place, after which the applied electric field can be removed. This process typically yields values of 10^{-8} to 10^{-7} esu.[3] This is comparable to $LiNbO_3$ with a value of 196×10^{-9}. The electric field can be applied by either parallel plates or by a corona induced by a tungsten needle above the sample. Poling with parallel plates has the advantage of greater uniformity of the field. The advantage of the corona method is simplicity of the setup and the ability to apply a stronger electric field.

Unfortunately, the chromophores tend to loose their alignment over time resulting in a decay of the $\chi^{(2)}$. In some cases, this decay can be quite large. For example, Hampsch *et al.* studied Disperse Orange 25 in polystyrene. At room temperature, the decay in $\chi^{(2)}$ was been measured to be 80% in the first 200 hours.[4] The decay rate increases with increasing temperature. Above the glass-transition temperature, the decay is nearly instantaneous.

Attempts have been made to reduce the $\chi^{(2)}$ decay by crosslinking polymers through UV radiation. In one example, the UV radiation was applied for 10 minutes at an intensity of 3 mW / cm^2 and a wavelength of 254 nm. Crosslinked polymers have less rotational freedom which results in a 50% lower initial $\chi^{(2)}$ but also in a lower decay rate (10% in 500 hours at room temperature).[5] Further stability in $\chi^{(2)}$ has been achieved by doping the chromophores in polyamic acid followed by conversion to polyimide and subsequent densification.[6, 7] Polyimides are chemically stable at temperatures as high as 400°C and are used extensively in the semiconductor industry as a thin film dielectric insulator. Polymides with high optical transparency are readily available. The chromophores are doped in the precursor polyamic acid, heated, and exposed to the high electric field to align the chromophores. Further heat curing above T_g (> 250 ºC) causes the polyamic acid to irreversibly form imide rings. These imide rings reduce the rotational mobility of the chromophores which results in films that have a higher thermal stability. A side product of the imidization is water, and therefore as a final step, water is removed from the film which can reduce the film thickness up to 40%.[6] This step is called densification and requires elevated temperatures (340-380 ºC) for about half an hour. This further restricts the mobility of the chromophores. Finally, the sample is cooled to room temperature and the electric field is removed. This process has significantly increased the temporal stability at room temperature, showing an initial drop of 5% in $\chi^{(2)}$, and only a small decay after that. The high temperatures needed for this process are higher than the decomposition temperature for most nonlinear chromophores, a fact that seriously limits the choice of chromophores. Development of chromophores with large β values and thermal stability above 300 ºC has been an active research area over the past decade.

Davey *et al.* attempted to overcome the thermal stability issue by using high T_g (~400 ºC) diamine functionalized chromophores.[8] In this procedure, the chromophore is imbedded in the polyimide after which the polyimide is spin-casted. This results in chromophore-functionalized polyimides. This procedure greatly improves the temporal stability at room temperature, with an initial drop of 5% and no significant loss in 50 days. Unfortunately, the thermal stability did not show much improvement. At a temperature of 0.65 $T_{g,}$ 20% of the SHG signal was lost irrecoverably. This was followed by a complete loss of SHG signal beyond 0.65 T_g. A survey of the current state of the art in poled polymers is given in reference 9.

Langmuir-Blodgett Deposition

To improve on the temporal stability, various attempts have been made to self-assemble films with intrinsic structural asymmetry. The oldest method is Langmuir-Blodgett deposition. This deposition consists of two steps, a densely packed monolayer of the desired material is created on a water surface, and then the material is transferred to the substrate one monolayer at a time. The material to be deposited must consist of amphiphilic molecules; molecules that are hydrophobic on one end and hydrophilic on the other end. On the whole, the molecule must not be soluble. Rayleigh was the first to create monolayer films by spreading on liquids.[10] Langmuir[11] first accomplished transferring the layer to a solid substrate. The Langmuir-Blodgett deposition works in the following manner. A monolayer of molecules that are amphiphilic (hydrophobic on one end and hydrophilic on the other) is spread on an air-water interface. The layer is compressed until the molecules are densely packed and therefore aligned. A hydrophobic substrate is immersed in a vertical direction through the monolayer. This causes the deposition of the first layer as illustrated in Figure 2.1.1. When the substrate is extracted from the water, a second layer is deposited. The layer construction formed this way is called Y-type. X- and Z- types are formed when the layer is deposited on insertion or withdrawal only. The X- and Z- type layers are inherently asymmetric while the Y-type is symmetric and has by itself zero $\chi^{(2)}$. The highest $\chi^{(2)}$ values with LB deposition have been achieved with a variation on Y-type deposition. This was accomplished by using two alternating LB films comprised of a donor- and acceptor- substituted polyene. The sample was immersed through a monolayer with the electron donor substituted polyene and moved through a gate, while immersed, to a second bath containing the electron acceptor substituted polyene. The sample was then extracted through this monolayer. Films deposited in this manner have shown non-linear susceptibilities of $\chi^{(2)} = 2 \times 10^{-6}$ esu.[12]

LB deposition is a difficult process, complicated by the need for a constant pressure on the monolayer. Too little pressure and the molecules are not closely packed and misaligned. Too much pressure and the molecules stack on top of each other. The deposition procedure is also very sensitive to contaminants. The most important disadvantage of LB films is the poor mechanical and thermal stability, since the layers are held together by only van der Waals forces. Highly anisotropic order of the LB film has been measured right after production with $\chi^{(2)} = 2 \times 10^{-6}$ esu, but the SHG response vanished within days.[12] Langmuir Blodgett films with large number of bilayers tend to collapse, thereby randomizing chromophores, when heat is applied or just as time passes.

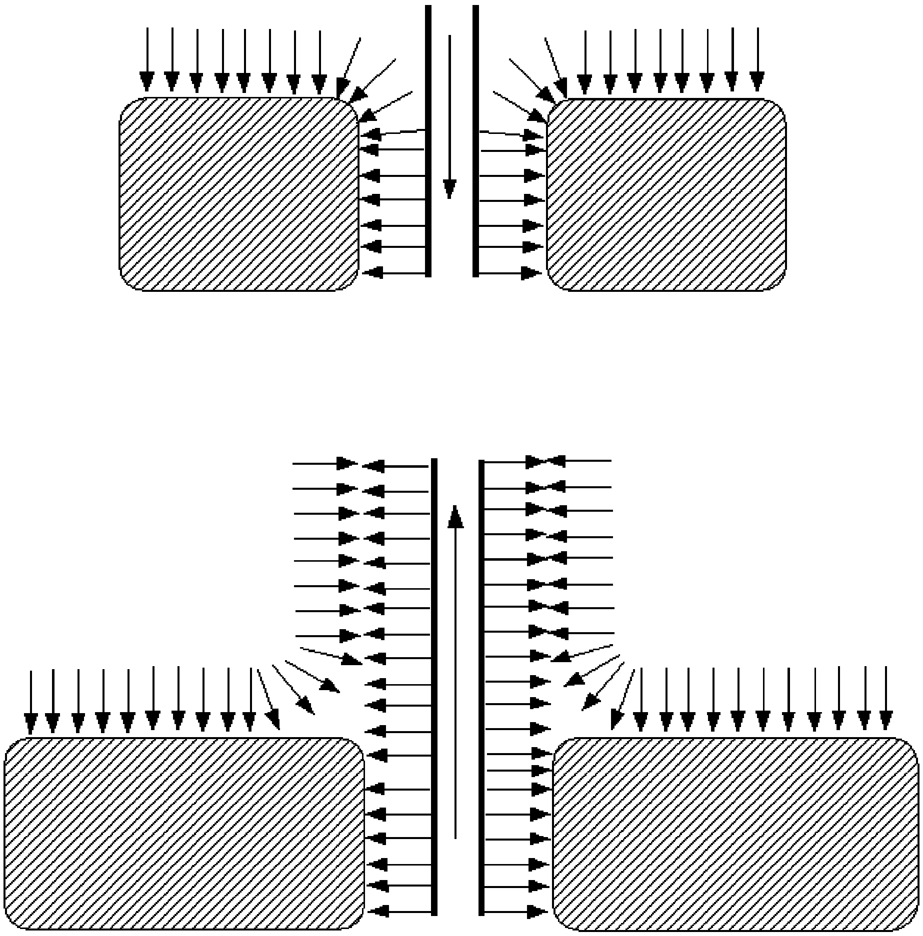

Figure 2.1.1. Langmuir-Blodgett deposition. An amphiphilic material is spread over the surface of water. Compression forces the material to be in the closest posible packing, which forces the chromophores to be aligned. Layers are deposited by immersion and removed from the solution.

Covalent Self-Assembly

Another common form of assembling polar thin films is covalently self-assembled monolayers (SAMs).[13] For example, hydroxylated substrates are immersed in amphiphile fluids to produce a covalently bonded film to the substrate. Adsorption by itself leads to films of only one monolayer. Surfaces covered by monolayers exposing nonpolar parts such as methyl groups become inert to further bonding of molecules from the fluid phase. This prevents uncontrolled deposition resulting in poorly defined thick layers. Additional layers may be deposited by chemically activating the new surface layer and reimmersing the substrate in the solution. In this manner, highly structured films can be made that are exceptionally mechanically and chemically robust. SAMs result in stable, structurally well-defined two dimensional aggregates with close packed, oriented molecules. Therefore, these films are well suited for nonlinear optical applications with $\chi^{(2)}$ of up to 3.0×10^{-7} esu.[14]

One issue with SAMs is that they are extremely time consuming to fabricate. Immersion time for each reaction step ranges from a half an hour to several days.[15] Also, the adsorption steps as well as the chemical activation steps often have to be done at elevated temperatures.

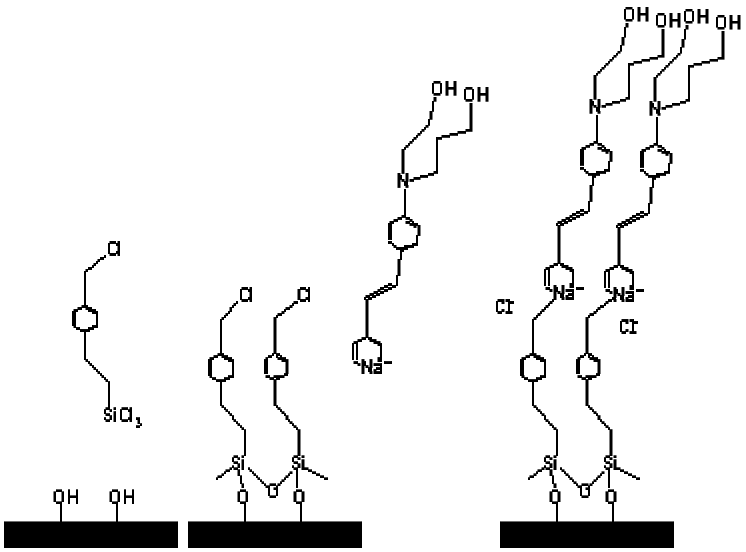

Figure 2.1.2. Covalent deposition process. (Reference 14). The covelent deposition process can lead to very robust highly organised films but is difficult and extremely time consuming to produce.

2.2 ISAM Film Deposition Process

The ionically self-assembled monolayer (ISAM) technique bypasses many of the problems in the previously described techniques. This technique was first developed by Decher *et al.*[16] ISAM films are grown monolayer by monolayer by alternately immersing a charged substrate in anionic and cationic polymer solutions. Each monolayer reverses the charge on the surface and thus primes the sample for the next layer. As a monolayer is deposited, the deposition halts as the adsorbed polymers repel the similarly charged polymers in the solution. Upon immersion in the oppositely charged solution, a new layer is grown. Thus, the growth of the film is controlled with an accuracy of one monolayer at a time.

This relatively quick and simple procedure is carried out at room temperature with no special equipment needed and results in smooth, homogeneous, and physically and chemically robust films. In principle, there is no restriction on the choice of polyelectrolytes. This method has been applied to polymers, monomers, DNA, clay platelets, proteins, and viruses.[16-19] These films have been studied in applications such as light-emitting diodes, photovoltaics, anti corrosion layers, and electrochromics.[20-24] In this thesis, we are interested in production of ISAM films with a second order nonlinear optical response. These films show substantial $\chi^{(2)}$ values with outstanding thermal and temporal stability.[25-29] In a thermal stability experiment, ISAM films consisting of PAH/PS-119 were heated to 150 ºC for 18 hours. After cooling, the SHG signal was completely restored.[28] The $\chi^{(2)}$ for PAH / PS-119 film under a particular set of solution parameters has been measured to be equal to 1.53×10^{-9} esu.[28] As a reminder, the $\chi^{(2)}$ for lithium niobate is 196×10^{-9}.

In our experiments, it is always the anionic polymer that contains the NLO chromophores. Figure 2.2.1 demonstrates the building of the sample layer structure. The arrows in the figure represent of the chromophore side groups on the polyanions. Net polar order is presumably achieved because more chromophores are pointing in the direction of the substrate than in the opposite direction. Although Figure 2.2.1 is beneficial from a conceptual point of view, it is incorrect in its suggestion that the layers are discrete. Bragg peaks indicative of well defined multi-layer structures are not observed by X-ray reflectivity or small angle neutron reflectivity.[30-33] However, as first order peaks are observed, variations in concentration must be present. This leads to the conclusion that films made by ISAM are stratified but do not consist of well separated, distinguishable alternating layers. The layers are in fact deeply interpenetrated as shown in Figure 2.2.2.

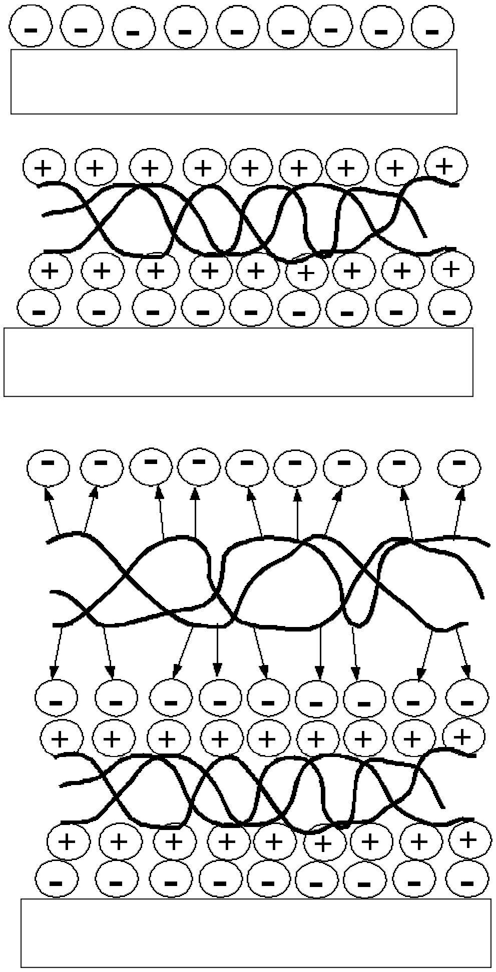

Figure 2.2.1. Schematic of ISAM deposition process. The glass slide is negatively charged on contact with water. In the first solution, a cationic NLO-inactive polymer is deposited. In the second solution, an anionic polymer with an NLO chromophore is deposited.

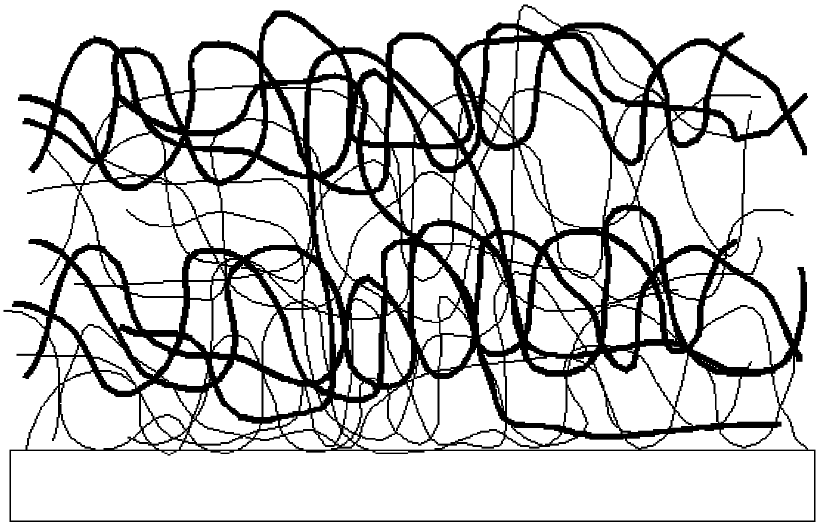

Figure 2.2.2. A more realistic picture for the ISAM process. The oppositely charged polymers are highly interpenetrated.

Before the films are deposited, the glass microscope substrates are cleaned with the RCA cleaning process.[34] The RCA cleaning procedure starts with a 20 minute bath at 70ºC in a 5:1:1 solution of $NH_4OH:H_2O_2:H_2O$. The slides are rinsed in DI water and immersed for 20 minutes in a 6:1:1 solution of $HCl:H_2O_2:H_2O$ at room temperature. Finally, the slides are rinsed again and dried at 130 ºC for one hour.

The glass surfaces are negatively charged on contact with water by dissociation of silonol groups[35]

$$\mathrm{SiOH} \Leftrightarrow \mathrm{SiO}^- + \mathrm{H}^+ \ . \qquad (2.2.1)$$

The deposition process starts by immersing the substrate in a polycation solution. Coulombic attraction will bind the polycation to the surface quickly and homogeneously, resulting in a reversal of the surface charge which ends the deposition. The substrate is rinsed in DI water and immersed in the polyanion solution where another monolayer is deposited and the surface charge is reversed again. This process continues until the desired number of bilayers is reached. The DI water used in the solutions and in the rinsing process was obtained from a Barnstead Nanopure II filtration / deionization system.

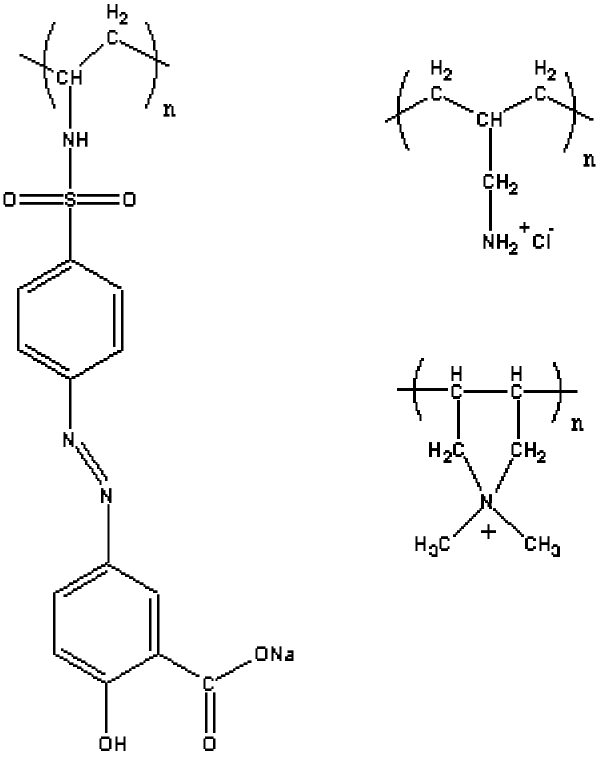

Figure 2.2.3. The structures poly{1-[4-(3-carboxy-4 hydroxyphenylazo) benzenesulfoamido]-1,2-ethanediyl, sodium salt} (PCBS) (left), poly(allylamine hydrochloride) (PAH) (right top), and poly(diallyldimethylammonium chloride) (PDDA) (right bottom).

The structures of the polymers most commonly used in the experiments of this thesis are depicted in Figure 2.2.3. As polycations, we used poly(allylamine hydrochloride) known as PAH and poly(diallyldimethylammonium chloride) further abbreviated as PDDA. The structure on the left is the NLO-active poly{1-[4-(3-carboxy-4 hydroxyphenylazo) benzenesulfoamido]-1,2-ethanediyl, sodium salt} known as PCBS. All polymers were obtained from Sigma Aldrich. It is important to note that PAH and PCBS do not only bond electrostatically but that they may also form hydrogen bonds.

A typical absorbance spectrum for a PAH/PCBS ISAM film is shown in Figure 2.2.4. The peak absorbance value of PAH / PCBS films, at $\lambda = 360$ nm, as a function of bilayers is shown in Figure 2.2.5. Both polymers were deposited at a pH of 7.0 and no salt was added. The figure shows that the absorbance increases linearly with increasing number of bilayers. This indicates that the amount of polymer deposited with each successive layer is constant. Similarly, ellipsometry shows that the thickness of ISAM films increases linearly with the number of bilayers.[36] This means that the absorbance increases linearly with film thickness and therefore the layer density is constant from bilayer to bilayer.

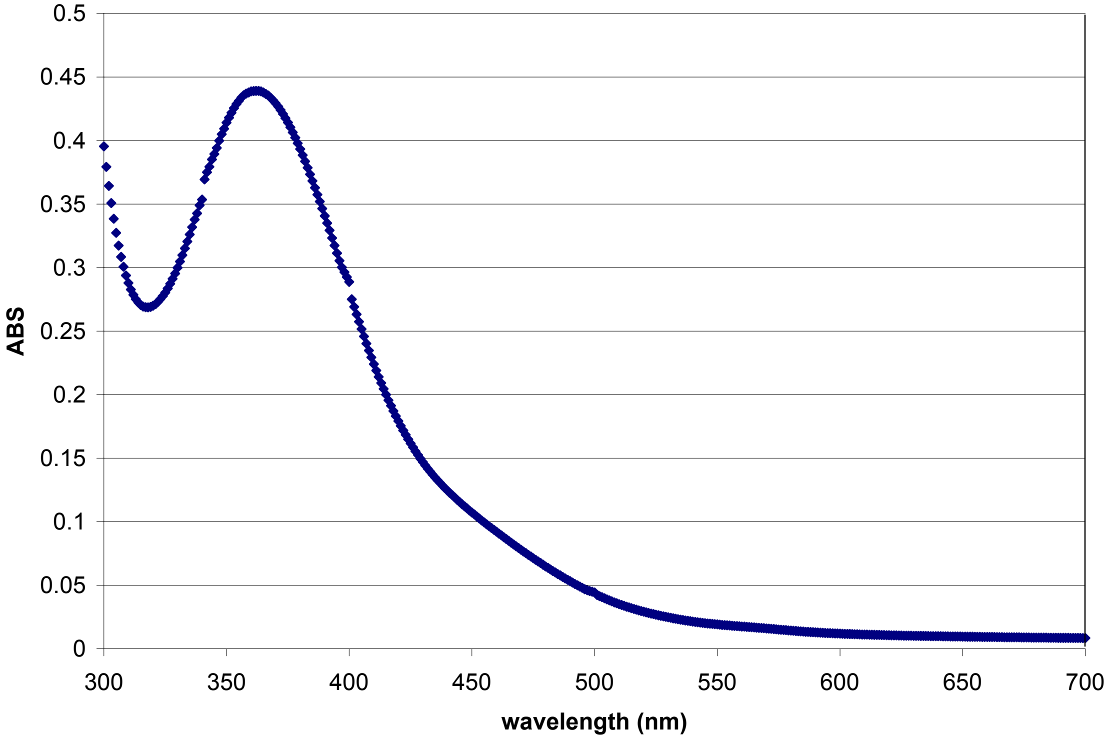

Figure 2.2.4. Typical absorbance spectrum for PAH / PCBS sample.

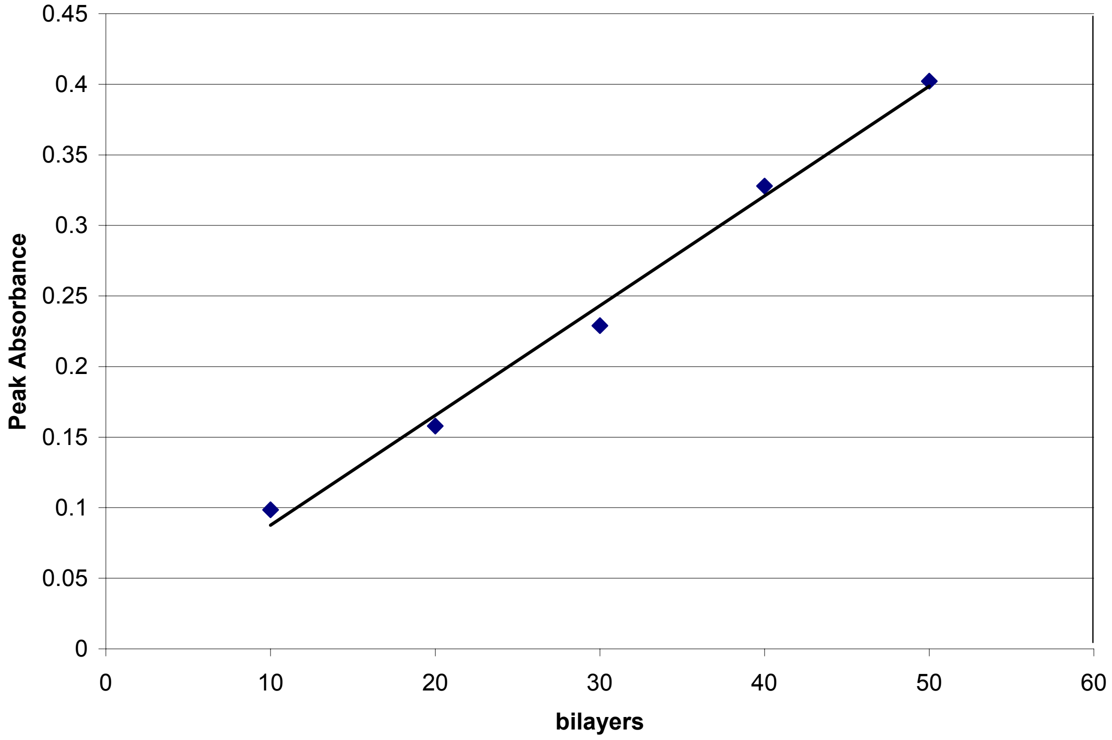

Figure 2.2.5. The peak absorbance of PAH / PCBS films as function of the number of bilayers.

In Figure 2.2.6, the square root of the SHG signal is plotted as a function of the number of bilayers for the same films shown in Figure 2.2.5. The figure shows that the square root of the SHG signal increases linearly with increasing number of bilayers. Since the film thickness increases linearly with the number of bilayers, it follows that the square root of the SHG signal increases linearly with film thickness. This was to be expected from the discussion in Section 1.5. This indicates that the net orientation of the chromophores is independent of the amount of bilayers deposited and was first demonstrated by Virginia Tech researchers.[37] The ability to grow thick films with uniform polar order throughout the film is critical for NLO applications.

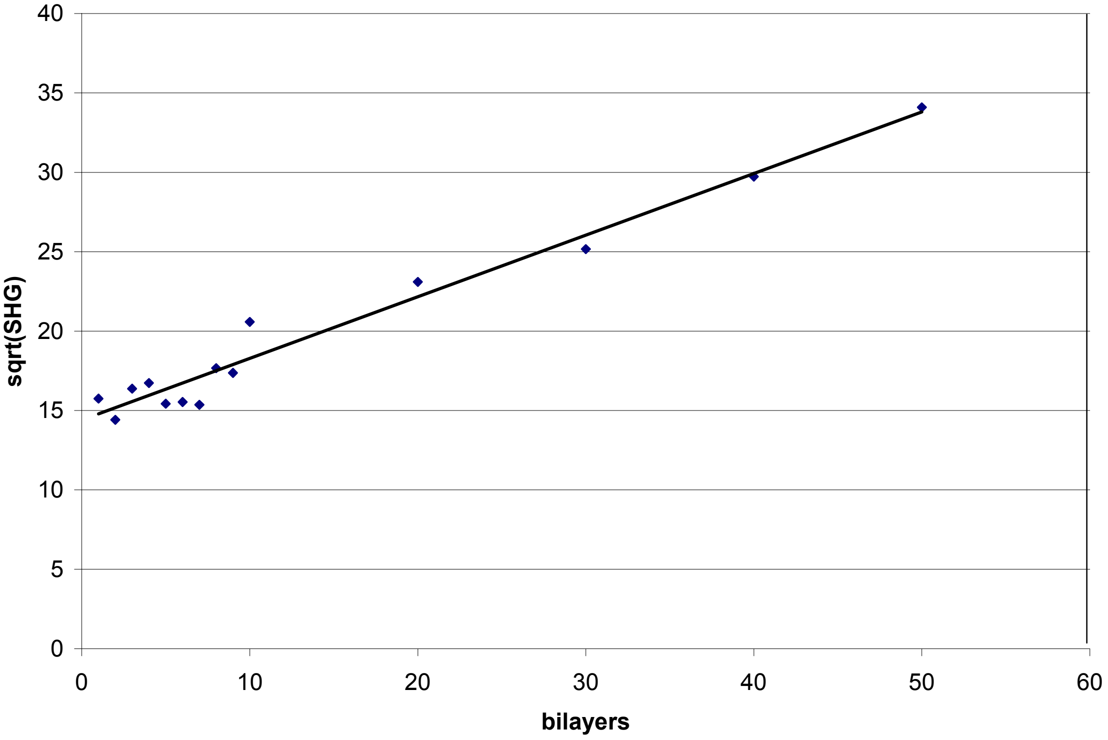

Figure 2.2.6. The square root of the SHG signal generated by PAH / PCBS films as a function of the number of bilayers.

In contrast, the combination of PDDA and PCBS does not show a significant growth of SHG with the number of bilayers. One main difference between PDDA and PAH in combination with PCBS is that the bond between PDDA and PCBS is purely electrostatic while between PAH and PCBS there is also the possibility of hydrogen bonding. When a given bilayer is deposited, say bilayer X, there is an electrostatic attraction to the previously deposited layers resulting in a net orientation of the chromophores. However, when additional bilayers are deposited on top, bilayer X experiences a symmetric situation. The chromophores of this bilayer are equally attracted to other bilayers on top of it and below it. One would expect that this leads to randomly oriented chromophores and zero $\chi^{(2)}$ with exception of the bilayers at the air and glass interfaces. This appears to describe the situation for the PDDA / PCBS films accurately. However, the PAH / PCBS films show a significant $\chi^{(2)}$ in the bulk layers. While still not fully understood, one possible explanation is as follows. As noted above, there may be both an hydrogen bond and an electrostatic bond between a PCBS chromophore and PAH. The hydrogen bond is stronger than the electrostatic bond and both bonds must break at the same time for the chromophore to "flip over" to another direction. Presumably, this will largely reduce the "flip over" probability compared to only an electrostatic bond. Also, those chromophores that do break free must find another free charge before they fall back to their original position; in order to change the position permanently. This further reduces this probability. Although the chromophores in ISAM films can change orientation, the films usually show good aging properties.[38, 39]

2.3 Hybrid Covalent / Ionic Deposition

As discussed above, the ISAM deposition method has many advantages over deposition methods such as poled polymers, Langmuir-Blodgett, and covalent self-assembly. A potential disadvantage of ISAM is that a large fraction of the chromophores is randomly or oppositely oriented which limits the SHG response (see Figure 2.2.1)[28]. In fact, additional layers would not deposit if it were not for chromophores pointing in the opposite of the desired direction.

In order to increase the $\chi^{(2)}$, variations of the classic ISAM method have been investigated. One of these variations is called hybrid covalent / ionic deposition.[40,41] The materials first used in this method are PAH and Procion Red. Figure 2.3.1 shows a schematic of the deposition scheme and the Procion Red structure. The PAH is deposited as described in the previous section at a pH of 7.0. The Procion Red is deposited at a pH of 10. At this pH, the PAH is weakly charged ($pK_a \sim 9$), so there is little electrostatic attraction of the Procion Red to the PAH substrate. However, a covalent bond can form between the reactive triazine ring of the Procion Red and an unprotonated amine group of PAH. After a monolayer of Procion Red is deposited, the sample is immersed into PAH again which is at 7.0 pH. At this pH, the PAH amine is protonated and the next PAH layer can bind electrostatically with the sulfonates of Procion Red.

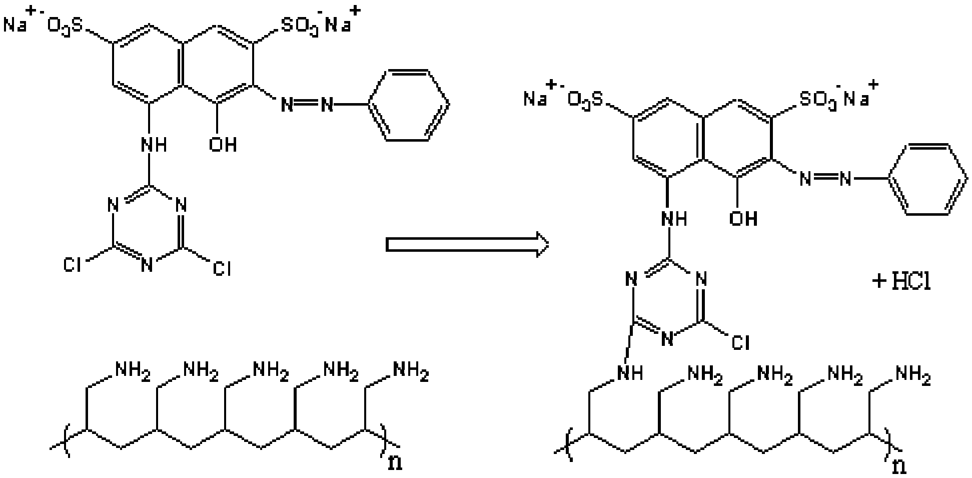

Figure 2.3.1. The covalent reaction between Procion Red and the PAH substrate. The reactive triazine covalently couples with an amine group of PAH.

Figure 2.3.2 shows a typical absorption spectrum of a PAH / Procion red sample. Figure 2.3.3 shows the peak absorbance values for PAH / Procion Red, at λ = 522 nm, as a function of the number of deposited bilayers. As in the case for classical ISAM films, the absorbance increases linearly with the number of bilayers indicating that in hybrid covalent / ionic assembly the amount of material deposited per bilayer is again independent of the amount of bilayers deposited.

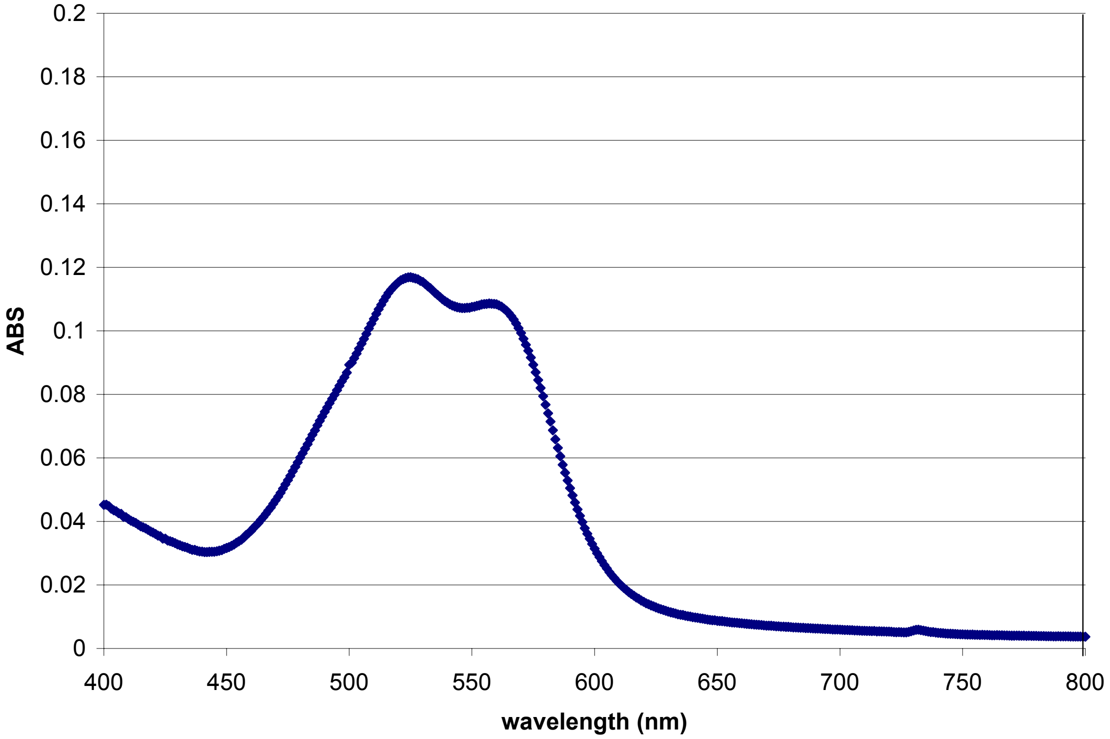

Figure 2.3.2 The absorbance spectrum of a 50 bilayer PAH / Procion Red sample.

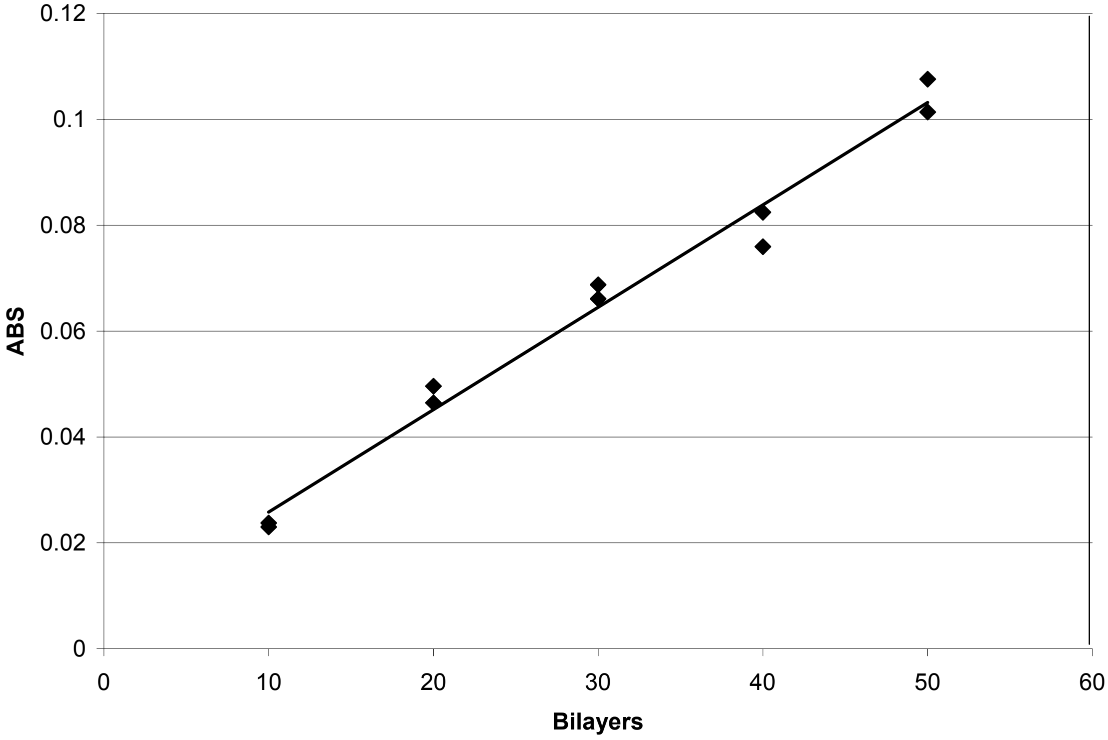

Figure 2.3.3. Absorbance as a function of deposited bilayers of PAH / Procion Red. The pH of PAH and Procion Red were 7.0 and 10.0 respectively. This allows for covalent deposition of Procion Red on PAH and ionic deposition of PAH on Procion Red.

The square root of the SHG signal as a function of the number of bilayers is depicted in Figure 2.3.4. Similarly to the case of PCBS, the square root of the SHG signal for PAH / Procion Red increases linearly with increasing bilayer numbers. Variations on Procion Red have been tested and have the largest $\chi^{(2)}$ values (12 x 10^{-9}) yet observed in ISAM films.[37] Procion Red was used because it is commercially available. It does not have a structure appropriate for large β value however. It is expected that significant further increases in $\chi^{(2)}$ can be achieved through the use of molecules that are optimized both for hybrid covalent / ionic deposition and their NLO response. These efforts are the subject of another students' Ph.D. research.

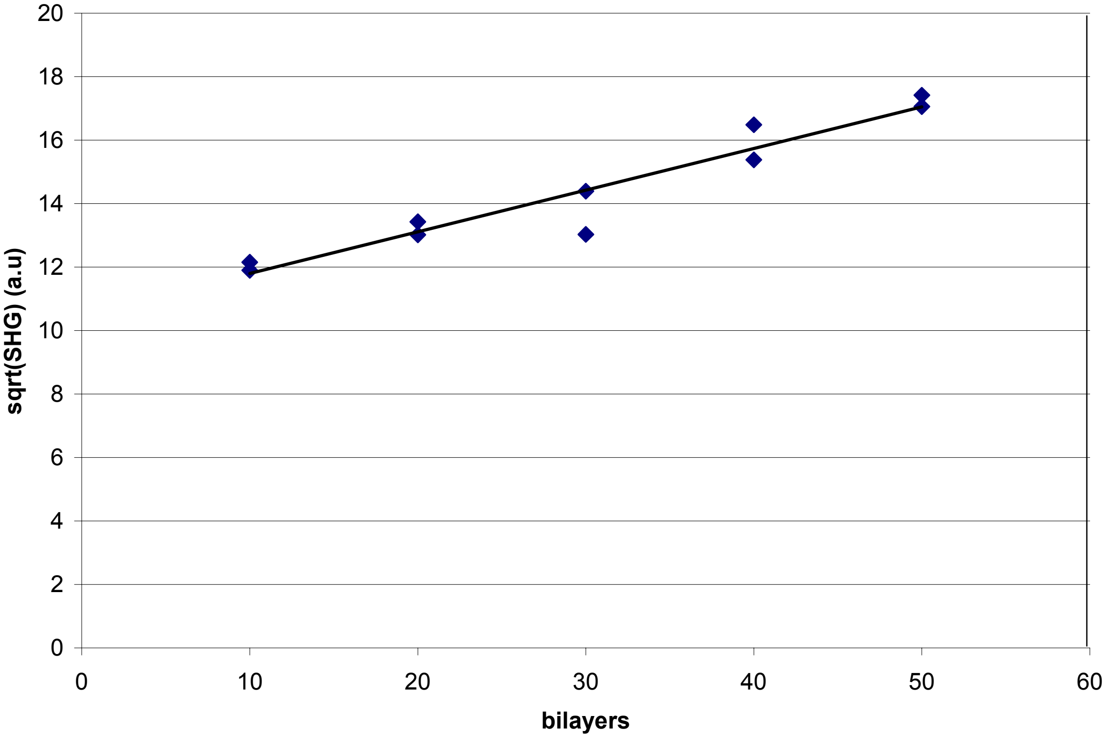

Figure 2.3.4. The square root of the SHG signal as a function of bilayers for PAH / Procion Red samples.

2.4 Multivalent monomer Deposition

Multivalent monomer deposition is very similar to the ISAM deposition process. As before, a polymer (usually PAH) is used as polycation. As anion, an NLO-active monomer is used that has multiple charges on one end and a single charge (same sign) on the other. The multiple charges are more strongly attracted to the polycation than the single charge resulting in a preferred orientation for the monomer. After the multivalent monomers are deposited, the sample is immersed in the polycation to start a new bilayer. The structure for one of these multivalent monomer materials, Acid Blue 92, is shown in Figure 2.4.1. Acid Blue 92 is obtained from Sigma Aldrich.

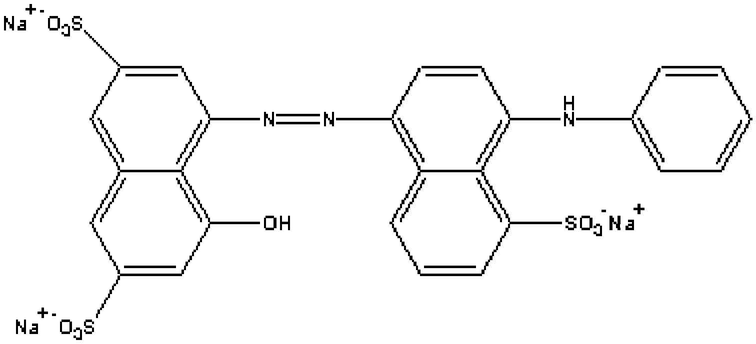

Figure 2.4.1. Structure of Acid Blue 92.

Figure 2.4.2 shows a typical spectrum for Acid Blue 92. The peak absorbance as a function of bilayers is depicted in Figure 2.4.3. Once again, the absorbance shows a linear dependence on the number of bilayers, indicative of a reproducible amount of material deposited with each bilayer.

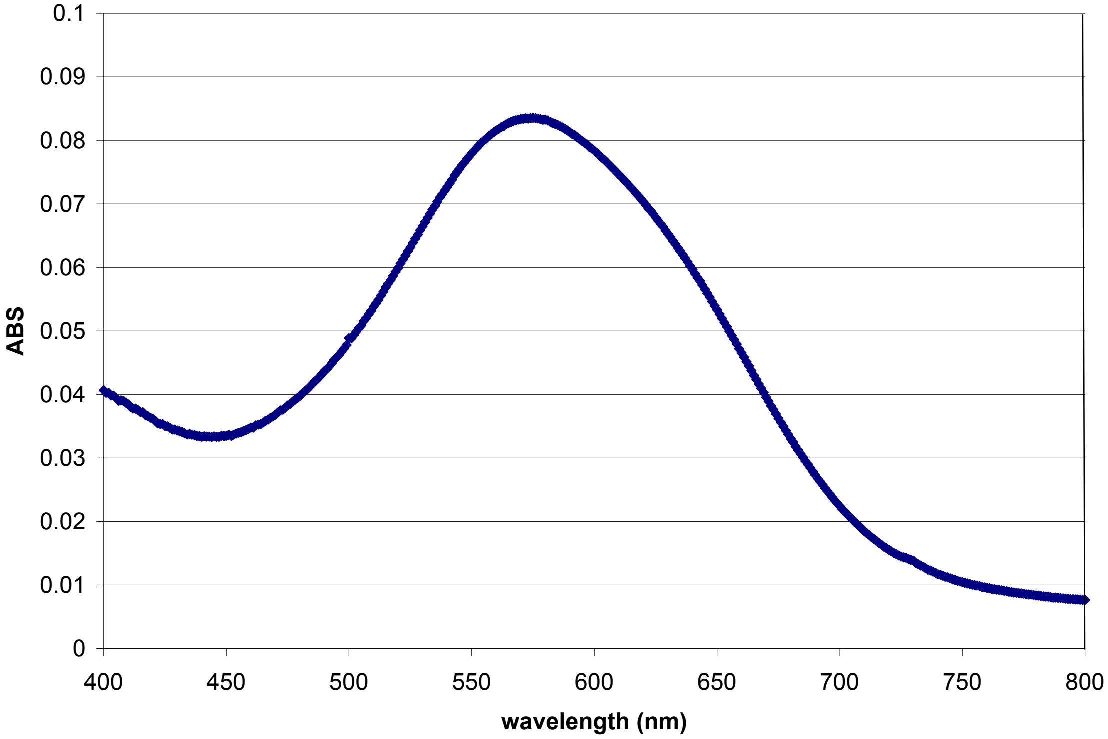

Figure 2.4.2. Typical spectrum of a PAH / Acid Blue 92 sample.

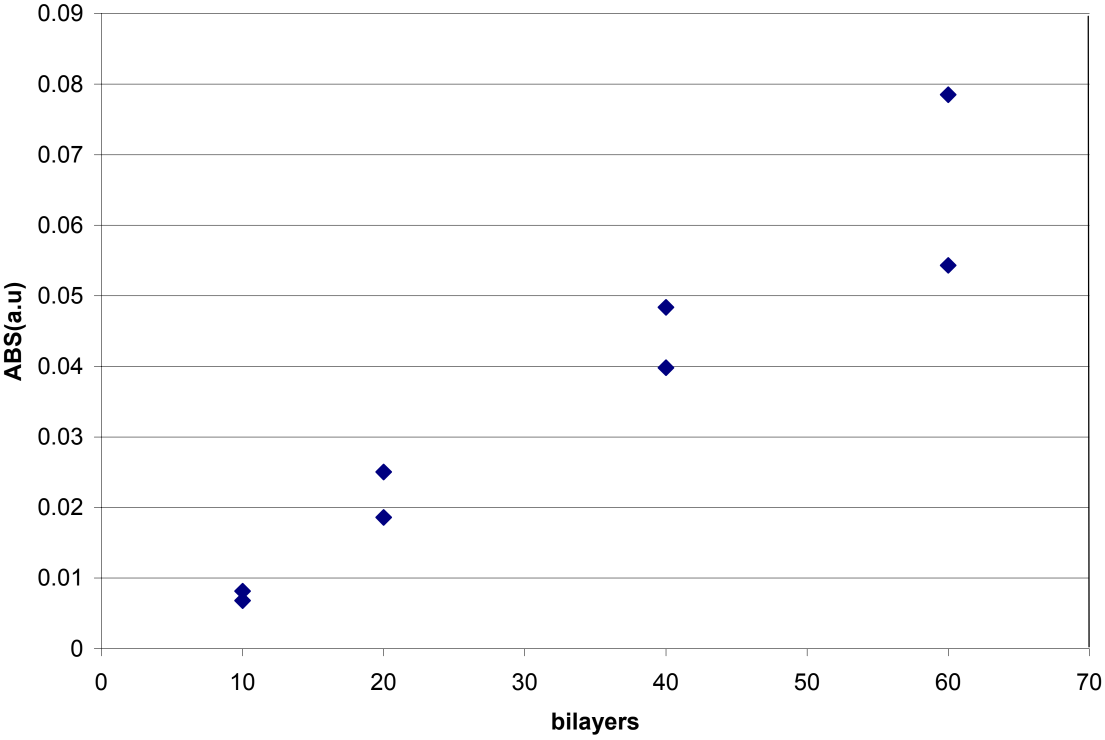

Figure 2.4.3. The peak absorbance value for PAH / Acid Blue 92 as a function of bilayers for two different sets of films.

The square root of the SHG signal as a function of the number of bilayers for Acid Blue 92 is shown in Figure 2.4.4. It is important to note that despite thorough rinsing, the polycation solution showed some small discoloration after depositing a large number of bilayers. This indicates that the binding of multivalent monomers to the polycation is weaker than the binding of a polyanion. Considering that polyanions possess thousands of charges, this is no surprise. Comparison of the SHG signals for PCBS, Procion Red, and Acid Blue 92 reveals that the Acid Blue 92 starts off much stronger than PCBS or Procion Red but does not exhibit as much growth with additional bilayers. This alternative approach of film fabrication, along with a few variations, will be discussed in more detail in Chapter 3.

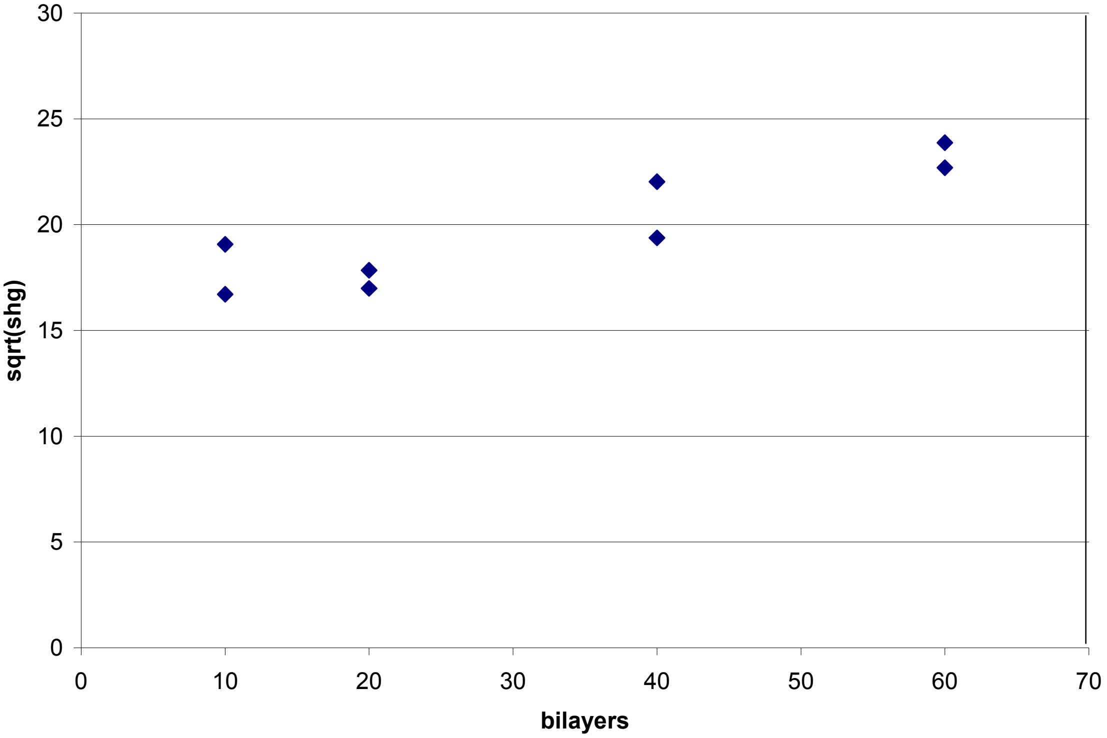

Figure 2.4.4. The square root of the SHG signal for PAH / Acid Blue 92 films as a function of bilayers.

References

[1] K.D. Singer, J.E. Sohn, S.J.Lalama, *Appl. Phys. Lett.* **49** (1986) 248.

[2] K.D. Singer, M.G. Kuzyk, J.E. Sohn, *J. Opt. Soc. Am. B* **4** (1987) 968.

[3] L. Cheng, R. Foss, G. Meredith, W. Tam, F. Zumsteg, Mat. *Res. Soc. Symp. Proc*. **247** (1992) 27.

[4] H.L. Hampsch, J. yang, G.K. Wong, and J.M. Torkelson, *Macromolecules* **23** (1990) 3648.

[5] R. Yeng, Y. Chen, B. Mandal, J. Kumar, S. Tripathy, *Mat.Res.Soc.Symp. Proc*. **247** (1992) 111.

[6] J. Wu, J. Valley, S. Ermer, E. Brinkley, J. Kenney, G. Lipscomb, R. Lytel, *Appl. Phys. Lett*. **58**, (1991) 225.

[7] J. Wu, E. Brinkley, J. Kenney, R. Lytel, A. Garito, *J. Appl. Phys*. **69** (1991) 7366.

[8] M.H. Davey, V.Y. Lee, L.M. Wu, C.R. Moylan, W. Volksen, A. Knoesen, R.D. Miller, T.J. Marks, *Chem. Mater.* **12** (2000) 1679.

[9] H. Ma, S. Liu, J. Luo, S.H. Kang, M. Haller, T. Sassa, L.R. Dalton, A.K.Y. Jen, *Ad. Funct. Mater* **12** (2002) 565.

[10] Lord Rayleigh, *Phil. Mag*. **48** (1890) 337.

[11] I. Langmuir, *J. Am. Chem. Soc.* **39** (1917) 1848.

[12] S. Allen, T.D. McLean, P.F. Gordon, B.D. Bothwell, P. Robin, I. Ledoux, *SPIE Proc*., **971** (1988) 206.

[13] L. Netzer, J. Sagiv, *J. Am. Chem. Soc*. **105** (1983) 674.

[14] S. Yitzchaik, S.B. Roscoe, A. K. Kakkar, D.S. Allan, T.J. Marka, Z. Xu, T. Zhang, W. Lin, G.K. Wong, *J. Phys. Chem*. **97** (1993) 6958.

[15] Wenben Lin, Weiping. Lin, G.K. Wong, T.J. Marks, *J. Am. Chem. Soc.* **118** (1996) 8034.

[16] G. Decher, J.D. Hong, *Thin Solid Films* **210** (1992) 831.

[17] S. Watanabe, S. Regen, *J. Am. Chem.Soc*. **116** (1994) 8855.

[18] X. Zhang, M. Gao, X. Kong, Y.Sun, J.Shen, *J. Chem. Soc. Chem. Commun*. (1994) 1055.

[19] Y. Lvov, K. Ariga, T. Kunitake, Chem. Lett. (1994) 2323.

[20]W. Kong, X. Zhang, M. Gao, H. Zhou, W. Li, J. *Shen, Macromol.. Rapid. Commun.* **15** (1994) 405.

[21]E. Kleinfeld, G. Ferguson, *Science* **265** (1994) 370.

[22]M. Gordon. *A Nacreous Selfp-Assembled Nanolaminate for Corrosion Resistance on 2024-Al Alloy, Masters Thesis Virginia Polytechnic Institute and State University* (2001).

[23]D. Marciu, M.B. Miller, J.R. Heflin, M.A. Murray, A.L. Ritter, P.J. Neyman, W. Graupner, H. Wang, H.W. Gibson, R.M. Davis, *MRS Proc.* **598** BB11.50.1 (2000).

[24]C. Brands, T. Piok, P.J. Neyman, A. Erlacher, C. Soman, M.A. Murray, R. Schroeder, J.R Heflin, W. Graupner, D. Marciu, A. Drake, M.B. Miller, H. Wang, H. Gibson, H.C. Dorn, G. Leising, M. Guzy, R.M. Davis, *SPIE Proc.* **3937** (2000) 51.

[25]J.R. Heflin, C. Figura, D. Marciu, Y. Liu, and R.O. Claus, *SPIE Proc*. **3147** (1997) 10; *Appl. Phys. Lett.* **74**, (1999) 595.

[26]Y. Lvov, S. Yamada, and T. Kunitake, *Thin Solid Films* **300** (1997) 107.

[27]X. Wang, S.Balasubramanian, L.Li, X. Jiang, D. Sandman. M.F. Rubner, J. Kumar, and S.K. Tripathy, Macromol. *Rapid Commun.* **18** (1997) 451.

[28]C. Figura, *Second Order Nonlinear Optics in Ionically Self-Assembled Thin Films, Thesis, Virginia Polytechnic Institute and State University* (1999).

[29]C. Figura, P.J. Neyman, D. Marciu, C. Brands, M.A. Murray, S. Hair, M.B. Miller, R.M. Davis, and J.R. Heflin. *MRS Proc*. **598** BB4.9.1-6 (2000).

[30]M. Losche, J. Schmitt, G. Decher, W.G. Bouwman, K. Kjaer, *Macromolecules* **31** (1998) 8893.

[31]J. Schmitt, T. Grunewald, K. Kjaer, P. Pershan, G. Decher, M. Losche, *Macromolecules* **26** (1993) 7058.

[32]G.J. Kellog, A.M. Mayes, W.B. Stockton, M. Ferreira, M.F. Rubner, R. Hsieh, *J. Appl. Phys*. **79** (1996) 5109.

[33]T. Salditt, Q. An, A. Plech, C. Eschbaumer, U.S. Schubert, *Thin Solid Films* **354** (1999) 208.

[34]W. Kern, D.A. Poutinen, *RCA Rev*. **31** (1970) 187.

[35]R.K. Iler, *The Chemistry of Silica Wiley, New York* (1979).

[36]Y. Liu, *Thesis, Virginia Polytechnic institute and state university*, 1996.

[37]J.R. Heflin, C. Figura, D. Marciu, Y. Liu, R.O. Claus, *Appl. Phys. Lett*. **74**, 495 (1999).

[38]C. Figura, D. Marciu, Y. liu, Y.X. Wang, K. Lenahan, R.O. Claus, *Polym. Prep. Am. Chem. Soc., Div. Polym. Chem.* **39(2)** (1998) 1122.

[39]R. Bijlsma, A.A. van Well, M.A. Cohen Stuart, *Physica B* **234** (1997) 254.

[40]P.J. Neyman, M. Guzy, S.M. Shah, R.M. Davis, K.E. Van Cott, H. Wang, H. Wang, H.W. Gibson, C. Brands, J.R. Heflin, *MRS Proc*. **708** BB4.4 (2000).

[41]K. Van Cott, M. Guzy, P. Neyman, C. Brands, J.R. Heflin, H.W. Gibson, R.M. Davis, *Angewandte Chemie International edition* **41** (2002) 3719.

Chapter Three: Multivalent Monomer Deposition Process

A consequence of ISAM film formation using polymers is that a significant percentage of the chromophores are pointing in a direction away from the glass substrate, opposing the net orientation. This is both necessary and unfortunate. Necessary because the chromophores pointing in the opposing direction provide the charges on which the new layer is built. Unfortunate because opposing chromophores cancel each other therefore reducing the net orientation and thus reducing the $\chi^{(2)}$. In this chapter a novel deposition method, a variation on ISAM called multivalent monomer deposition, is investigated in an attempt to overcome these issues. In this method, the polyelectrolyte with NLO sidechains is replaced by NLO monomers with charges of different strength on each side of the molecule. The possible advantages of this method are increased NLO activity due to increase in net orientation and a decrease in layer thickness. Also, attempts are made to complex the multivalent monomer molecules with cyclodextrins to increase the SHG signal even further.

3.1 Multivalent Monomer Deposition Method

In an attempt to overcome the issue of opposing chromophore orientation, we have fabricated ionically self-assembled films incorporating multivalent monomer NLO chromophores. The difference between the ISAM deposition process and the multivalent monomer deposition process is that the optically active polymer is replaced by an optically active monomer with charges on both ends of the molecule. The charges are of the same sign (negative in the experiments described in this thesis) but not equal in strength. The idea is that the end of the monomer with the larger charge will have a higher probability of deposition, resulting in a net orientation of the chromophores. The smaller charges on the other side of the monomer will provide the sites for deposition of the next polymer layer.

It was known from literature that ISAM films could still be built if one of the polymers is replaced by a multivalent monomer[1,2]. Figure 3.1.1 shows a schematic comparison between the polyelectrolyte ISAM and the multivalent monomer deposition process. Although the schematic for the ISAM shows a net orientation of the chromophores, many if not most of the chromophores are randomly oriented. In contrast, the schematic of the multivalent monomer deposition shows all chromophores pointing in the general direction of the glass slide. This increase in net orientation is expected to result in increased $\chi^{(2)}$.

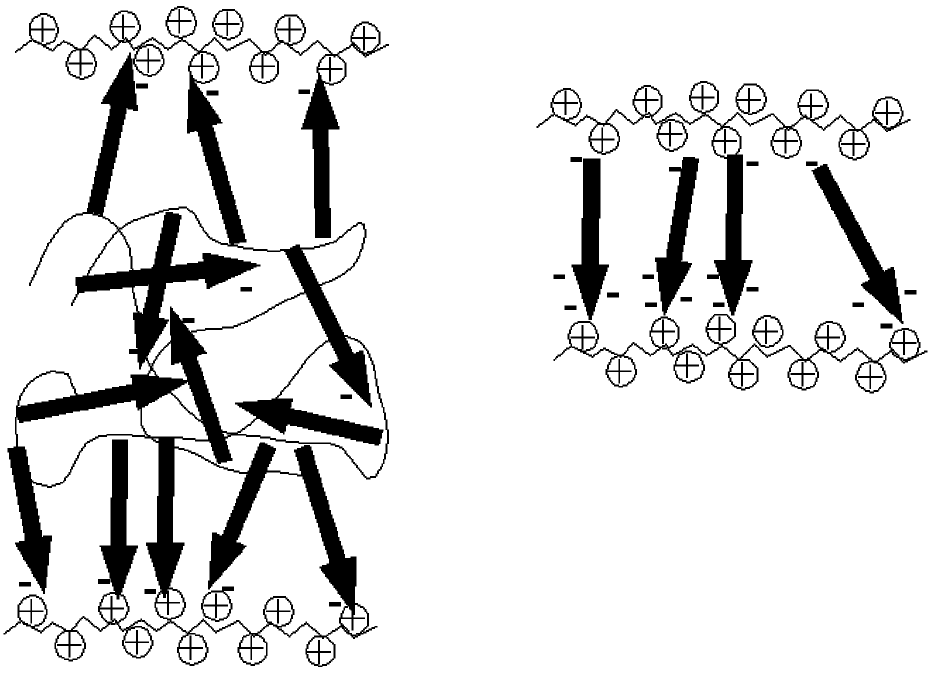

Figure 3.1.1 Schematic representation of a polyelectrolyte ISAM film (left) and the multivalent monomer deposition process (right).

3.2 Planarity

Figure 3.2.1 shows the chemical structure of Acid Blue 92, Solvent Blue 37, and Amaranth. The Amaranth is discussed in the next section. All materials were purchased from Sigma Aldrich. It was anticipated that the end of the molecules with two sulfonate groups would preferentially bind to the preceding PAH layer while the following PAH layer would bind to the remaining sulfonate group, thus yielding a high degree of polar order. The Acid Blue 92 and Solvent Blue 37 have very similar structures, the only difference being the extra OH group in Solvent Blue 37. It was hypothesized that the extra OH group forces a greater planarity in the Solvent Blue 37 molecule, which would result in a larger SHG response, similar to the results of Leslie *et al*[3]. For these experiments, the concentration was 10 mMol and the pH was 7.0. No salt was added. The absorbance as function of the number of bilayers is depicted in Figure 3.2.2. The absorbance of both Acid Blue 92 and Solvent Blue 37 increases linearly with the number of bilayers but the absorbance of Solvent Blue 37 is consistently higher. This makes sense as the extra OH group may be negatively charged, resulting in a denser absorption. However, the difference in absorbance could also be caused by difference in extinction coefficient ε. The extinction coefficient is defined through

$$T = 10^{-\varepsilon c l}, \qquad (3.2.1)$$

where c is the concentration in moles per liter, l is the thickness, and T is the % transmission.

To make sure that this is not the case, the absorbance was measured of 0.01 mMol solutions of Acid Blue 92 and Solvent Blue 37. The results of this test are shown in Table 3.2.1. The data show that the extinction coefficient for Solvent Blue 37 is not higher than the extinction coefficient of Acid Blue 92.

The SHG signal as a function of the number of bilayers is shown in Figure 3.2.3. The SHG signal does not increase with the number of bilayers as hoped, but shows a decrease. This indicates that the ordering is lost as additional bilayers are deposited. The SHG signal for Solvent Blue 37 is indeed much stronger than Acid Blue 92 for small number of bilayers, but with increasing bilayers the SHG signal decreases even more for

Solvent Blue 37. Planarity is a moot point if there is little or no net orientation of the chromophores.

Material	Peak Wavelength	Extinction Coefficient
Acid Blue 92	569	3.63×10^{-5} L mol^{-1} cm^{-1}
Solvent Blue 37	571	2.79×10^{-5} L mol^{-1} cm^{-1}
Amaranth	522	4.56×10^{-5} L mol^{-1} cm^{-1}

Table 3.2.1. Extinction coefficients of Acid Blue 92, Solvent Blue 37, Amaranth.

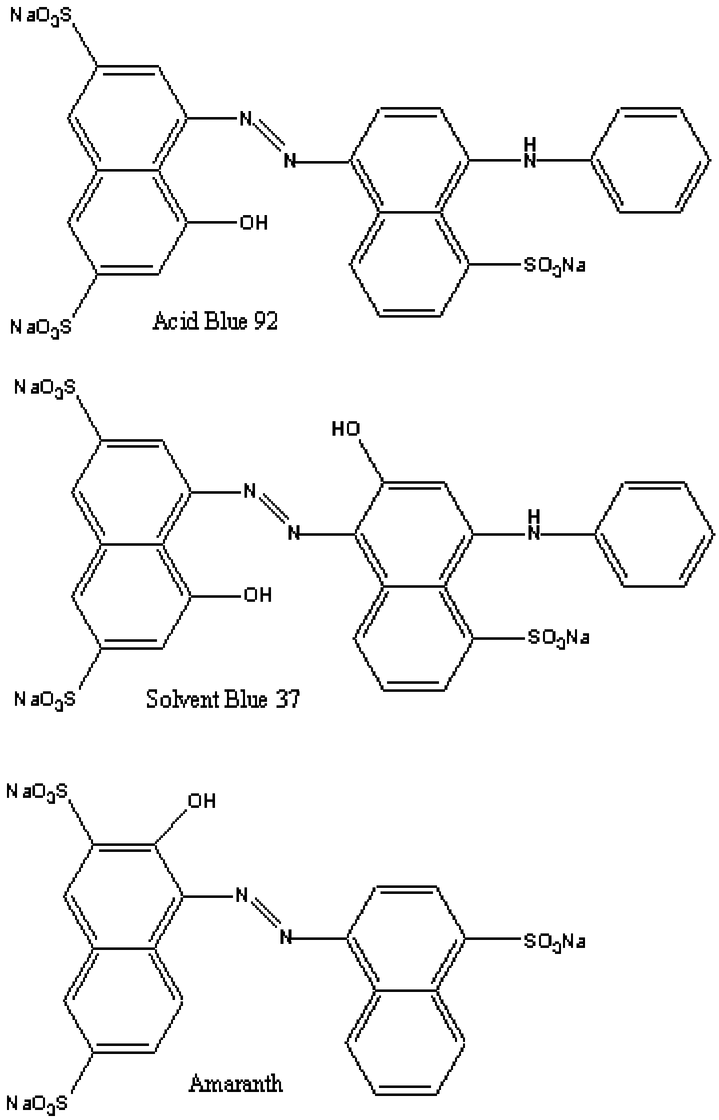

Figure 3.2.1. The chemical structures of Acid Blue 92, Solvent Blue 37, and Amaranth.

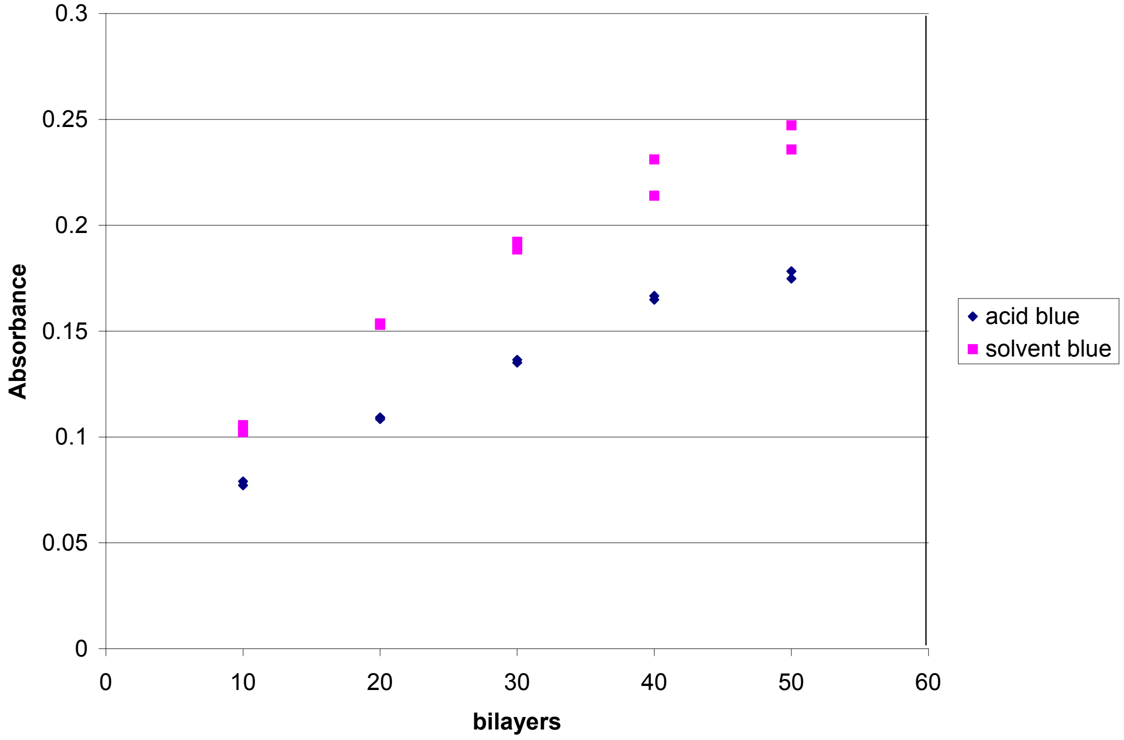

Figure 3.2.2. The absorbance of Solvent Blue 37 and Acid Blue 92 as a function of the number of bilayers.

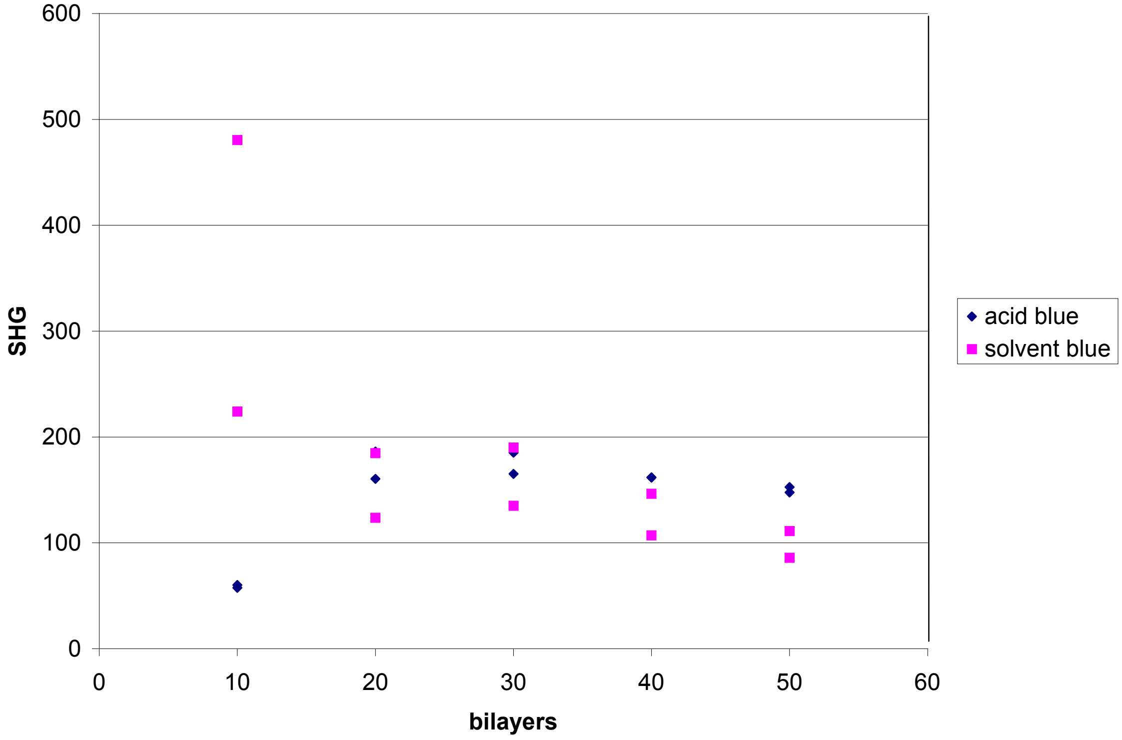

Figure 3.2.3. Second Harmonic generation as a function of deposited bilayers.

3.3 Functional groups

The chemical structure of Amaranth is also similar to Acid Blue 92. The important difference is that Amaranth is missing an amine group and a phenyl ring. The conjugation length is thus shorter and the amine group acts a an electron donor and therefore the Amaranth is expected to have a much lower SHG signal compared to Acid Blue 92. Figure 3.3.1 shows the absorbance as function of the number of bilayers for Amaranth. The absorbance increases linearly with the number of bilayers but at a rate that is an order of magnitude lower than the absorbances of Acid Blue 92 and Solvent Blue 37.

Figure 3.3.2 shows the SHG signal of Amaranth as a function of deposited bilayers. The SHG signal for Amaranth is extremely low and does not increase with the number of bilayers. This indicates that the presence of an electron donor is indeed essential and that the presence of electron acceptors alone results in a smaller hyperpolarizability β.

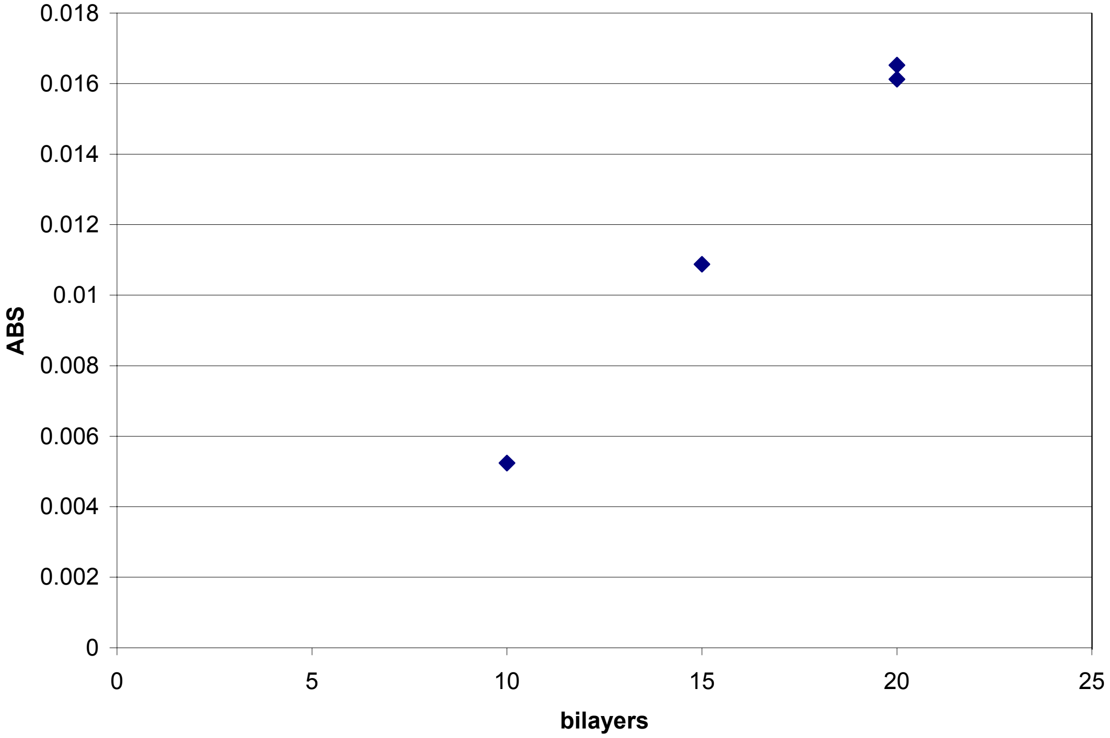

Figure 3.3.1. Absorbance as a function of bilayers for Acid Red 27 (Amaranth). The absorbance is smaller than the absorbance of Acid Blue 92 but does scale with increasing number of bilayers.

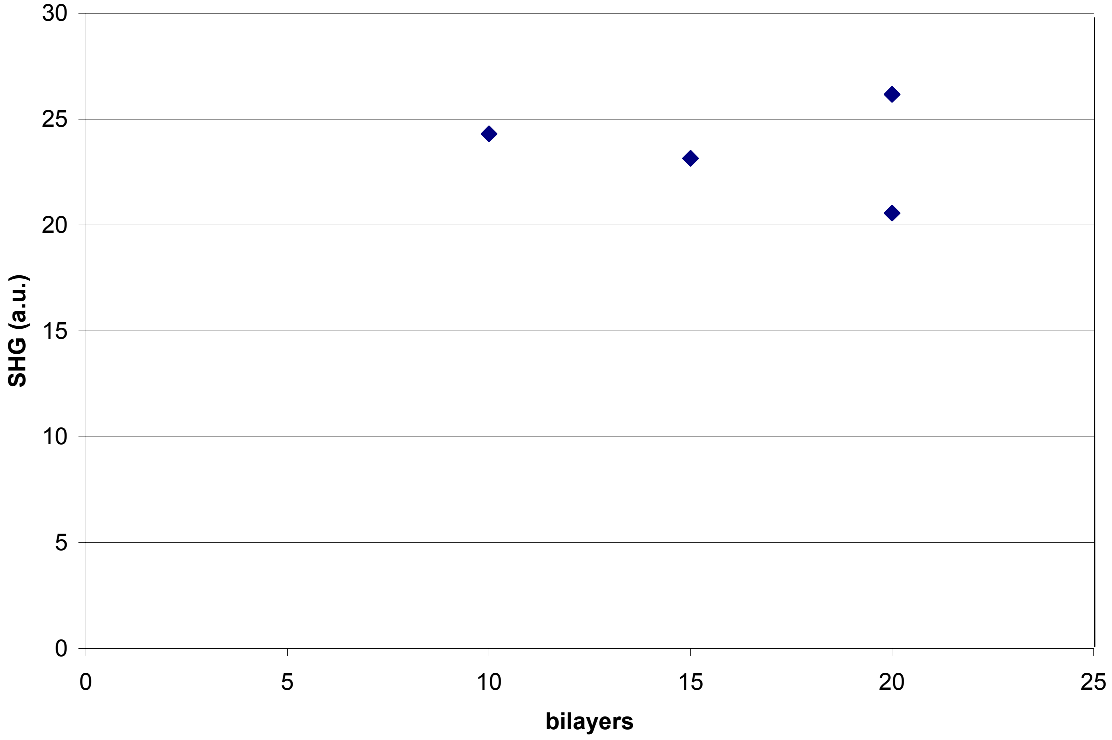

Figure 3.3.2. The SHG response as a function of the number of deposited bilayers. The signal is extremely small and does not increase.

3.4 Opposite charges

As an alternative to multivalent monomers, which are monomers with different number of charges on each end, we tried monomers with charges of opposite sign on each end. Figure 3.4.1 shows the structure of Mordant Yellow 12. It was hypothesized that the carboxy group of the Mordant Yellow 12 would bond with the preceding PAH layer, resulting in a Mordant Yellow 12 layer with nearly all monomers aligned. On top of the Mordant Yellow 12 layer, PAA (which would bind with the amine end of Mordant Yellow 12) and PAH would be deposited, after which a new Mordant Yellow 12 can be deposited. Researchers at Luna Innovations first proposed this deposition scheme[4]. It is quite different from the usual ISAM deposition scheme in which each layer consists of material that has exclusively one sign of charge. One potential concern with the Mordant Yellow 12 deposition is that the amine and carboxy groups of different Mordant Yellow 12 molecules would bind to one another, resulting in an uncontrolled, bulk deposition. Figure 3.4.2 shows the absorbance of these samples as a function of the number of trilayers. Surprisingly, it is found that this construction is a well-behaved ISAM film with the absorbance increasing linearly with increasing trilayers.

However, as depicted in Figure 3.4.3. the SHG response from these films does not scale quadratically with the number of bilayers. This indicates that Mordant Yellow 12 does initially deposit with polar order but that the net orientation decreases for subsequent layers. Most likely, this is because the Mordant Yellow 12 is bound electrostatically to the PAH with only one site and the molecule may reorient after the deposition of subsequent layers.

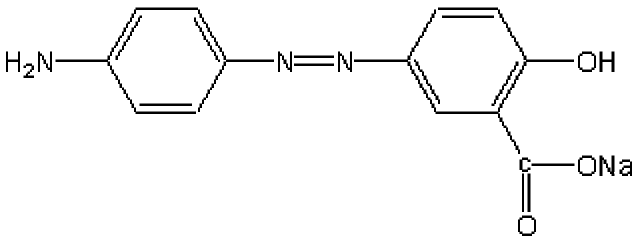

Figure 3.4.1. The chemical structure of Mordant Yellow 12.

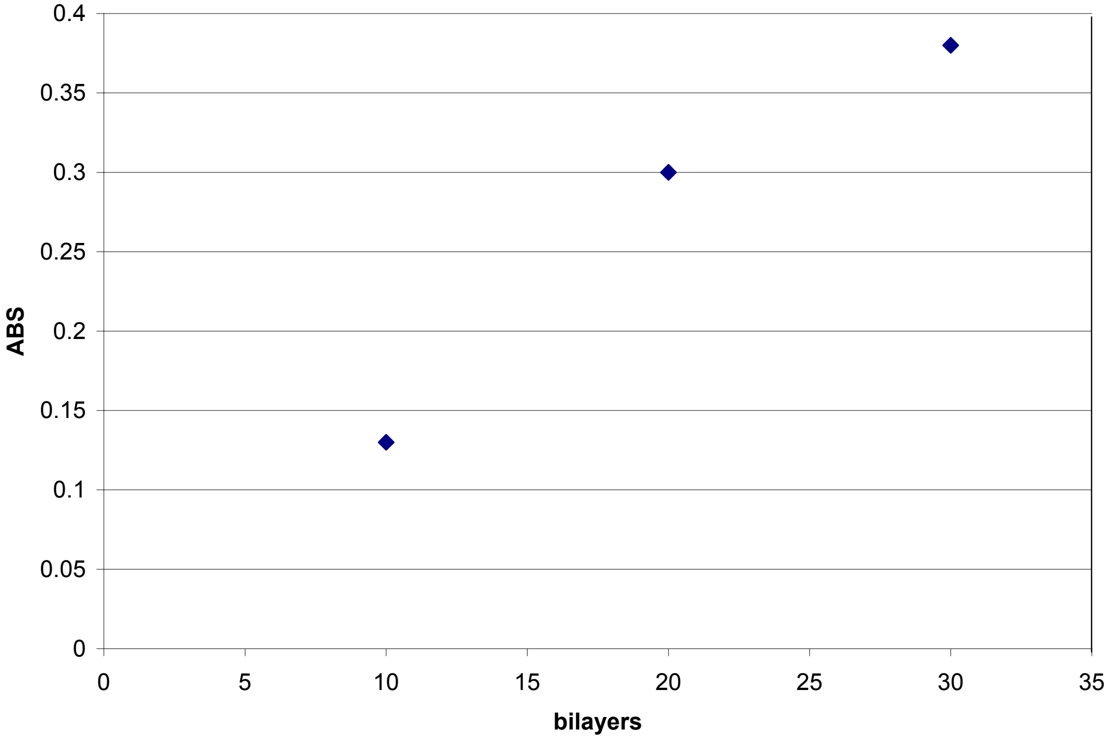

Figure 3.4.2. Absorbance as a function of the number of deposited trilayers for PAH / Mordant Yellow 12 / PAA.

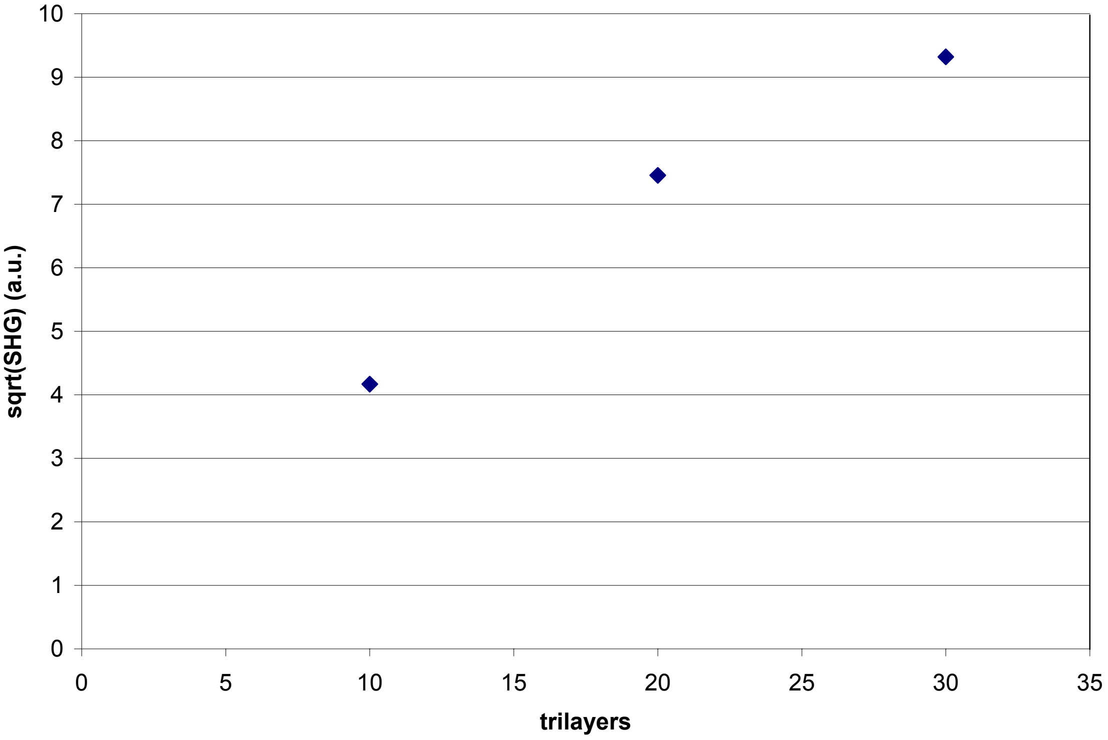

Figure 3.4.3. The square root of the SHG response as a function of deposited trilayers for Mordant Yellow 12.

3.5 Beta cyclodextrin

From the results of the previous sections, it appears that while ISAM films with multivalent monomers can exhibit polar order, they do not result in structures that are robust enough to scale over large number of bilayers. To achieve better scaling and larger SHG response, some additional mechanism is needed to cause the monomers to exhibit more uniform alignment. One possible way is to use the rather unique hydrophilic-hydrophobic nature of cyclodextrins. Cyclodextrins are cone shaped molecules that are hydrophobic on the inside and hydrophilic on the outside. Figure 3.5.1 shows the molecular structure, the hydrophobic and hydrophilic sites, and the geometrical arrangements of the most common cyclodextrins[5]. The hydrophilic exterior allows the cyclodextrins to be easily dissolved in water. Conjugated linear NLO monomers, such as those discussed in the preceding sections of this chapter, will easily complex with cyclodextrins due to the hydrophobic interior. That is, molecules will thread through the cyclodextrin sleeve.[5] In our experiments, we chose to use β-cyclodextrin as it has the proper inner diameter to allow phenyl rings to enter.

The features of cyclodextrins described above allow for multiple strategies to try to enhance net ordering and thus the SHG response. For example, to prevent the Mordant Yellow 12 molecules from bonding electrostatically to one another in solution due to opposite charges on each molecule, cyclodextrins can be added to the solution. The cyclodextrins will complex with the Mordant Yellow 12 molecules isolating each molecule from the others, and this solution is then used for deposition. The same deposition scheme as in Section 3.4 was used with the Mordant Yellow-cyclodextrin complex instead of just Mordant Yellow 12. Figure 3.5.2 shows a schematic of this process. Unfortunately, this scheme did not result in a significant deposition (absorbance values of the films were small), and therefore no SHG response was observed. What was observed was a strong discoloration of the PAA solution. This indicates that the Mordant Yellow-cyclodextrin complex does deposit on the PAH but that the one electrostatic bond is just not enough to keep the Mordant Yellow-cyclodextrin complex in place during the PAA deposition.

Another possibility is to deposit the cyclodextrins first on PAH, thus creating a layer with many hydrophobic cavities. Naturally, the cyclodextrins would have to be negatively charged for this. Then the film would be immersed in the Mordant Yellow 12 solution. The idea is that the positive end of the molecule would be attracted and the negative side repulsed. Therefore, the monomers would be aligned before they entered the cyclodextrin. On top of the negatively charged cyclodextrin, the next PAH layer is deposited. This idea is depicted schematically in Figure 3.5.3. This approach was tried with β-cyclodextrin sulfate and carboxymethyl β-cyclodextrin polymer. In both cases, no significant deposition took place. The PAH solution did not discolor, hence the Mordant Yellow 12 did not come off in the PAH solution. So it either did not deposit at all or, possibly, was washed off in the rinsing process. Apparently, the one electrostatic bond is simply not strong enough to keep the Mordant Yellow 12 molecules bound to the PAH layer. Also, it seems possible that if the β-cyclodextrin sulfate is deposited first, then the Mordant Yellow 12 molecules may not thread through with the β-cyclodextrin sulfate but instead may bind electrostatically to its edge. Again, this one electro-static bond is not strong enough to survive the rinsing process. Figure 3.5.4 shows the absorbance as a function of trilayers for PAH/MY12/PAA, PAH/MY12-β-cyclodextrin complex/PAA, PAH/β-cyclodextrin-sulfonate/MY12, and PAH/carboxymethyl β-cyclodextrin polymer/MY12. Finally, Figure 3.5.5 shows the SHG as a function of trilayers for PAH/MY12/PAA, PAH/MY12-β-cyclodextrin complex/PAA, PAH/β-cyclodextrin-sulfonate/MY12, and PAH/carboxymethyl β-cyclodextrin polymer/MY12. The PAH/MY12/PAA combination exhibits the largest SHG response. Considering the absorbance data this is not surprising. A related approach was demonstrated by Fischer *et*

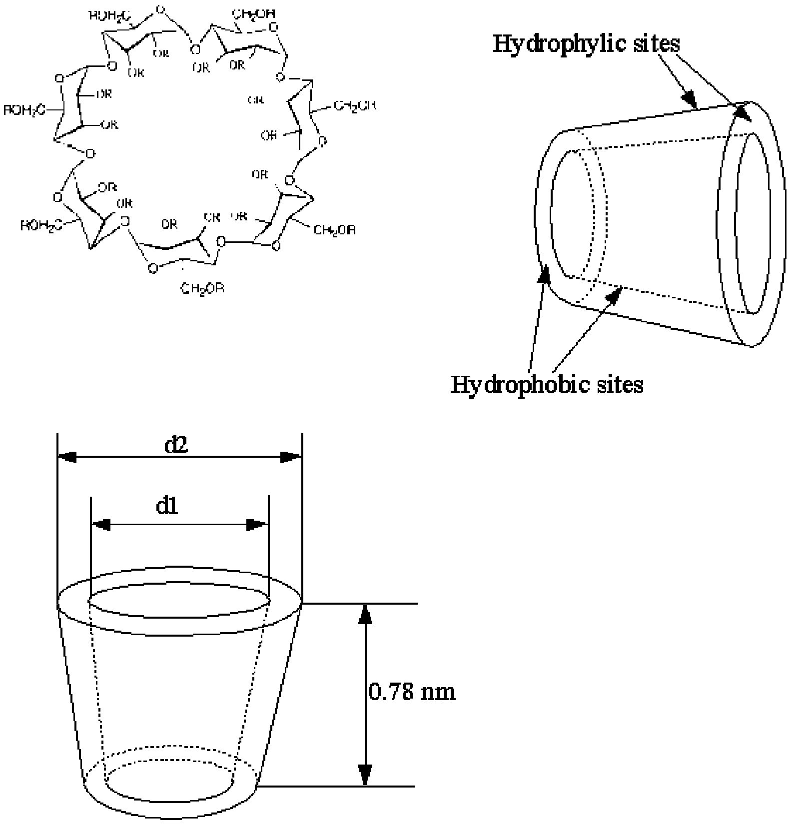

Figure 3.5.1. The chemical structure of β-cyclodextrin, the hydrophobic and hydrophilic sites, and the sizes of cyclodextrins. The inner and outer diameters are:

Cyclodextrin	Inner diameter	Outer diameter	Inner volume
α-cyclodextrin	0.57 nm	1.37 nm	174 Å^3
β-cyclodextrin	0.78 nm	1.53 nm	262 Å^3
γ-cyclodextrin	0.95 nm	1,69 nm	427Å^3

al.[6] They used cyclodextrins that were positively charged on one surface with an anionic copolymer that possessed sulfonate groups both close to the backbone as well as the end of azo chromophores side groups. Quadratic scaling of SHG was observed up to 30 bilayers.

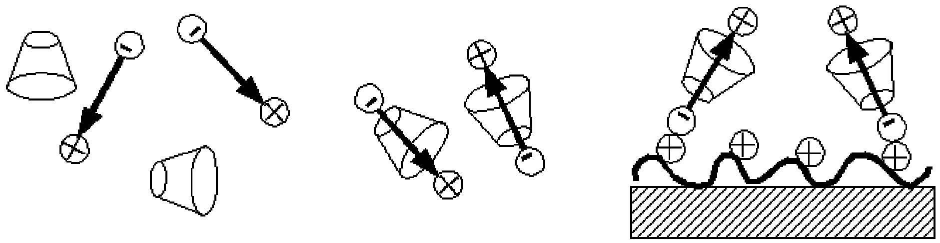

Figure 3.5.2. Mordant Yellow 12 and β-cyclodextrin molecules are mixed in solution and form complexes. The Mordant Yellow 12-β-cyclodextrin complex is then used for deposition.

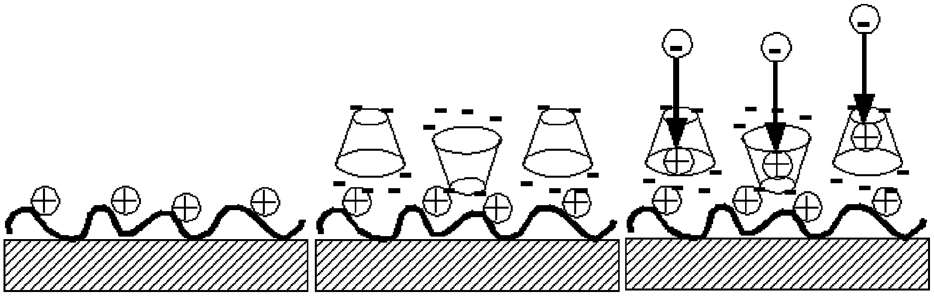

Figure 3.5.3. On top of a PAH layer, β-cyclodextrin sulfate is deposited. Then the slide is immersed in Mordant Yellow 12 solution so complexes can be formed. It was hypothesized that due to the charges on the molecules, the complexation would take place with the Mordant Yellow 12 molecules aligned.

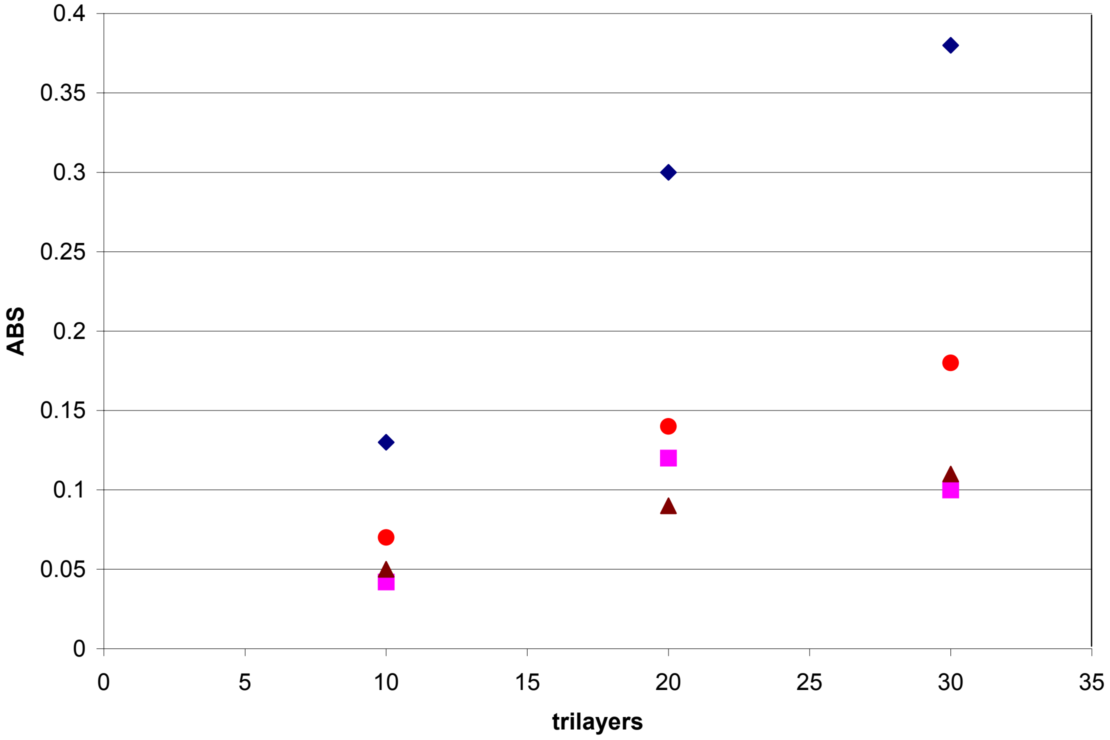

Figure 3.5.4. The absorbance as a function of deposited trilayers for PAH/MY12/PAA (diamonds), PAH/MY12-β-cyclodextrin complex/PAA (squares), PAH/β-cyclodextrin-sulfanate/MY12 (triangles), and PAH/carboxymethyl β-cyclodextrin polymer/MY12 (circles).

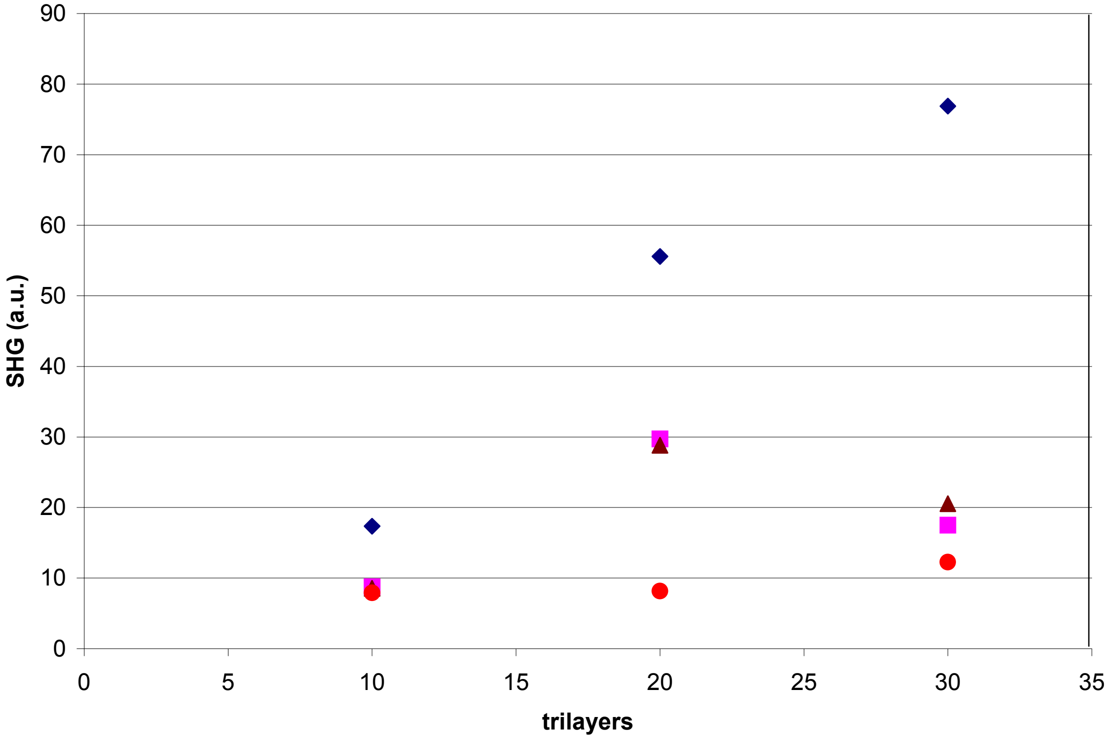

Figure 3.5.5. The SHG response as a function of deposited repeat units for PAH/MY12/PAA (diamonds), PAH/MY12-β-cyclodextrin complex/PAA (squares), PAH/β-cyclodextrin-sulfanate/MY12 (triangles), and PAH/carboxymethyl β-cyclodextrin polymer/MY12 (circles).

3.6 Acid Blue 92 β-cyclodextrin complex

In the previous section, we attempted to increase the alignment of multivalent monomers by complexing the monomers in solution as well as by depositing β-cyclodextrins before depositing the monomer. Both methods failed to produce films with a significant amount of deposited NLO active material. In this section, the reverse is attempted. First the monomer Acid Blue 92 is deposited on PAH then uncharged β-cyclodextrin is deposited.

The idea is that the β-cyclodextrin molecule may increase the perpendicular orientation of the Acid Blue 92 monomers while leaving the charges on the end of the Acid Blue 92 molecule free for the next PAH layer. Figure 3.6.1 shows the SHG as a function of repeat units for this construction. The addition of β-cyclodextrin molecules increases the SHG response consistently. The increase is rather small for Acid Blue 92 and there is still not a proper quadratic scaling of SHG with the number of bilayers. But these results indicate that it may be possible to increase alignment with the addition of β-cyclodextrins.

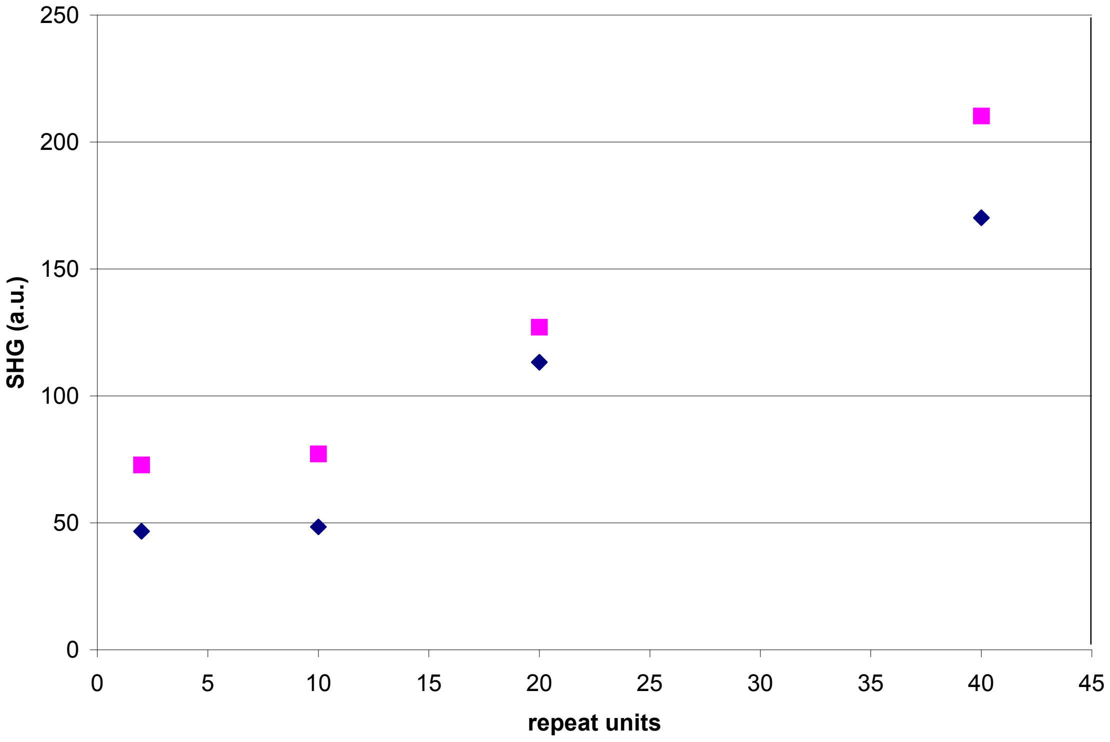

Figure 3.6.1. The SHG response as a function of repeat units for PAH/Acid Blue 92 and PAH/Acid Blue 92/β-cyclodextrin.

3.7 Miscellaneous multivalent materials

Figure 3.7.1 shows the chemical structures of additional multivalent monomers that we tested for use in the fabrication of second order NLO-active films. These materials are Direct Blue 71, Mordant Orange 10, Ponceau S, and Direct Yellow 8. All materials were purchased from Sigma Aldrich. The deposition schemes for Direct Blue 71, Ponceau S, and Direct Yellow 8 were the same as that for Acid Blue 92 (PAH/monomer, both at pH = 7.0). The Mordant Orange 10 was deposited at pH = 3.0 against PAH at pH = 7.0. The Mordant Orange 10 has a sulfonate and a carboxy group. At pH = 3.0 the sulfonate group will be charged while the carboxy group is neutral. This is expected to cause deposition with a preferential orientation with the sulfonate group to the surface. When the substrate is subsequently immersed into PAH at pH = 7.0, the carboxy groups are charged so the PAH can deposit.

The absorbance as a function of bilayers for these materials is shown in Figure 3.7.2. All materials show a roughly linear increase in absorbance with increasing bilayers. Note that no comparison can be made between the relative thicknesses between materials from this figure. Only within one series is thickness proportional to absorbance.

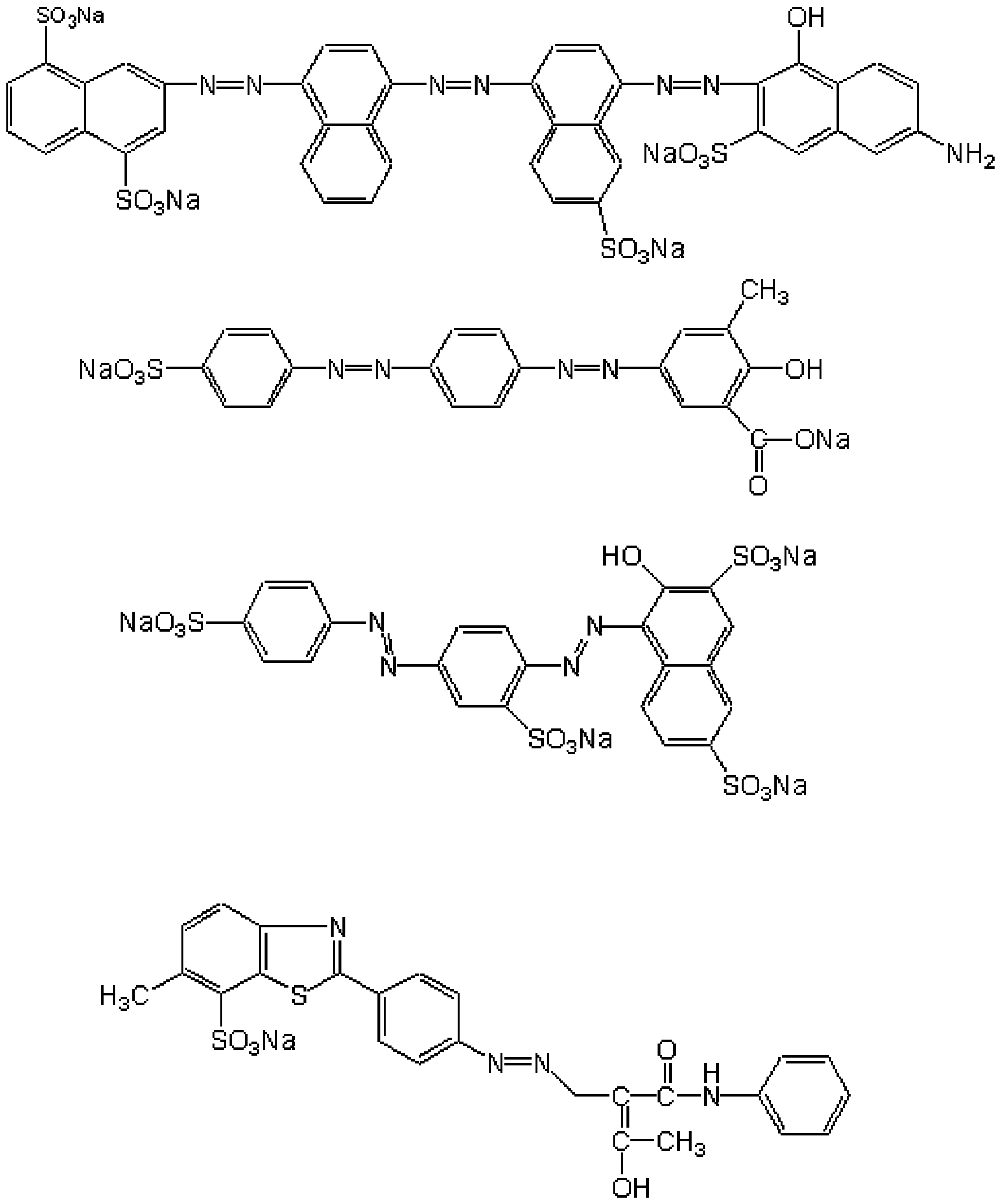

Figure 3.7.1. The Chemical structures for a selection of monomers. From top to bottom Direct Blue 71, Mordant Orange 10, Ponceau S, and Direct Yellow 8.

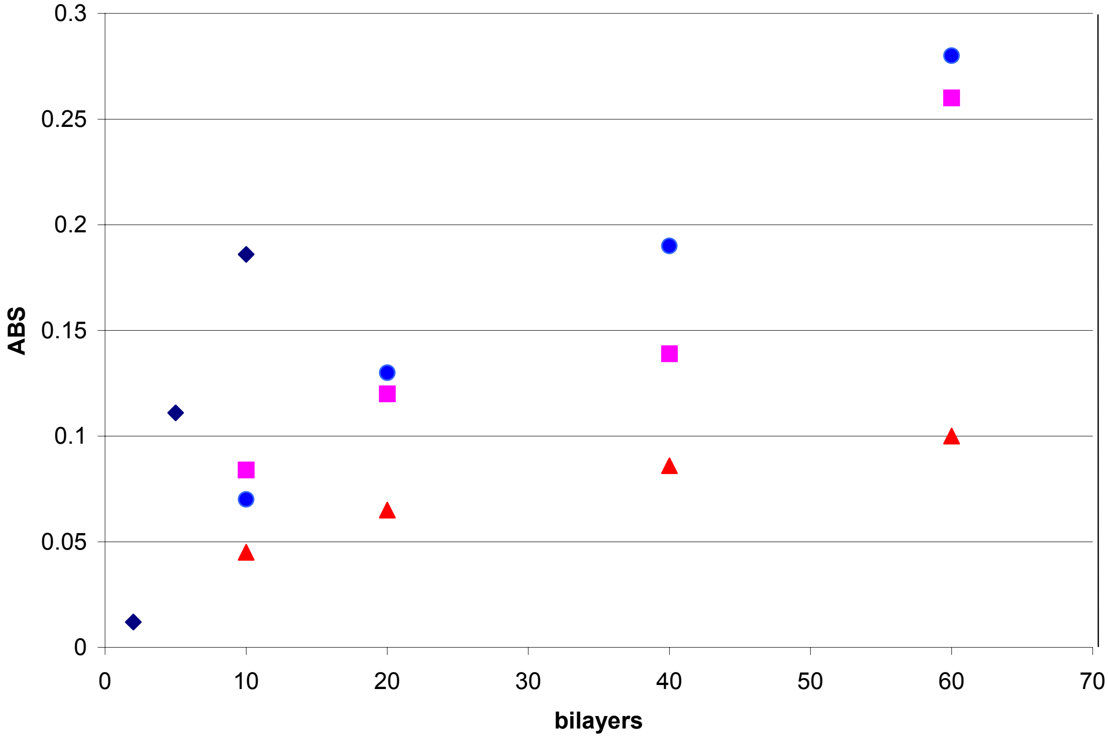

Figure 3.7.2. The absorbance as a function of bilayers for Mordant Orange 10 (diamonds), Direct Blue 71(circles), Ponceau S (squares), and Direct Yellow 8(triangles).

The SHG signal as a function of bilayers of Direct Blue 71 and Mordant Orange 10 are depicted in Figure 3.7.3 and 3.7.4 respectively. Both show a significant increase in SHG for small number of bilayers. So far, Mordant Orange 10 has not been measured for bilayer numbers larger than 10. The SHG signal of Direct Blue 71 plateaus at 20 bilayers. Unlike Acid Blue 92 and Solvent Blue 37, the SHG signal does not decrease at higher numbers of bilayers.

The SHG signals as a function of bilayers for Ponceau S and Direct Yellow 8 are depicted in Figure 3.7.5. For both materials the SHG is low and does not increase with increasing number of bilayers. It is not surprising that Ponceau S does not show a significant SHG response. Ponceau S does not have an electron donor and therefore does not show SHG for reasons similar to Amaranth in Section 3.2. Direct Yellow 8 does have an electron donor but the orientation of the charges suggest that the molecule might be oriented flat to the surface which could explain the lack of SHG response.

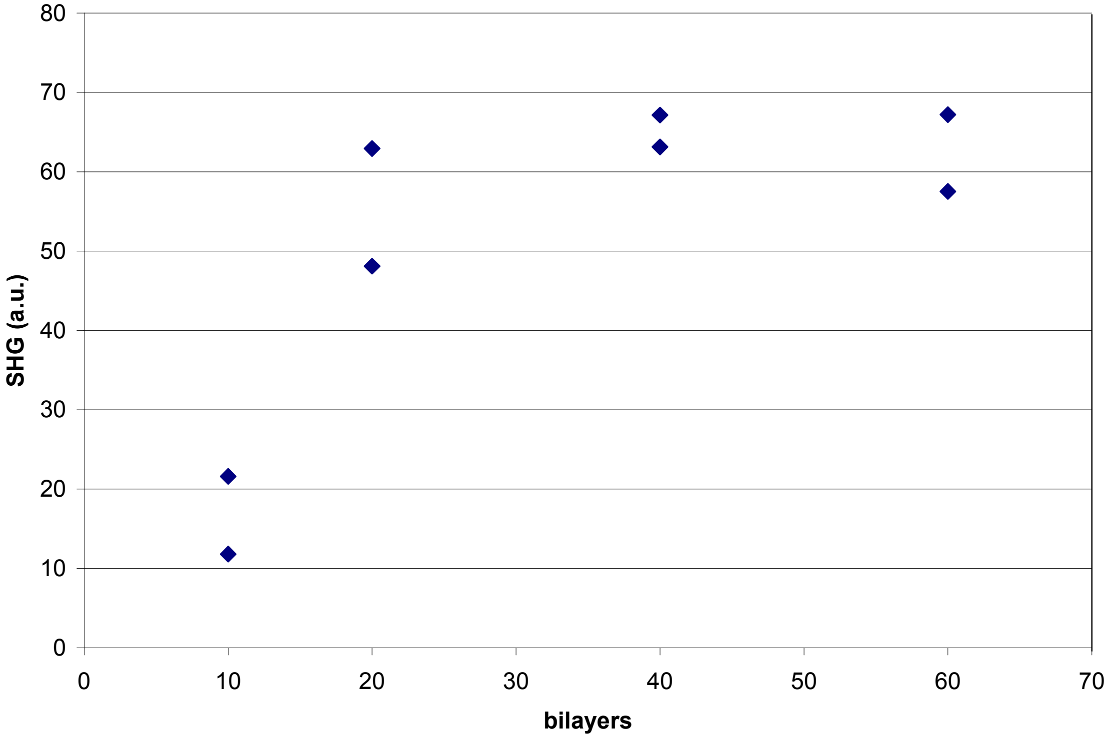

Figure 3.7.3. The SHG signal as a function of bilayers for Direct Blue 71.

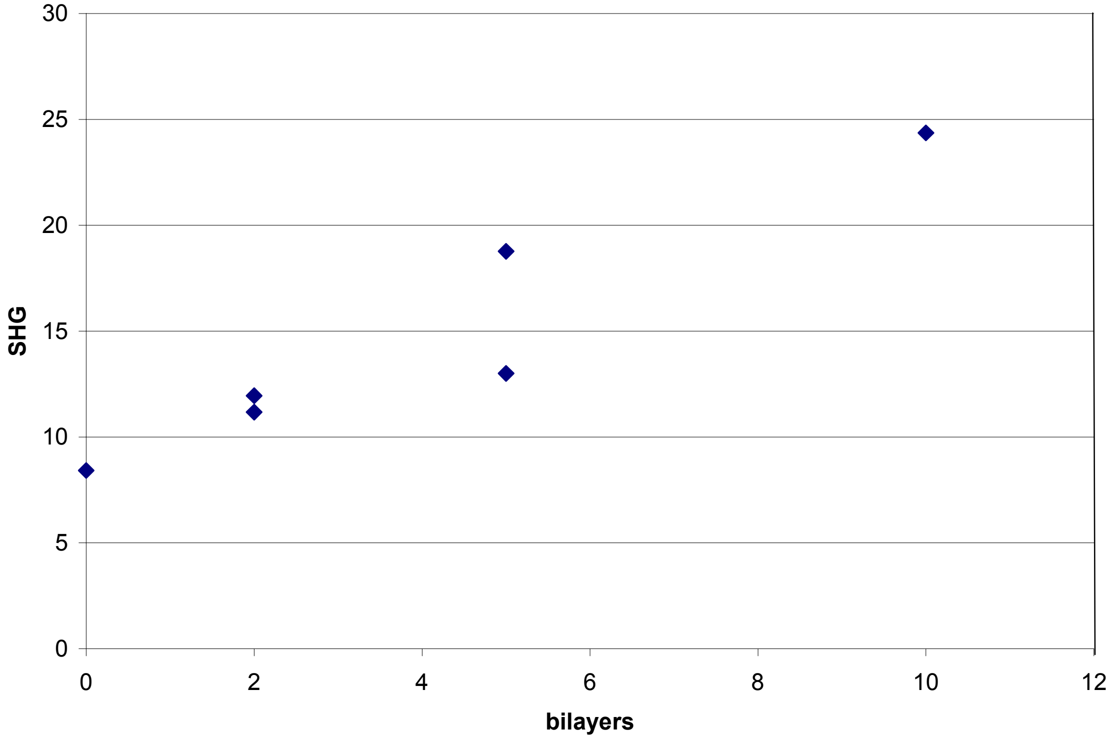

Figure 3.7.4. The SHG signal as function of bilayers for Mordant Orange 10.

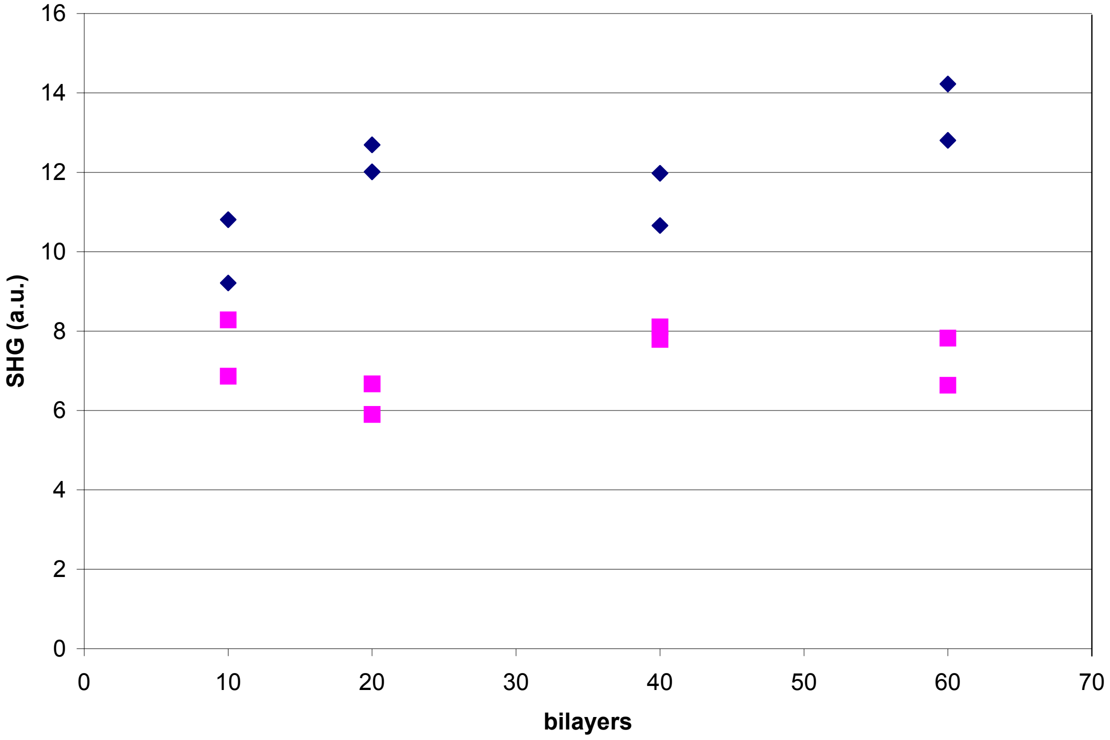

Figure 3.7.5. The SHG signal as function of bilayers for Ponceau S and Direct Yellow 8.

3.8 Conclusions

Multivalent monomer deposition is a possible alternative to the “classic” polyelectrolyte ISAM films for the production of thin layer NLO films. The SHG response for some multivalent monomer films is better than that of typical polyelectrolyte ISAM films for small number of bilayers. Growth of the SHG signal with increasing bilayers is observed for smaller number of bilayers, but there is not quadratic scaling of the SHG and even a decrease in SHG is observed in some cases at higher number of bilayers. Increase in chromophore alignment using β-cyclodextrins has been attempted with several combinations of chromophores and cyclodextrins. So far, only limited improvement has been observed for the Acid Blue 92 / β-cyclodextrin combination. It appears that the use of multivalent monomer deposition may have some potential, but much work remains to be done in order to achieve a uniform polar orientation throughout the film as large numbers of layers are deposited.

References

[1] G. Mao, Y. Tsao, M. Tirrell, H.T. Davis, *Langmuir* **11**, (1995) 942.

[2] K. Ariga, Y. Lvov, T. Kunitake, *J. Am. Chem. Soc.* **119**, (1997) 2224

[3] T.M. Leslie, R.N. De Martino, E.W. Choe, G. Khanarian, D. Hass, G. Nelson, J.B. Stamatoff, D.E. Stuetz, C.C.Teng, and Y.N. Yoon, *Mol. Cryst. Liq. Cryst.* **153** (1987) 451.

[4] Luna Innovations, 2851 Commerce street, Blacksburg, VA 24060, http://www.lunainnovations.com.

[5] J. Szejtli, *Chem. Rev.* **98** (1998) 1743.

[6] P. Fischer, M. Koetse, A. Laschewsky, E. Wischerhoff, L. Jullien, A. Persoons, T. Verbiest, *Macromol*. **33** (2000) 9471.

Chapter Four: Interface Dependence of Second Harmonic Generation in Thin Films Fabricated from Ionically Self-Assembled Monolayers.

In Chapter 2, it was shown that, for certain preparation conditions of ISAM films, the SHG increases quadratically with the number of bilayers for large number of bilayers, which is indicative of a bulk $\chi^{(2)}$ response with uniform polar order throughout the film[1-3]. Under other preparation conditions, ISAM films exhibit subquadratic or no growth of SHG with the number of bilayers. Interestingly, even for those films that exhibit quadratic scaling, for smaller number of bilayers the SHG is often much larger than expected[4] (see Figures 2.2.6 and 2.3.4). This suggests a strong interface SHG signal combined with bulk polar order. It is therefore desirable to understand this interface effect, and ideally, reproduce the strong interface effect throughout the bulk of the film. This chapter represents a study of this interface effect and the first attempts to recreate it in the bulk.

4.1 Separating the interface effect from the bulk contribution

There are two interfaces for every film, an air-film interface and a glass-film interface. For the first few bilayers, the SHG is much stronger than for the same number of bilayers in the bulk. This interface effect can be investigated with the use of optically inactive buffer layers. As cations, the following materials were used: PAH (introduced in chapter 2) and poly (diallyldimethylammonium chloride) (PDDA) and as an anionic material poly (acrylic acid) (PAA) was used. The chemical structures of PAH and PDDA are depicted in Figure 4.1.1. All materials were purchased from Aldrich Chemical Company Inc.

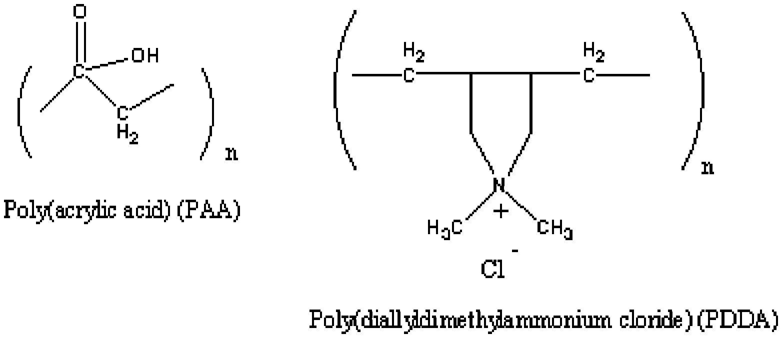

Figure 4.1.1. The chemical structures of PAA and PDDA.

Figure 4.1.2 shows the square root of the SHG signal as function of the number of PAH/PCBS bilayers with and without 10 bilayers PAH/PAA on top and bottom. The PAH/PAA bilayers were deposited to eliminate the effect of the glass-film and air-film interfaces on the PCBS NLO-active layers. The deposition scheme is depicted in Figure 4.1.3. We see that without the interface effects, the SHG is much weaker for a given number of bilayers. In this series, the square root of the SHG signal grows linearly with the number of bilayers from the start indicating that the interface effect can be removed by simply adding ten PAH/PAA buffer bilayers on both sides of the optically active film. Without the buffer layers, the SHG signal is dominated by the interface effect for the first few bilayers after which the quadratic behavior of the bulk contribution takes over. In the bulk region, the slope of the square root of the SHG signal as a function of bilayers is the same with and without buffer layers. This is to be expected if the second harmonic electric fields from the interfaces and the bulk film coherently combine to yield a total SHG intensity given by

$$I^{2\omega} \propto \left(A_{\text{int}} + \chi^{(2)} l\right)^2 \qquad (4.1.1)$$

where A_{int} is the electric field generated at the second harmonic frequency by the interface. The interface thus yields a non-zero intercept of square root of the SHG versus the number of bilayers but does not affect its slope.

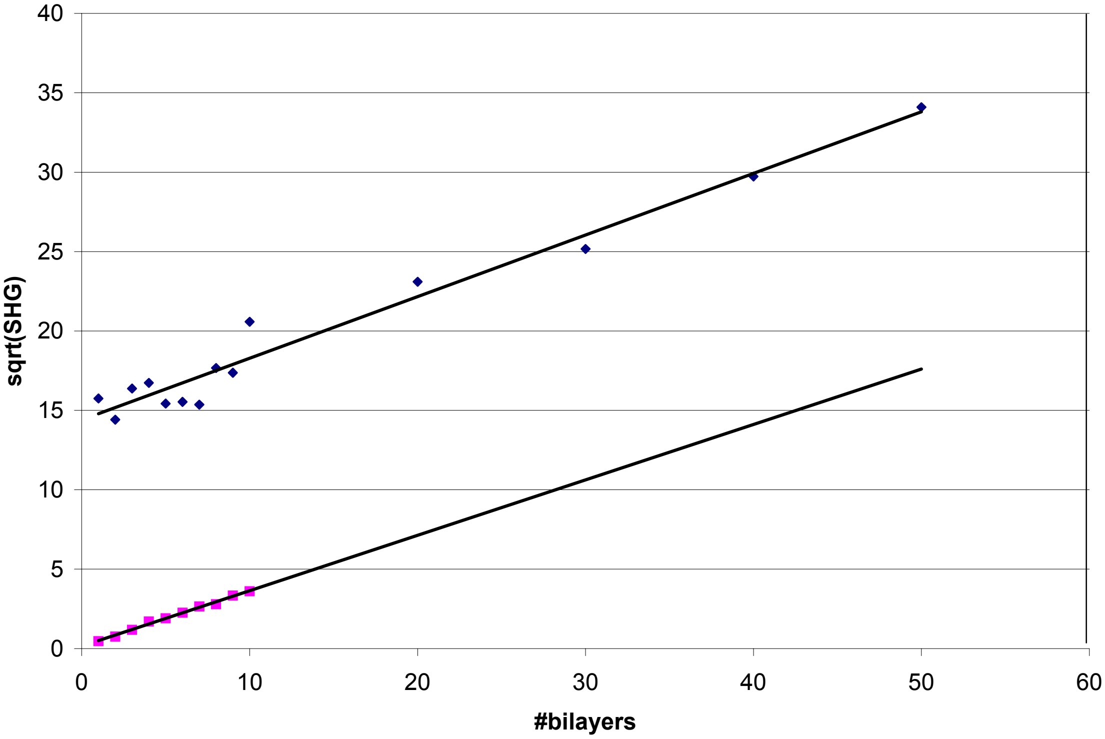

Figure 4.1.2. The square root of the SHG signal as a function of bilayers for a sample with (squares) and without (diamonds) ten bilayers of PAH/PAA above and below of the active PAH/PCBS bilayers.

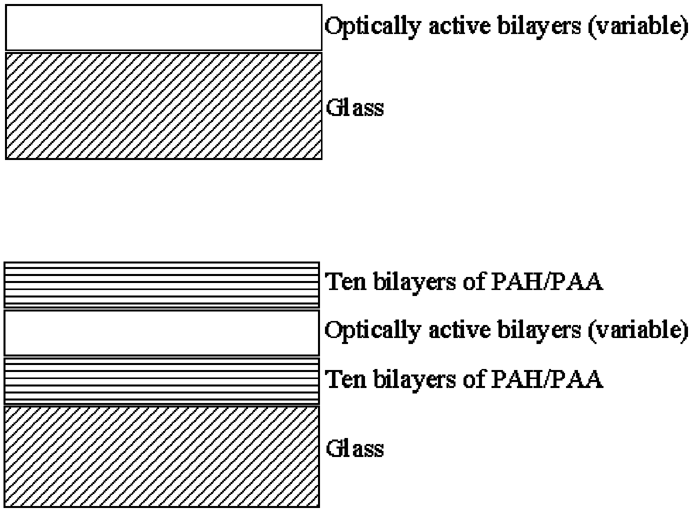

Figure 4.1.3. The deposition scheme used to demonstrate the interface effect. In one series, the PAH/PCBS bilayers are deposited directly on the glass substrate. In the other series, ten buffer bilayers were deposited before and after the PAH/PCBS bilayers.

Figure 4.1.4 shows the absorbance for the same series. This figure clearly shows that the absorbance of a PAH/PCBS sample is not influenced by the buffer bilayers. The same amount of PCBS is deposited in each bilayer in both cases. This indicates that the interface effect is not caused by a difference in bilayer thickness between bilayers at the interface and in the bulk.

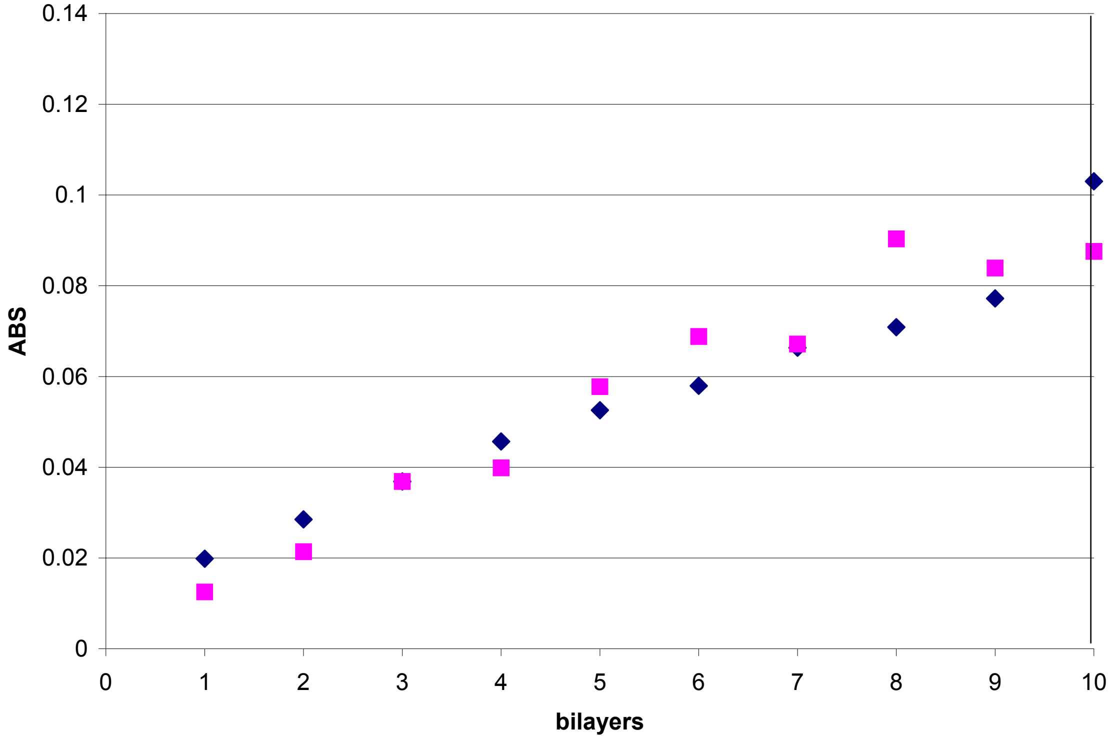

Figure 4.1.4. The absorbance at 360 nm as a function of bilayers for PAH/PCBS samples with (squares) and without (diamonds) ten PAH/PAA buffer bilayers above and below of the active PAH/PCBS bilayers. Notice that the presence of buffer layers does not influence the absorbance.

4.2 The interface effect of PCBS

Figure 4.2.1 shows the deposition scheme used to investigate the influence of the glass-film interface. In this series, all samples had one bilayer of PAH/PCBS with 10 bilayers of PAH/PAA on top to eliminate the contribution of the air-film interface effect. The samples differed in the number of PAH/PAA bilayers between the glass and optically active PAH/PCBS bilayer. The SHG signal as a function of the buffer bilayers between the glass substrate and the optically active PAH/PCBS bilayer is shown in Figure 4.2.2. It is evident that a PAH/PCBS bilayer bordering the glass interface produces a much stronger SHG signal than other PAH/PCBS bilayers. The glass-film interface effect has a significant effect only on the first bilayer deposited.

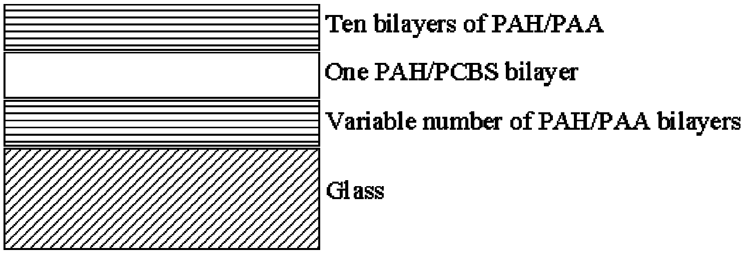

Figure 4.2.1. The deposition scheme used to investigate the influence of the glass interface. All samples had one optically active PAH/PCBS bilayer and were capped with ten PAH/PAA buffer layers. The difference between the samples was the number of buffer bilayers between the glass substrate and the PAH/PCBS bilayer.

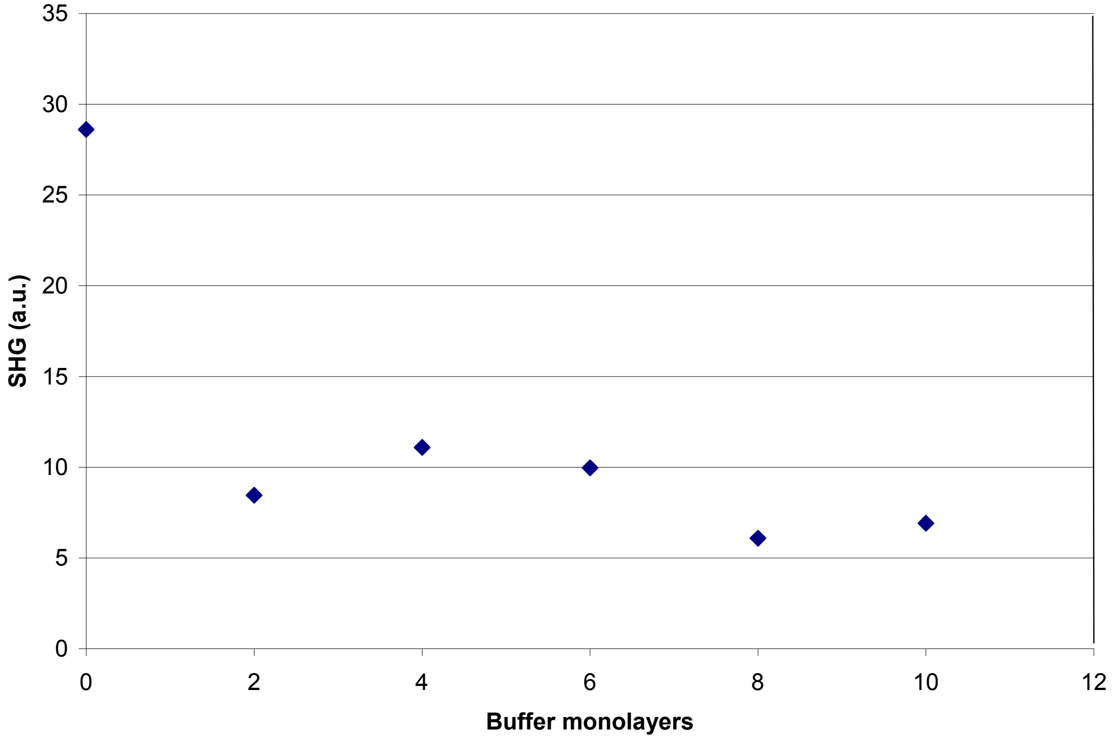

Figure 4.2.2. Influence of the glass interface. All samples have one PAH/PCBS bilayer and ten PAH/PAA bilayers on top. The samples differ in the number of buffer bilayers between the glass interface and the PAH/PCBS bilayer. It is clear that the glass interface significantly boosts the SHG response of a PAH/PCBS bilayer deposited on it.

Figure 4.2.3 shows the deposition scheme used to investigate the influence of the air-film interface. In these series, all samples had 10 bilayers of PAH/PAA followed by one bilayer of PAH/PCBS. The samples differed in how many monolayers were deposited afterward. For one series the top-layers were alternatively PAH and PAA, for the other series it was PDDA and PAA. The main differences between PDDA and PAH is that the interaction between PDDA and PCBS is purely electrostatic while PAH can also form a hydrogen bond with PCBS. In separate studies, we have found that PAH/PCBS films exhibit quadratic scaling of SHG intensity with the number of layers while PDDA/PCBS films exhibit only interface SHG with no additional SHG with increased layers. In both cases, the SHG signal decreases with increasing number of top layers deposited. The results are shown in Figure 4.2.4. The decay as a function of capping layers is larger for PDDA/PAA capping. In both cases, it is clear that the air-film interface effect reaches much deeper than the air-glass interface effect. This is probably due to the fact that the film is built layer by layer and that the film-air interface is “softer” than the glass-film interface due to the amorphous nature of the polymers. The chromophores are perpendicular to the PCBS polymer backbone, and therefore the chromophores generate the largest signal when the PCBS backbone is parallel to the surface. When the optically active PCBS polymer is deposited, not all of the polymer is adsorbed flat on the substrate. Parts of the polymer will be in loose loops and tails illustrated in Figure 4.2.5. However, these loops and tails will tend to flatten on the surface when the film is dried if no additional layers are deposited. When additional layers are deposited on top of the optically active polymer, these loops will be pulled up and incorporated in the new layers thereby reducing the signal as the chromophores are oriented more parallel to the surface. This will continue as layers are being deposited until the loops and tails can no longer reach the surface and interact with additional layers. Studies have indicated that the layers of ISAM films are highly interpenetrated with each layer extending roughly four bilayers above and below its central location,[5] consistent with the results of Figure 4.2.4. Beyond roughly four buffer bilayers, additional bilayers do not interact with (and reorder) the PAH/PCBS layer. The glass interface reaches only one bilayer deep, as the optically active polymers can not easily penetrate layers that are already deposited. When PCBS is capped with PDDA/PAA, the signal decays faster with each additional layer than in the case of capping with PAH/PAA. Therefore, the PDDA appears to have a larger disordering effect on PCBS.

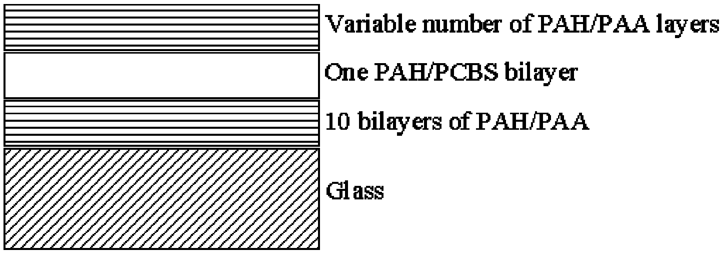

Figure 4.2.3. Deposition scheme used to investigate the air interface effect. Ten bilayers of PAH/PAA were deposited followed by one PAH/PCBS bilayer. The samples differ in the number of capping layers deposited on top of the PCBS layer.

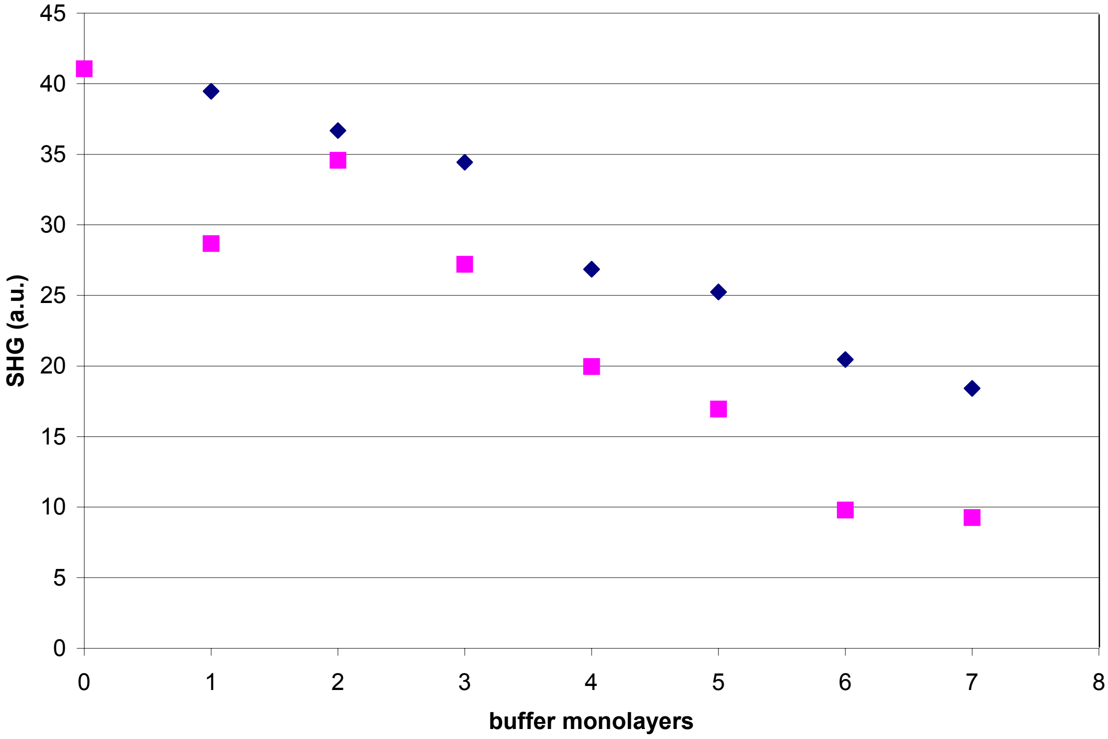

Figure 4.2.4. The influence of the air interface on the SHG signal. All samples had ten bilayers of PAH/PAA followed by one PAH/PCBS bilayer. The samples differed in the number of monolayers on top. The top layers were alternatively PAH and PAA for the diamond series and PDDA and PAA for the square series. Note that the air interface effect is spread out over multiple layers.

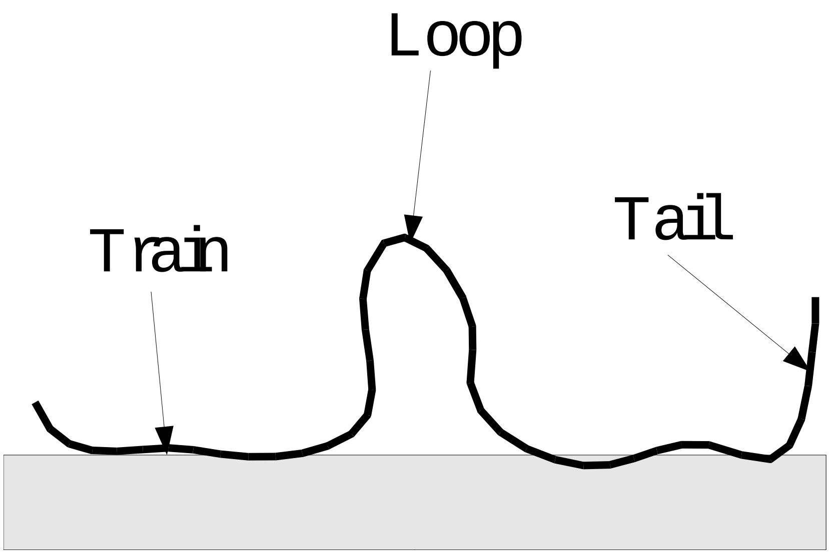

Figure 4.2.5. A deposited polymer chain schematic showing loop, train, and tail.

Since the square root of the SHG signal is proportional to $\chi^{(2)}$ one would expect that

$$A_{\text{glass-film}} + A_{\text{film-air}} + (l\chi^{(2)}{}_{\text{bulk}})_{\text{one bilayer}} = E_{\text{total}}. \qquad (4.2.1)$$

From Figure 4.1.2 we get the value of $(l\chi^{(2)}{}_{\text{bulk}})_{\text{one bilayer}} = 0.5$ (first sample of the second series). From Figures 4.2.2 and 4.2.4 we get the values of $[(A_{\text{glass-film}} + (l\chi^{(2)}{}_{\text{bulk}})_{\text{one bilayer}}]^2 = 28.6$, and $[(A_{\text{air-film}} + (l\chi^{(2)}{}_{\text{bulk}})_{\text{one bilayer}}]^2 = 41.1$ (in both cases first sample from the left). Finally, From figure 4.1.2 we get $E_{\text{total}} = 15.8$ (first sample from the left in the first series. Therefore we have

$$A_{\text{glass-film}} + A_{\text{film-air}} + \chi^{(2)}{}_{\text{bulk}} =$$

$$\sqrt{28.6} - 0.5 + \sqrt{41.1} - 0.5 + 0.5 =$$

$$5.35 + 6.41 - 0.5 = 11.26 = 71\% \text{ x } 15.8. \qquad (4.2.2)$$

It is conceivable that the glass-film and air-film interface effects influence each other and thus cause the discrepancy.

4.3 The interface effect of Acid Blue 92

The interface effects were also investigated for the PAH / Acid Blue 92 deposition scheme. Figure 4.3.1 shows the glass interface effect for Acid Blue 92. The samples were deposited as follows: first n bilayers of (PAH/PAA), where n is 0, 1, 2…, then one bilayer of PAH / Acid Blue 92, and finally 10 bilayers of PAH / PAA to eliminate the air interface effect. This is the same deposition scheme shown in Figure 4.2.1 except the PCBS is replaced by Acid Blue 92. The glass interface effect of Acid Blue 92 is similar to that of PCBS, the signal is much stronger if the PAH / Acid Blue 92 bilayer is deposited directly on the glass slide and drops off rapidly with the incorporation of buffer layers. The main difference is that the interface effect is even stronger in Acid Blue 92 than in PCBS. In fact, the interface effect is stronger in Acid Blue 92 than in any other material we have encountered so far.

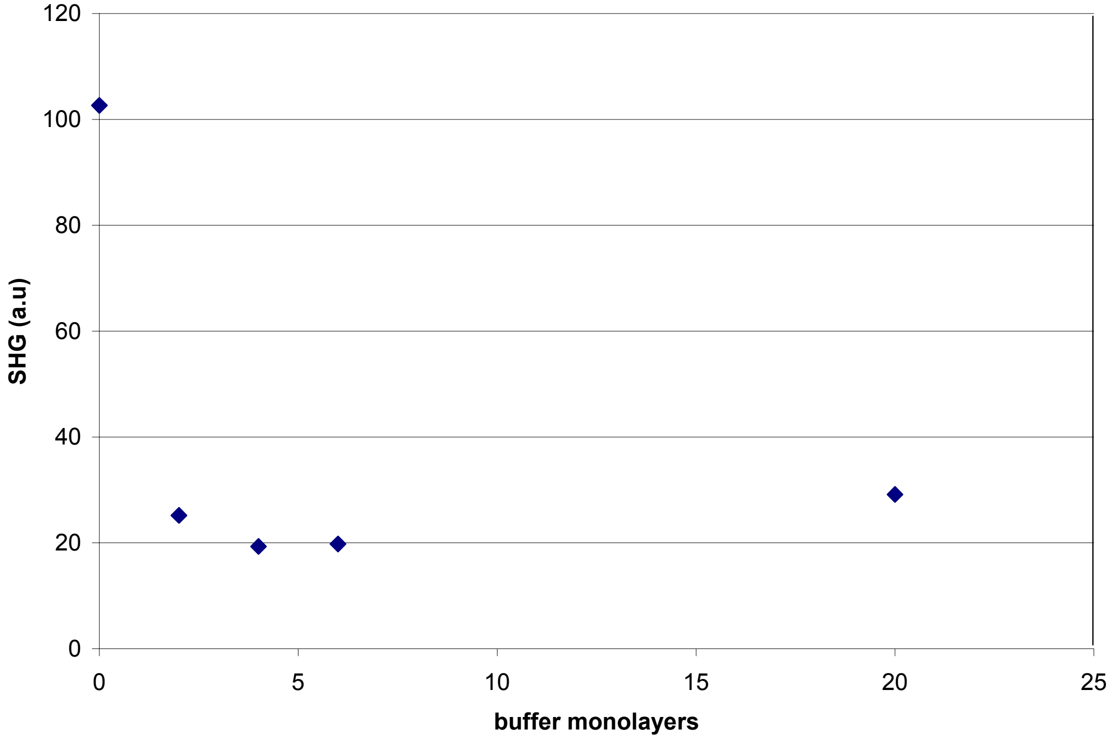

Figure 4.3.1. The influence of the glass interface effect on the SHG response of Acid Blue 92. All samples had one PAH / Acid Blue 92 bilayer and ten PAH / PAA bilayers on top. Depicted is SHG as function of the number of monolayers (alternately PAH and PAA) between the PAH / Acid Blue 92 bilayer and the glass interface.

The influence of the air interface effect on the SHG response of Acid Blue 92 is shown in Figure 4.3.2. All samples were first covered with 10 PAH / PAA bilayers to eliminate the influence of the glass interface followed by one PAH / Acid Blue 92 bilayer. This is the same deposition scheme used to investigate the air interface effect in PCBS as shown in Figure 4.2.3. In the figure, the SHG response is plotted against the number of top bilayers consisting of PAH / PAA. We see that the decay of the SHG signal with increasing top layers is much faster in Acid Blue 92 than in the case of PCBS. This is most likely because Acid Blue 92 is a monomer that cannot interpenetrate with other layers. Since it cannot exhibit tails and loops that can reach through many top layers, the final SHG value is reached earlier.

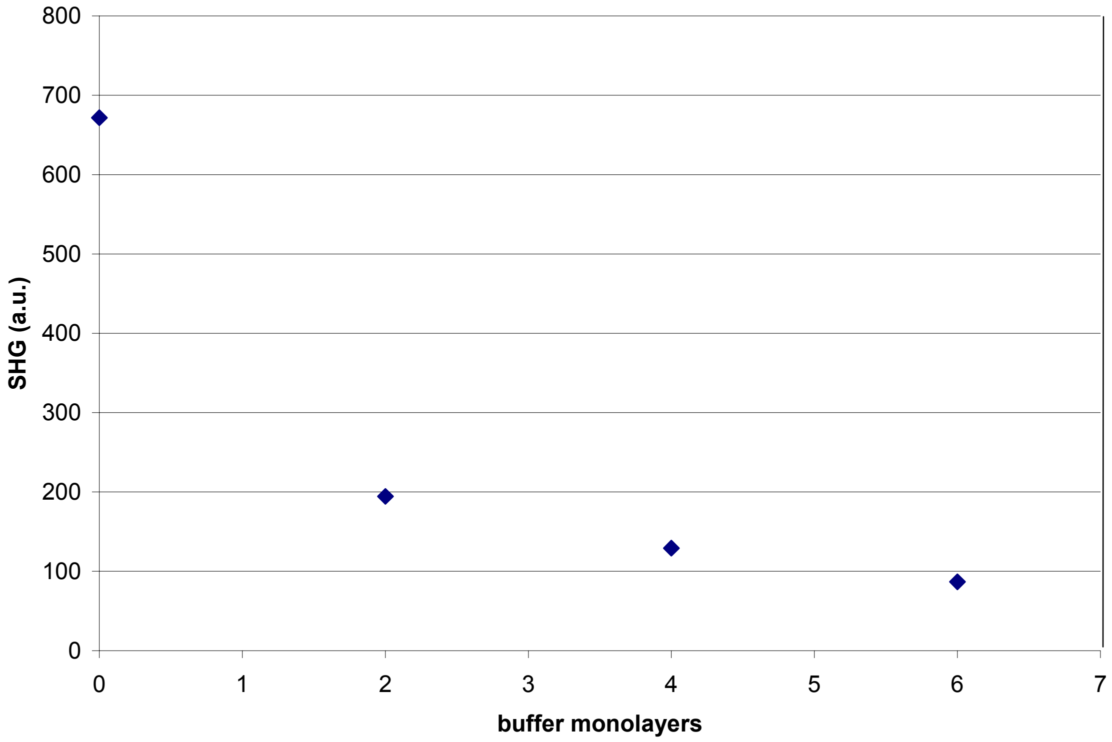

Figure 4.3.2. The influence of the air interface on the SHG response for Acid Blue 92. All samples were covered with 10 PAH / PAA bilayers and one PAH / Acid Blue 92 bilayer. Depicted is the SHG response as a function of buffer monolayers on top (alternately PAH / PAA).

Also note that the difference between the final SHG value and the SHG signal from an uncapped sample is larger (percentage wise) in the case of Acid Blue 92 than in PCBS.

This could be due to two things: either the randomization due to the top layers is larger in the case of Acid Blue 92 or perhaps the PAA polymer replaces the Acid Blue 92 which becomes redissolved in the solution. The latter is a serious possibility since Acid Blue 92 is connected to the film with only two charge groups. Table 4.2.1 shows the peak absorbance values for the samples discussed above. As there is only one Acid Blue 92 layer the values are extremely weak and therefore the noise is relatively large. It is clear however that the absorbance, and therefore the amount of Acid Blue 92 deposited, does not show a significant decay with larger number of top layers. Therefore the decay of the SHG signal with increasing number of top layers is due to randomization. It is not surprising that the randomization of chromophores is larger in Acid Blue 92 than in PCBS as the chromophores in PCBS are bound to a polymer chain and it is much harder to move a chain around than it is to simply deflect the orientation of a monomer.

number of top layers	peak absorbance value
0	0.00992
2	0.00945
4	0.00411
6	0.01382

Table 4.3.1. The peak absorbance values as a function of top bilayers of PAH / PAA for samples that already contain ten PAH / PAA bilayers and one PAH / Acid Blue 92 bilayer.

4.4 The interface effect of Procion Red

Figure 4.4.1 shows the glass interface effect for Procion Red. The deposition scheme was the same as for PCBS and Acid Blue 92. First n PAH / PAA bilayers were deposited, followed by one PAH / Procion Red bilayer, and finally ten PAH / PAA layers to eliminate the air interface effect. As before, n represents an integer number. The deposition times were 15 minutes for Procion Red and 3 minutes for PAH and PAA. The pH was 10.0 for Procion Red and 7.0 for PAH and PAA. In light of the results for PCBS and Acid Blue 92, the glass interface effect of Procion Red is unsurprising. The signal is much stronger if the first PAH / Procion Red bilayer is deposited directly on the glass substrate and much weaker for all the other samples.

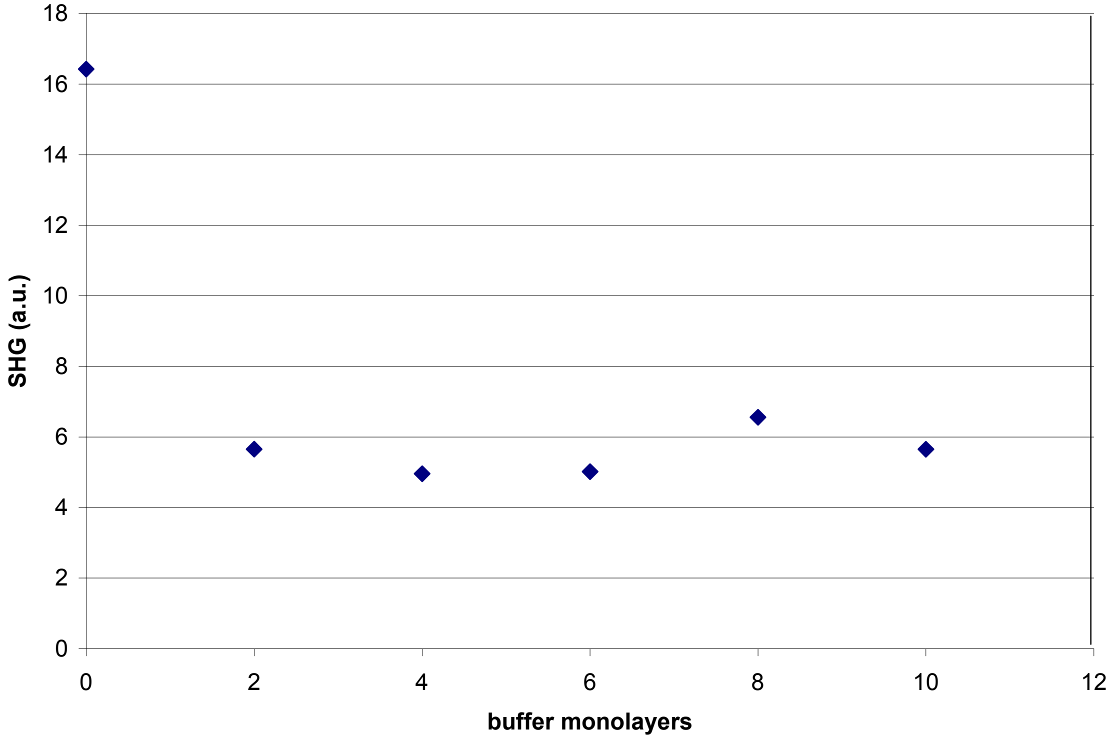

Figure 4.4.1. Glass interface effect of Procion Red. All samples consisted of one PAH / Procion Red bilayer and ten PAH / PAA bilayers on top. Depicted is the SHG signal as function of the number of buffer monolayers between Procion Red and the glass interface.

The air interface effect is shown in Figure 4.4.2. All samples had first ten PAH / PAA bilayers deposited followed by one PAH / Procion Red bilayer. Finally, an integer number of monolayers were deposited on top of the Procion Red layer. The capping layers were alternatively PAH and PAA. In the figure, the SHG signal is plotted against the number of top layers. Similar to Acid Blue 92, there is a fast drop in signal with increasing top layers. Both Acid Blue 92 and Procion Red are monomers but with different deposition techniques. The fact that both monomers show a rapid decay in SHG with increasing top layers supports the theory that the slow decrease in SHG signal for PCBS under similar circumstances is caused by the loops and tails inherent in polymer deposition. Although both Acid Blue 92 and Procion Red show a rapid decline when top layers are added, the extent of the decay is much larger for Acid Blue 92. This is most likely due to the fact that the covalent bond between Procion Red and PAH is much stronger than the electrostatic bond between Acid Blue 92 and PAH and the Procion Red molecule likely can not be reoriented as much.

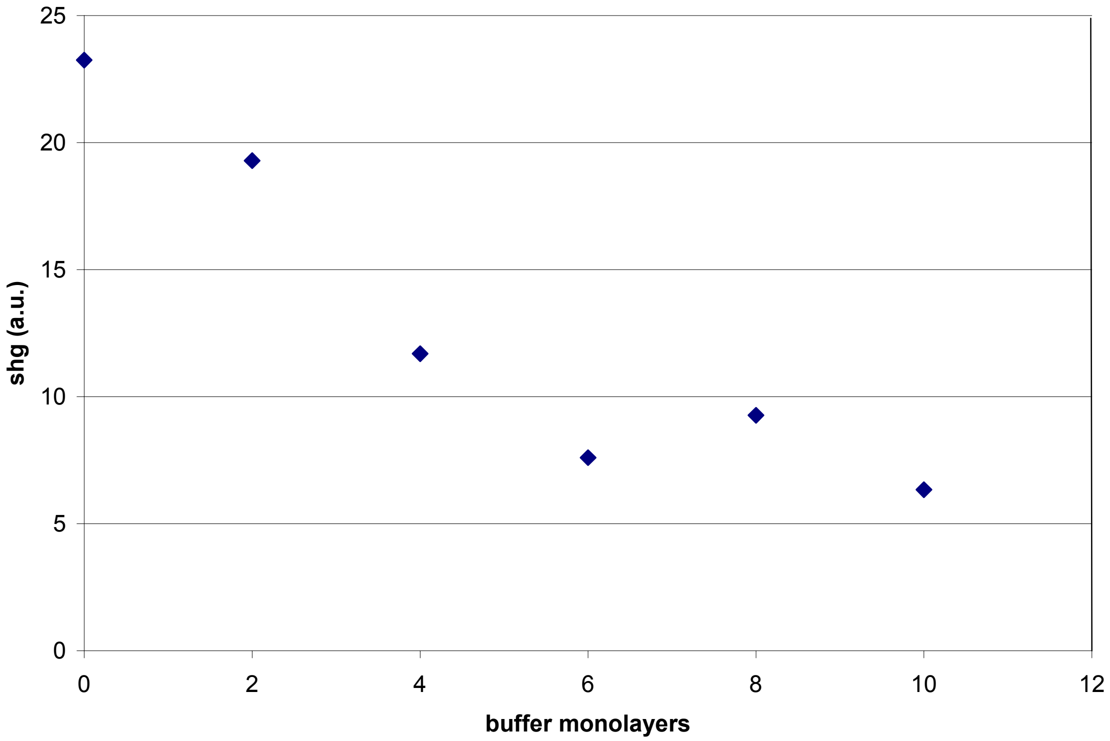

Figure 4.4.2. Air interface effect of Procion Red. All samples consisted of ten PAH / PAA bilayers followed by one PAH / Procion Red bilayer. Depicted is the SHG signal as function of the number of buffer monolayers on top of the Procion Red.

4.5 Attempts to recreate the interface effect in the bulk

It is clear from the previous sections that for every material and deposition method we have tested, the nonlinear optical response of bilayers at the interface is much larger than the contribution from bilayers in the bulk. This section will describe the first attempts to recreate the interface effect in the bulk. In these attempts, we have tried to create hard interfaces using laponite, colloidal silica, and colloidal gold.

Laponite

In recent years, the interest in organic-ceramic nanocomposite films has increased as these films possess unique physical properties.[6] Various multilayer assembly techniques, such as Langmuir Blodgett and ISAM, have been used in these organic-ceramic films studies.[7,8] Van Duffel *et al.* investigated the SHG response of glass/clay/PDDA/NAMO films.[9] NAMO stands for 4-{4-{N-allyl-N-methylamino]phenylazo}benzenesulfonic acid, sodium salt. The clays used were laponite, smectite, and hectorite. From these films, the ones incorporating laponite showed the largest response. Unfortunately, no comparison with a film without clay (i.e. glass/PDDA/NAMO) was shown. Also, no attempt was made to form structures with multiple quad layers.

Laponite is an entirely synthetic product and has a layer structure, which in dispersion in water is in the form of disc-shaped crystals. The outer rim is positively charged while the rest of the molecule is negatively charged with typical dimensions as shown in Figure 4.5.1. The laponite was purchased from Southern Clay Products. It was hoped that incorporation of a hard, impenetrable, flat layer would have a similar effect to the glass-film interface.

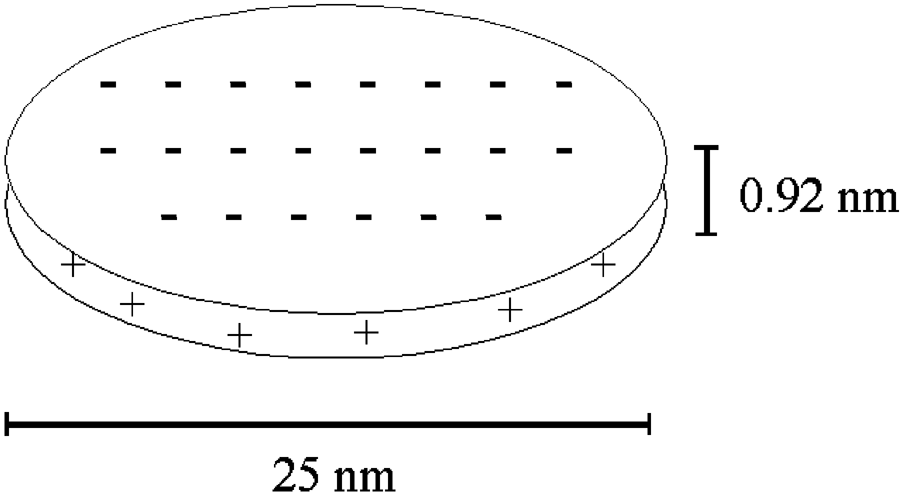

Figure 4.5.1 Dimensions of a laponite crystal.

Figure 4.5.2 shows the SHG signal for one PAH / PCBS bilayer, one PAH / laponite / PAH / PCBS quad layer, ten PAH / PCBS bilayers, and ten / PAH / laponite / PAH / PCBS quad layers. All samples were sandwiched between 10 PAH / PAA bilayers to eliminate the glass and air interface effects. No salt was added to the solutions. The concentration for the PAA, PAH, PCBS, and Acid Blue 92 was 10 mMol. The pH for these solutions was 7.0. The laponite concentration was 0.1 % and the pH was 10.0. It is evident that the inclusion of laponite does not contribute to the SHG signal. Van Duffel *et al.* showed that the ordering of laponite plates is extremely dependent on the magnitude of the PDDA concentration in PDDA/laponite films.[10] It is therefore possible that lowering the PAH concentration in our films will have a positive effect.

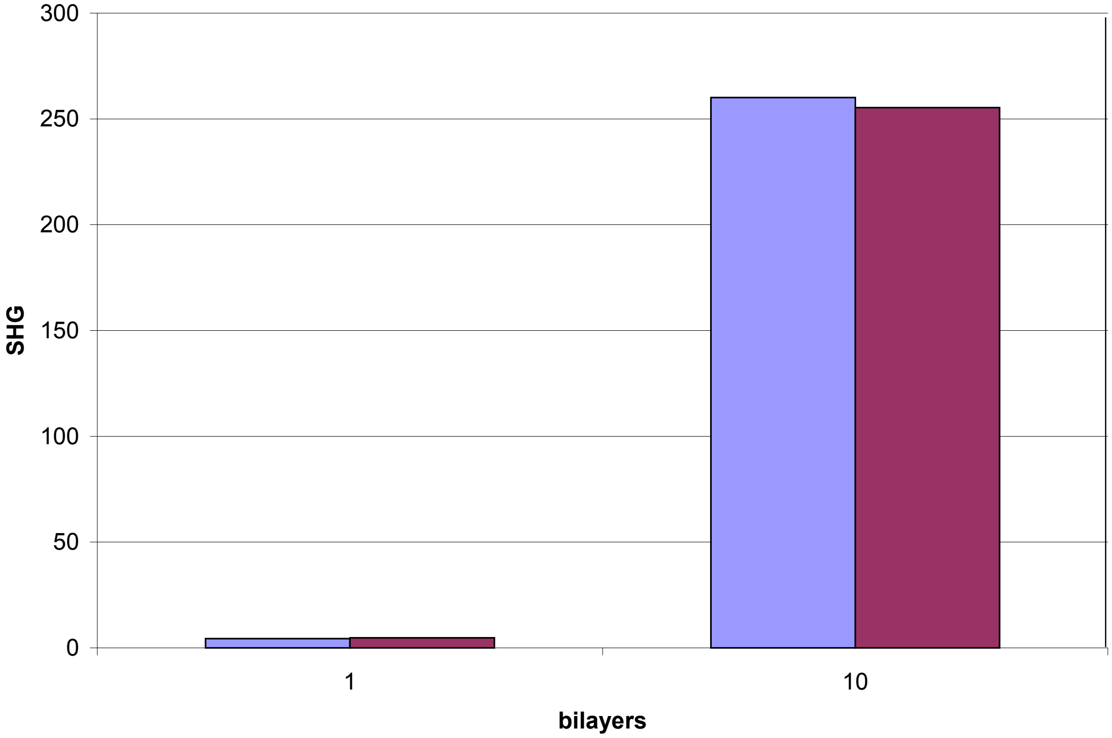

Figure 4.5.2. SHG for ten PAH / PCBS bilayers and ten PAH / laponite / PAH / PCBS quad layers. Both samples has ten PAH / PAA bilayers on top and bottom of the optically active film.

Figure 4.5.3 shows the results of laponite / Acid Blue 92 combinations. The first sample had PAH /Acid Blue 92 directly deposited on glass followed by ten bilayers on top to eliminate the air-film interface effect. The second (from the left) had 10 buffer PAH / PAA bilayers deposited below and above one PAH / Acid Blue 92 bilayer. As before the addition of buffer layer largely reduces the SHG signal. The sample denoted as “pdda” is the same as “10-buffer” except the PAH is replaced by PDDA. Replacing the PAH with PDDA had no effect. The sample denoted with laponite has 10 PAH /PAA bilayers deposited above and below one quad-layer of PAH/Laponite/PAH/Acid Blue 92. The addition of laponite slightly restores the signal lost due to the buffer layers. The difference is very small and does not justify the inclusion of Laponite, considering that the PAH / Laponite layer substitutes for of a PAH / Acid Blue 92 layer if one were to make multilayer films of this sort.

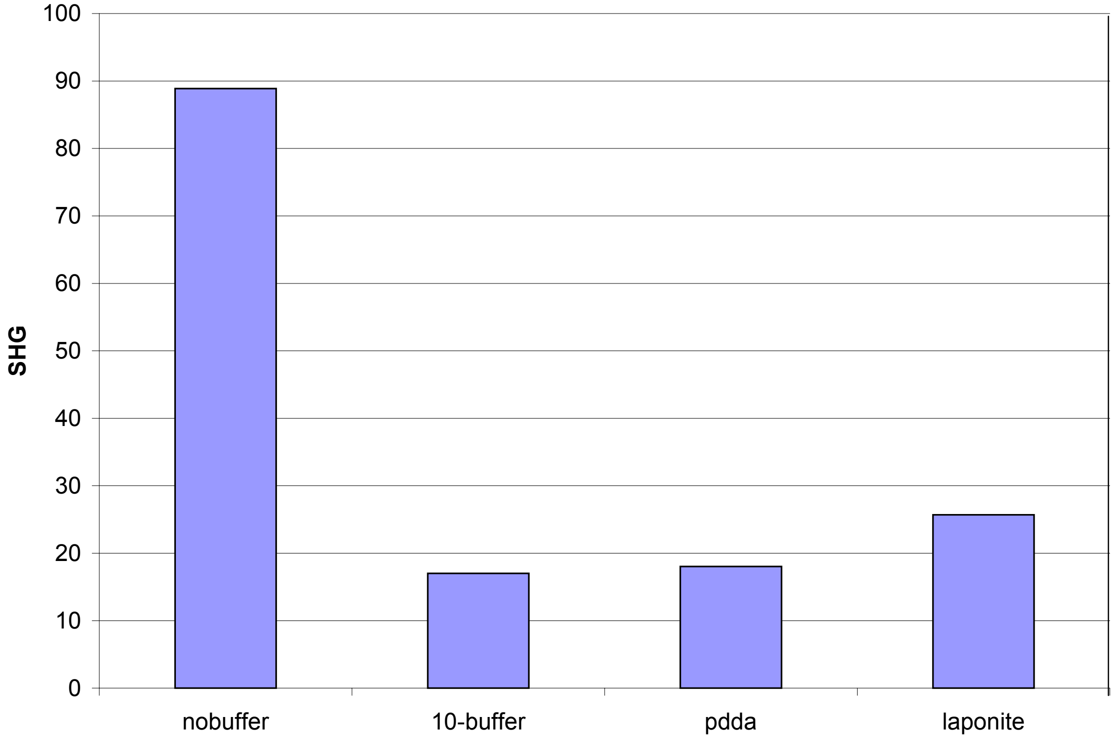

Figure 4.5.3. The SHG signal for different one bilayer PAH / Acid Blue 92 samples.

One sample had PAH /Acid Blue 92 directly deposited on glass (nobuffer) followed by 10 buffer bilayers of PAH / PAA on top. One sample had 10 buffer PAH / PAA bilayers deposited below and above one PAH / Acid Blue 92 bilayer(10-buffer). The sample denoted as “pdda” is the same as 10-buffer except the PAH is replaced by PDDA. The sample denoted with “laponite” has 10 PAH /PAA bilayers deposited above and below one quad-layer of PAH/Laponite/PAH/Acid Blue 92.

Ludox colloidal silica

The experiments in the previous section were repeated with colloidal silica particles instead of laponite. The colloidal silica consist of spheres with a diameter of 12 nm and were obtained from Ludox. Lvov *et al.* showed that ISAM films with polymers (PDDA) and colloid silica (45 nm) resulted in homogeneous films with a surface coverage of 40%.[11] Correcting for the shape factor (0.63 for hexagonal packing of spherical particles) leads to a surface coverage of approximately 70%. Figure 4.5.4 shows the SHG signal for one PAH / PCBS bilayer, one PAH / silica / PAH / PCBS quad layer, ten PAH / PCBS bilayers, and 10 / PAH / silica / PAH / PCBS quad layers. All samples were sandwiched between 10 PAH / PAA bilayers to eliminate the glass and air interface effects. It is evident that the inclusion of colloidal silica does not significantly contribute to the SHG signal.

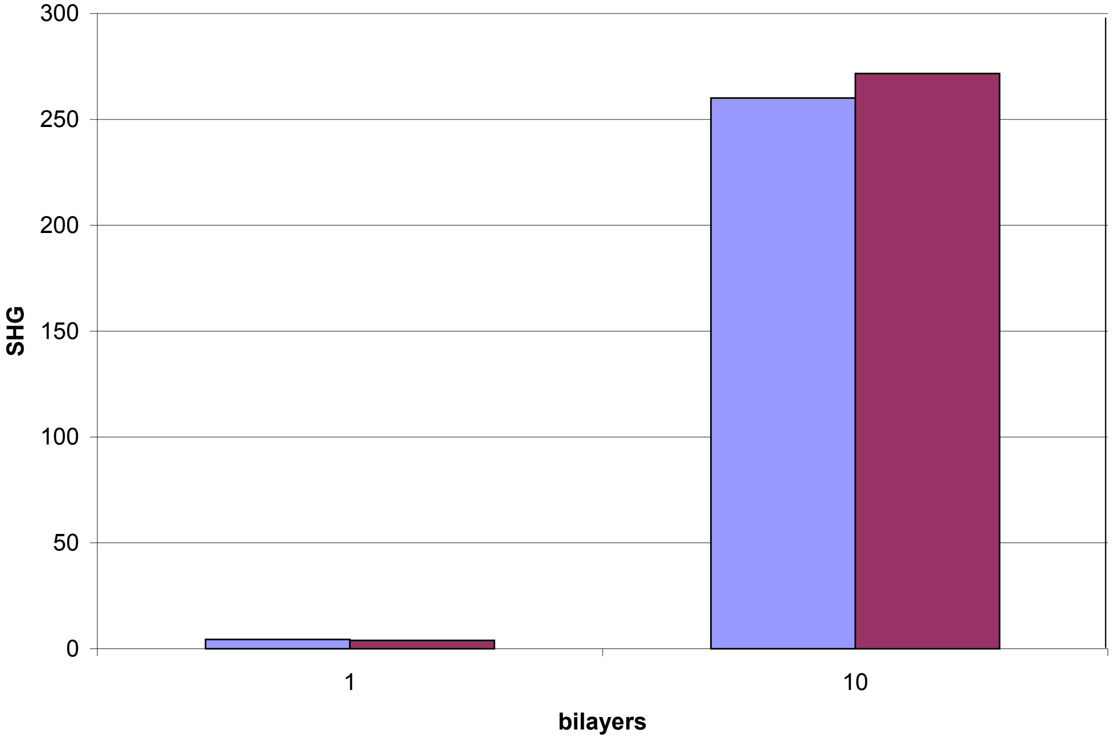

Figure 4.5.4. The SHG for ten PAH / PCBS bilayers and ten PAH / silica / PAH / PCBS quad layers.

The SHG for one bilayer of PAH / Acid Blue 92 and one PAH / silica / PAH / Acid Blue 92 quad layer (again sandwiched between ten PAH / PAA bilayers) is shown in Figure 4.5.5. This figure also shows one PAH / Acid Blue 92 bilayer directly on the glass slide with only ten PAH / PAA bilayers to remove the air interface effect. It is clear that in this case the silica does partly restore the glass interface effect. Unfortunately, this does not scale with increasing layers. An attempt to create ten quad layer films PAH / silica / PAH / Acid Blue 92 resulted in extremely inhomogeneous films. As Acid Blue 92 is only connected to the polymer substrate through two charges, some of the Acid Blue desorbs during immersion in the oppositely charged PAH solution resulting in slight discoloration of the PAH solution in the growth of PAH / Acid Blue 92 films. This was also the case during the fabrication of PAH / Silica / PAH / Acid Blue 92 films. However, the silica solution, which has the same sign of charge as Acid Blue 92, turned dark blue indicating that large amounts of the Acid Blue desorbed in this solution. It is hypothesized that the silica spheres connect to the PAH polymer and by thermal motion rip the polymer off the substrate taking the Acid Blue with it. This results in a very inhomogeneous film and discoloration of the silica solution as is observed. No such discoloration took place in the creation of PAH / silica / PAH / PCBS quad layer films. This is explained by the fact that the polymer / polymer films are structurally much more sturdy than the polymer / monomer films as expected.

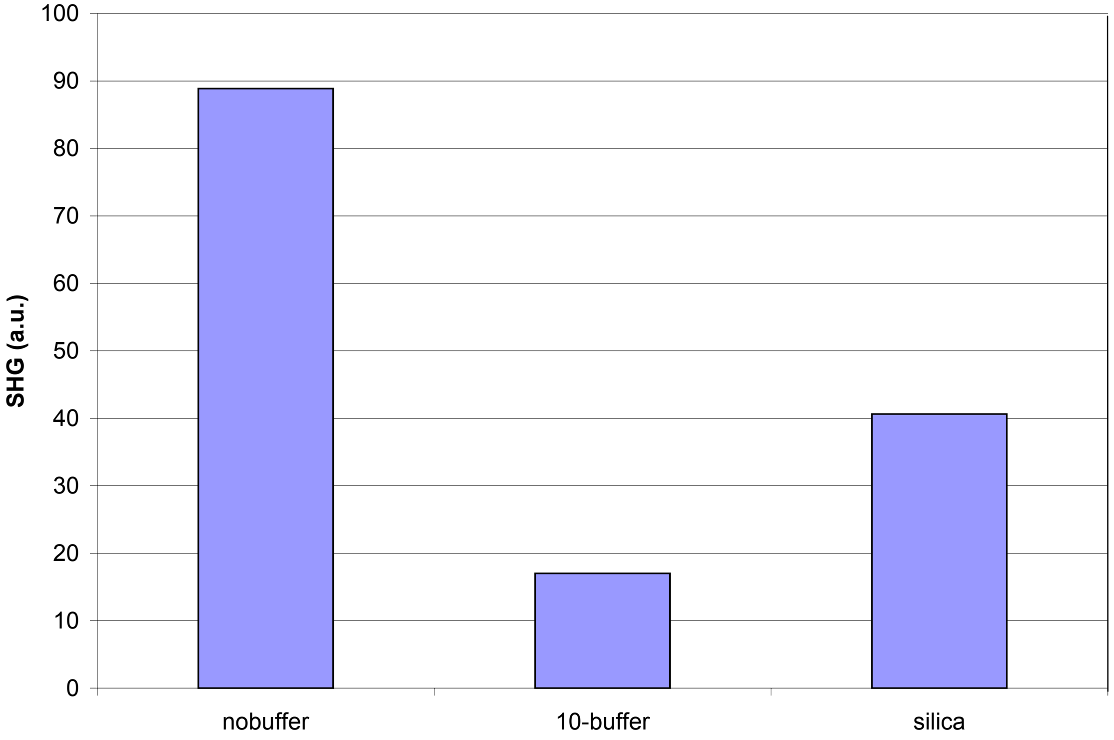

Figure 4.5.5. The SHG for different Acid Blue 92 samples. The sample denoted with "nobuffer" represents a PAH / Acid Blue 92 directly deposited on the glass slide with 10 PAH / PAA buffer bilayers on top. The sample denoted "10-buffer" has 10 buffer bilayers above and below the PAH / Acid Blue 92 bilayer. The sample with the name "silica" is the same as 10-buffer except the PAH / Acid blue 92 bilayer is replaced with a PAH / Silica / PAH / Acid Blue 92.

Colloidal gold

As a variation on colloidal silica, colloidal gold particles were used in a PAH/Au/PCBS triple layer construction. In this construction, the positive charges of PAH create negative image charges in the colloid gold particle. As the gold particle is electrically neutral, this results in a positive charge on the other side on which the PCBS deposits. Schmitt *et al.* incorporated negatively charged gold composite particles in ISAM films but no attempt was made to test for NLO activity.[12] The diameter of the colloidal gold particles used here was 5 nm. The pH was 7.0 and the concentration was 0.001 %. The colloidal gold was purchased from Sigma Aldrich.

Figure 4.5.6 shows the results of the PAH/Au/PCBS construction compared with the basic PAH/PCBS bilayer. Clearly, the inclusion of gold does not benefit the SHG response. Absorbance measurements show no evidence of the gold particles in the film. The lack of success in depositing the gold particles and perhaps restoring the interface effect in the bulk with colloid gold and colloid silica could be due to the chemicals included in the solution by the manufacturer to stabilize the solution. These chemicals could possibly screen the gold particles.

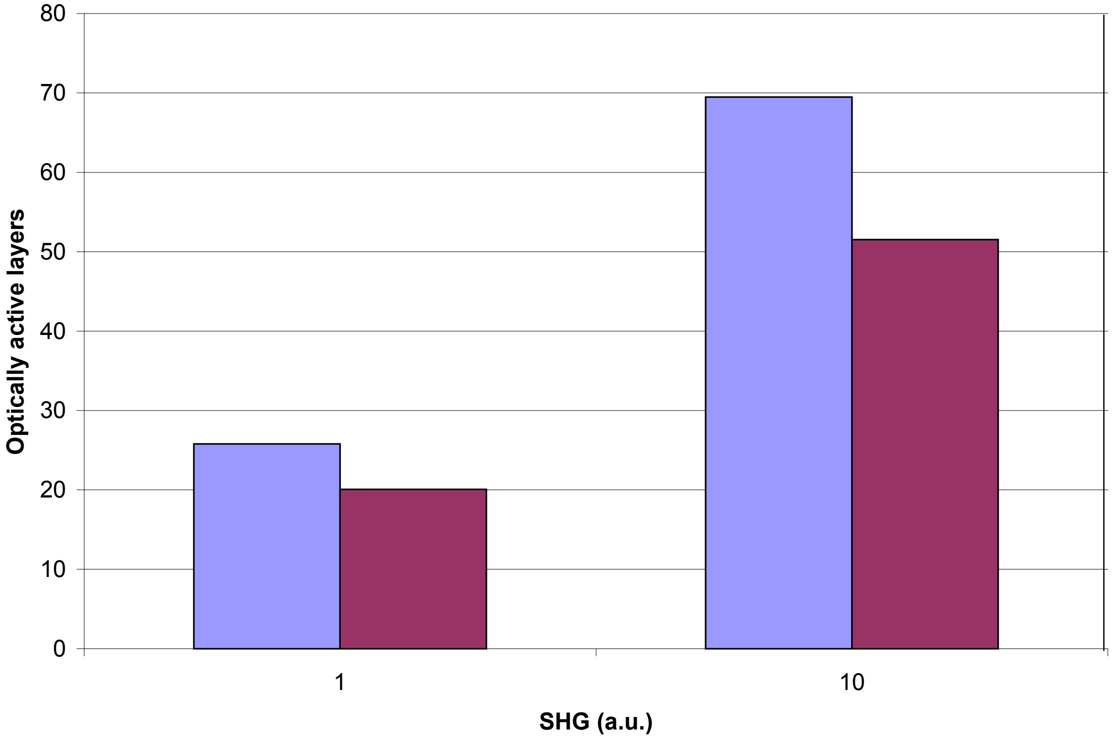

Figure 4.5.6. The SHG signal for one and ten repeat units of PAH / PCBS (blue) and PAH/Colloid Gold/PCBS (red) structures.

Conclusions

The square root of the SHG response of ISAM films with NLO active materials scales linearly with the number of bilayers for larger number of bilayers. For smaller number of bilayers, the response is much larger than expected due to large contributions from the interfaces. The interface effect can be separated into an air-film and a glass-film interface effect. For all materials tested the glass-film interface effect extends only one bilayer deep. The air-interface effect decays slowly with increasing top layers if the optically active material is a polymer but rapidly if it is a monomer. So far attempts to recreate the interface effect in the bulk have been unsuccesful.

References

[1] J.R. Heflin, Y. Liu, C. Figura, D. Marciu, R. Claus, *Proc. SPIE* **3147** (1997) 10.

[2] J.R. Heflin, Y. Liu, C. Figura, D. Marciu, R. Claus, *Appl. Phys. Let.* **74** (1999) 495.

[3] J.R. Heflin, Y. Liu, C. Figura, D. Marciu, R. Claus, *Organic Thin Films for Photonics Applications* **14** (1997) 78.

[4] C. Figura, *"Second Order Nonlinear Optics In Ionically Self-Assembled thin Films", Ph.D. thesis, Department of Physics, Virginia Polytechnic Institute and State University* (1999).

[5] G. Decher, *Science* **277** (1997) 1232.

[6] R. Vaia, H. Ishii, E. Giannelis, *Chem. Mater.* **5** (1993) 1694.

[7] N. Kotov, F. meldrum, J. Fendler, E. Tombacz, i. Dekany, *Langmuir* **10** (1994) 3797.

[8] E.R. Kleinfeld, G.S. Ferguson, *Science* **265** (1994) 370.

[9] B. Van Duffel, T. Verbiest, S. Van Elshocht, A. Persoons, F.C. De schryver, and R.A. Schoonheydt, *Langmuir* **17** (2001) 1243.

[10] B. Van Duffel, R.A. Schoonheydt, C.P.M. Grim, F.C. De schryver, *langmuir* **15** (1999) 7520.

[11] Y. Lvov, K. Ariga, M. Onda, I. Ichnose, and T. Kunitake. *Langmuir* **13** (1997) 6195.

[12] J. Schmitt, P. Machtle, D. Eck, H. Mohwald, and A. Helm, *Langmuir* **15** (1999) 3256.

Chapter Five: In Situ SHG Measurements of the Growth of Nonlinear Optical ISAM Films.

The interest in devices, sensors, special coatings, etc. has been one of the driving forces behind the ISAM technique in the past few years. This simple and effective fabrication method has been used to deposit a variety of thin films including inorganic[1], dyes[2], conducting polymers[3], proteins[4], DNA[5], and particles[6]. A deeper understanding of deposition kinetics is essential for further optimization of the fabrication procedures. Several theories have been proposed to model the adsorption of polyelectrolytes on solid surfaces[7,8]. The theoretical description of the deposition process is a daunting task due to the complexity of interactions and the non-equilibrium nature of the self-assembled film during formation[9-11]. It is shown here that polyelectrolyte deposition is much faster than film structure equilibration[12].

Unfortunately, there is little experimental information about the adsorption process itself due to the difficulty of tracking the interfacial process as each layer is grown. Only a few techniques can give sufficient time and mass resolution to investigate the adsorption process. The techniques that have been used include quartz crystal microbalance technique (QCM), surface plasmon spectroscopy (SPS), and Fourier transform infrared spectroscopy (FTIR)[13,14]. QCM is sensitive enough to mass changes that it can resolve the adsorption of monolayers. It is possible however that the use of QCM itself changes the adsorption and desorption kinetics. SPS is limited to metal substrates and FTIR provides a limited time resolution (≈40s)[15].

Second harmonic generation (SHG) has been successfully utilized to analyze surface properties, gas/liquid, and liquid/solid interfaces due to the intrinsic noncentrosymmetry of the interfaces.[16,17] As discussed in the preceding chapters, our group, as well as others, has been researching the use of the ISAM technique to create thin films with a large $\chi^{(2)}$ NLO response. The ease of fabrication and the excellent temporal and thermal stability of the $\chi^{(2)}$ response of ISAM films make them quite appealing for future device applications. In this chapter, the situation is somewhat reversed as SHG is used as a valuable tool to study the formation dynamics of multilayer ISAM films with high time resolution.

5.1 In Situ SHG Apparatus

The measurements were done using a standard SHG setup using a nanosecond pulsewidth Q-switched Nd:YAG laser. The fundamental wavelength is 1064 nm. The laser beam is p-polarized and weakly focused on the sample. Typical values for beam radius and pulse energy values were 100 μm and 1 mJ/pulse respectively. The SHG data were averaged over 10 shots (1 second) and 100 shot for *in situ* and *ex situ* measurements, respectively. The sample holder was constructed such that the sample could be immersed into a solution without moving the sample with respect to the incoming laser beam (Figure 5.1.1). Although the position of the sample is fixed with respect to the laser, the sample can be rotated about the axis that varies the angle of incidence of the fundamental beam. This arrangement enabled us to measure the SHG signal while the layer is growing and also as the sample is removed from the solution between deposition steps.

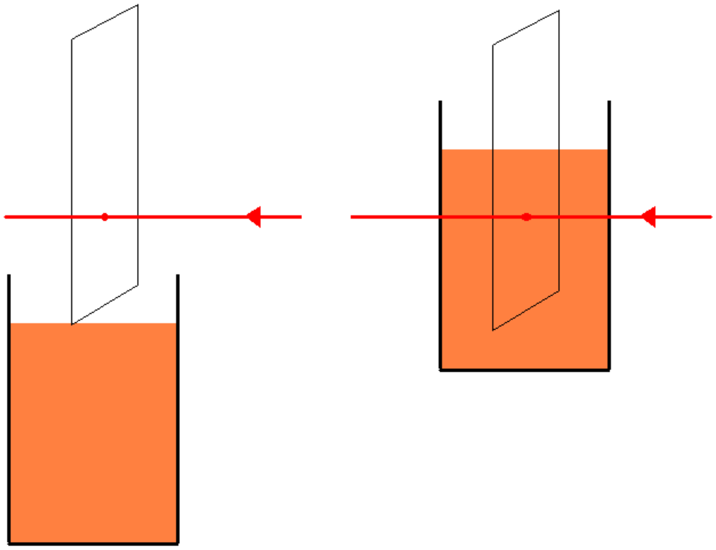

Figure 5.1.1. *In situ* deposition method. The sample is held fixed in position while the beaker with solution is moved. Therefore the beam is focused on the same spot for the complete measurement sequence.

A typical *in situ* measurement is depicted in Figure 5.1.2. A substrate with one monolayer of PAH was immersed in PCBS solution. The concentration was 1 mMol and the pH was 7.0. No salt was added. The data shows a rapid increase in SHG signal in the first minute followed by a slower increase. Comparison with *ex situ* absorption measurements shows that the deposition of a PCBS monolayer is essentially complete in less than a minute, which corresponds to the initial rapid increase in SHG signal. After deposition, the outer layer is likely to penetrate into the previous layers, and reorganize to an energetically more favorable conformation. The slower secondary increase in SHG signal is interpreted as this reorganization in the film.

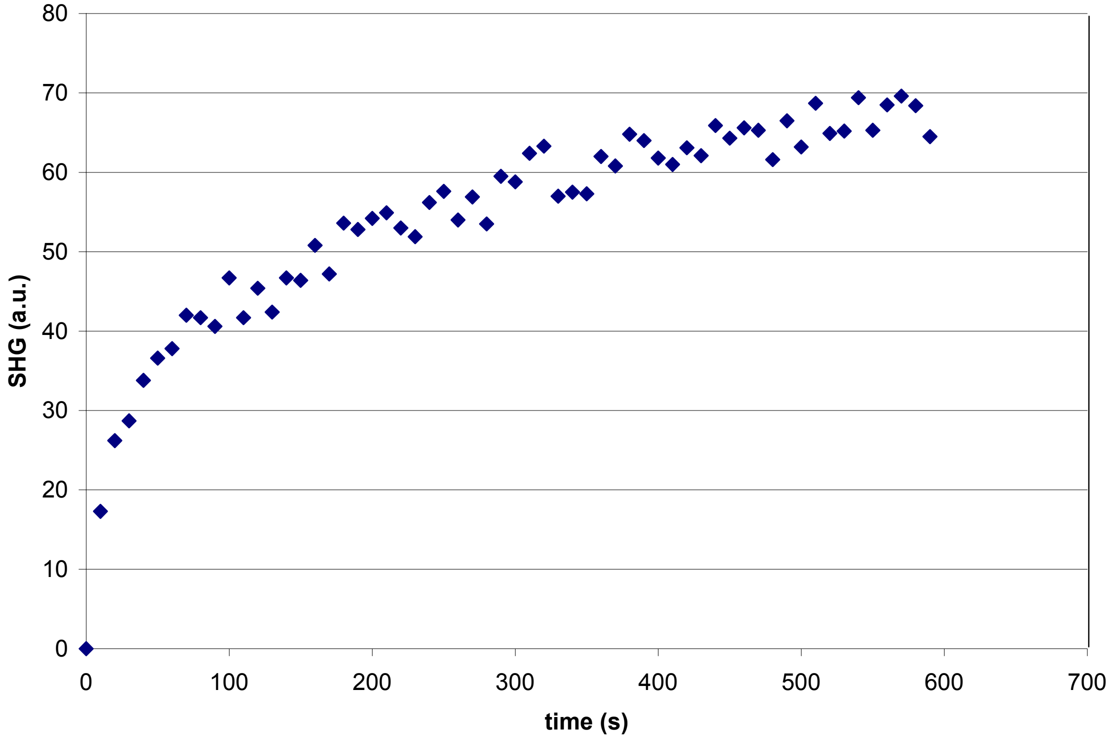

Figure 5.1.2. Typical *in situ* SHG measurement of PCBS on PAH. A rapid increase in the first minute is followed by a slower secondary increase.

In comparing *in situ* and *ex situ* measurements of a film, it is important to note that the SHG signals generated by the films on either side of the glass slide interfere with one other. The thickness of the glass slide, the angle of incidence of the laser beam, and the refractive indices of the glass slide and the surrounding medium determine the phase of the interference. The thickness of the deposited films is negligible compared to the SHG coherence length such that SHG from the entire film on either side can be considered to be identical in phase. Therefore, one would expect that the interface pattern of SHG versus angle of incidence is independent of layers deposited. In Figure 1.5.2, this was shown to be true for the bare glass substrate, a PAH layer, and a PAH/PCBS bilayer. It is clear that the signal strength is much stronger after deposition of PCBS, but the angular position of the maxima and minima is unaltered by depositing additional layers. The SHG signal observed from bare glass is due to the fact that the air-glass interface, like any other interface, is intrinsically non-centrosymetric.

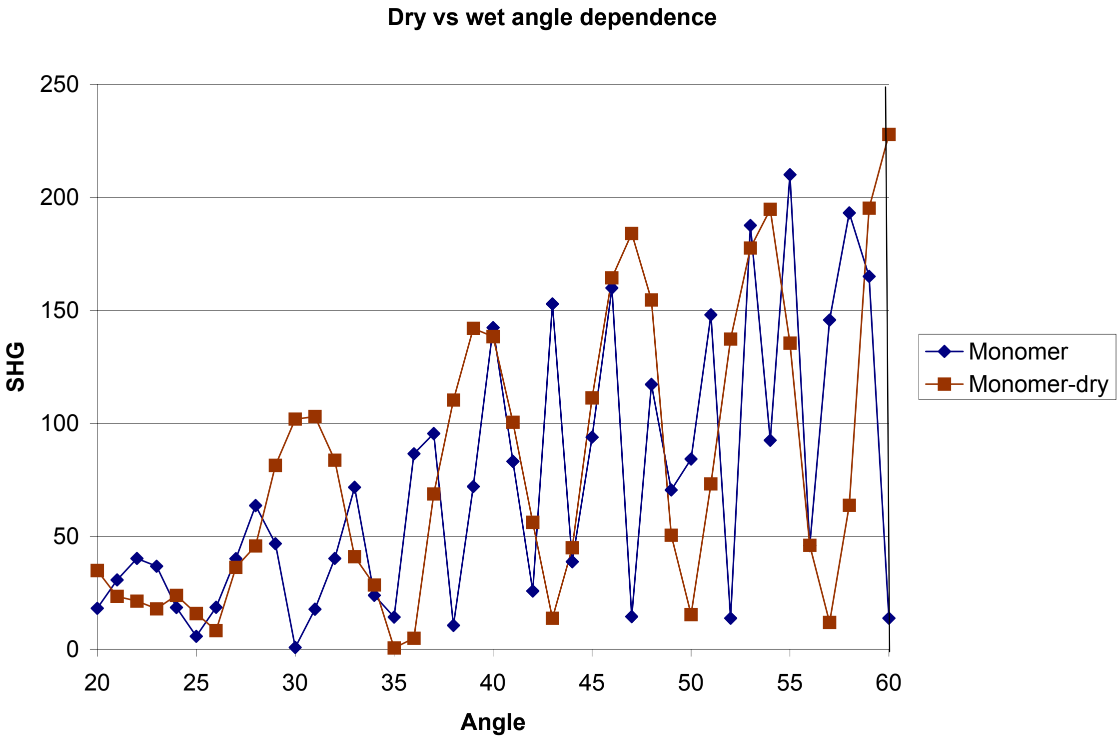

Figure 5.1.3. The SHG signal as function of incident angle for a PAH / Procion Red sample in air and in solution.

The interference between the SHG signals generated on opposite sides of the substrate is determined by the propagation distance through the glass, which is t/cos θ’, where t is the thickness of the glass slide (about 1 mm) and θ’ is the refracted angle in the glass. As the refractive index is wavelength dependent, the angle θ’ is different for the fundamental and second harmonic. The interference pattern is thus dependent on the refractive index of the surrounding medium. Figure 5.1.3 compares the interference patterns of a PAH / Procion Red sample in air with that of a sample in water. It is clear that the peaks are shifted closer together when the sample is in aqueous solution. This is due to the fact that the refractive index difference between water and glass is smaller than the refractive index difference between air and glass.

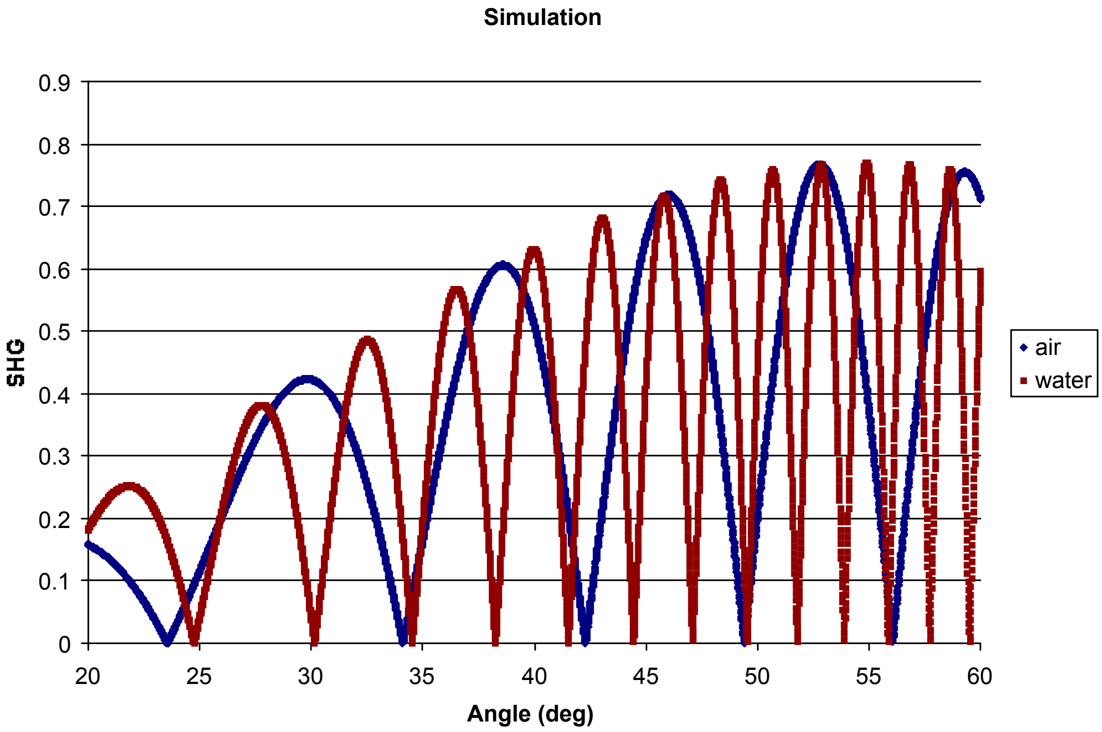

Figure 5.1.4. Calculated SHG signal as a function of incident angle for a glass slide with a NLO film on each side.

Figure 5.1.4 shows the calculated SHG interference pattern as a function of external incident angle for a glass slide (n=1.51, 1 mm) in air (n = 1.0) and water (n = 1.33). The calculation confirms the experimental finding that the peaks are closer together as the refractive index of the surrounding medium increases. For this calculation we used the results from Section 1.5 $I^{2\omega}(\theta) = I_{ENV}(\theta)\sin^2\left[\frac{\pi L_g(\theta)}{2l_{c,g}}\right]$ and $L_g(\theta) = L_0 / \cos\theta'$. When the refractive index of the surrounding medium increases cos θ' will decrease and therefore L_g will increase, resulting in smaller angular seperation between the peaks. In the remainder of this chapter, the angle of constructive SHG interference was determined for each slide both in air and aqueous solution. These two angles were then used for the remainder of the *in situ* and *ex situ* experiments, respectively.

One of the simplest and most common growth models is Langmuir kinetics. In this model, the adsorbed molecules are assumed to be non-interacting, but they do block molecules from landing on the same site. Therefore, the amount of material deposited per unit time is given by

$$\frac{dq}{dt} = K_f C(q_m - q) - K_r q \tag{5.1.1}$$

where q is the amount of material deposited, q_m is the maximum amount that can be deposited (one full monolayer), C is the concentration, K_f is adsorption rate, and K_r is the desorption rate. The density of coverage is defined as $Q = q / q_m$. The change in density of coverage per unit time can be calculated as

$$\begin{gathered} q_m \frac{dQ}{dt} = K_f C(q_m - q_m Q) - K_r q_m Q \\ \frac{dQ}{dt} = K_f C(1 - Q) - K_r Q = K_f C(1 - Q - LQ) \end{gathered} \tag{5.1.2}$$

where L is defined by $L = K_r / K_f C$. Integration gives the density of coverage

$$\begin{aligned}
&\int \frac{dQ}{1-(1+L)Q} = \int K_f C dt \\
&\frac{1}{-(1+L)}\ln\left[1-(1+L)Q\right] = K_f Ct \\
&1-(1+L)Q = \exp\left[-(1+L)K_f Ct\right] \\
&Q = \frac{1-\exp\left[-(1+L)K_f Ct\right]}{1+L}
\end{aligned} \quad . \tag{5.1.3}$$

For our experiments, $K_fC >> K_r$ and $L << 1$. So considering that the square root of the SHG signal of the film is proportional to the deposited material, equation 5.1.3 becomes

$$\sqrt{SHG_{film}} \propto Q = 1-\exp\left(-K_f Ct\right). \tag{5.1.4}$$

During the deposition there is no air-film interface but there is still a glass-film interface effect. Therefore, the square root of the total SHG will be equal to the square root of the SHG generated by the film plus the square root of the SHG generated by the glass-film interface effect. Figure 5.1.5 shows the calculated square root of the SHG generated by the film as a function of time for three different values of K_fC.

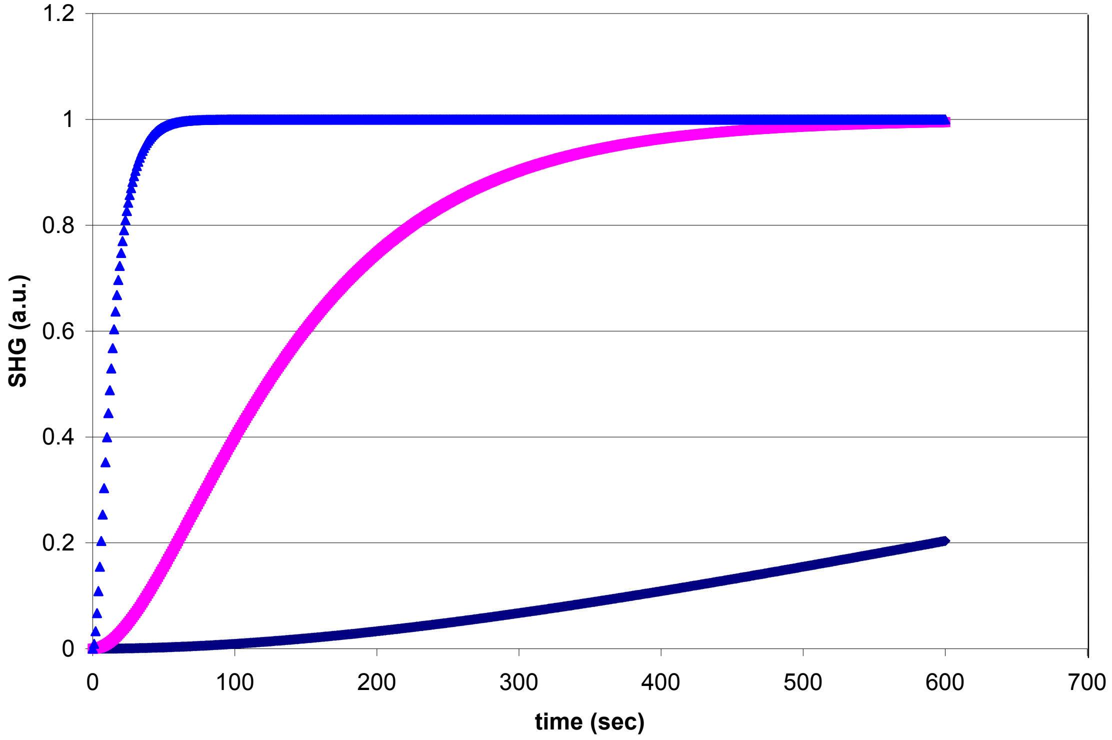

Figure 5.1.5. The calculated SHG values for a film as a function of time for three different values of K_fC. These values are 0.1 (blue), 0.01 (purple), and 0.001(dark blue) sec^{-1}.

5.2 Deposition rate as a function of various parameters

Concentration

The increase in SHG signal as a function of time for a sample with one monolayer of PAH in PCBS solution was monitored for PCBS solutions of four different concentrations. The results are shown in Figure 5.2.1. Consistent with earlier work, the deposition rate as well as the final SHG value proved to be constant over a large range. At low concentrations, on the order of 0.1 mMol, the final SHG value and deposition rate begin to drop, but even at 0.01mMol there is still significant deposition. It is important to point out that the cells with PCBS solution absorb light at the second harmonic wavelength. The measured *in situ* SHG values must be compensated for the absorption. Table 5.2.1 shows the absorbances (including reflection loss) at 1064 nm (the fundamental wavelength) and 532 nm (second harmonic) for the cell filled with PCBS solution of different concentration.

Concentration	Absorbance at 1064 nm	Absorbance at 532 nm
10 mMol	0.090	1.04
1 mMol	0.094	0.15
0.1 mMol	0.082	0.039
0.01 mMol	0.093	0.037

Table 5.2.1. Absorbance values for glass cell with PCBS solutions.

From the absorbance we can get the amount of light transmitted.

$$\begin{aligned} A &= \log_{10}\frac{I_{in}}{I_{out}} \\ T &= \frac{I_{out}}{I_{in}} = 10^{-A} \end{aligned} \tag{5.2.1}$$

where T is the transmittance, A is the absorbance, and I_{in} and I_{out} are the incoming and outgoing intensities. The sample substrate is approximately in the middle of the cell. There are two corrections to consider. First, some of the fundamental energy will be absorbed before it reaches the sample. Second, some of the generated second harmonic will be absorbed in the path between the sample and the end of the cell. For both corrections, the absorbance is half of the absorbance of the whole cell for a given wavelength. The calculation for the highest PCBS concentration is given as an example. First, the correction due to the absorption of the second harmonic.

$$\begin{aligned} A/2 &= 1.04/2 = 0.52 \\ T &= 10^{-0.52} = 0.30 \\ I_{532} &= T \cdot I_m = 3.33 \cdot I_m \end{aligned} \tag{5.2.2}$$

where I_m is the measured SHG and I_{532} is the SHG after correcting for the absorption of the second harmonic. The intensity of the incoming beam must be corrected as well.

$$\begin{aligned} A/2 &= 0.090/2 = 0.045 \\ T &= 10^{-0.045} = 0.90 \\ I_{1064} &= T \cdot I_i = 0.90 \cdot I_i \end{aligned} \tag{5.2.3}$$

where I_i is the intensity of the incoming fundamental and I_{1064} is the intensity after correction for absorption of the fundamental beam. Therefore, I_{1064} is the intensity that actually reaches the sample. Since the SHG is proportional to the square of the incident intensity, the total correction must be

$$I_c = \left(\frac{1}{0.90}\right)^2 \cdot 3.33 \cdot I_m = 4.11 \cdot I_m \tag{5.2.4}$$

where I_c is the SHG after all corrections.

As a check, the final corrected *in situ* SHG values were compared to *ex situ* SHG values of samples dipped in PCBS solutions of the same concentration. Figure 5.2.2 shows the final *in situ* SHG values and *ex situ* SHG values as a function of the PCBS concentration. Both graphs show constant SHG for 1 – 10 mMol and an initial decrease around 1 mMol.

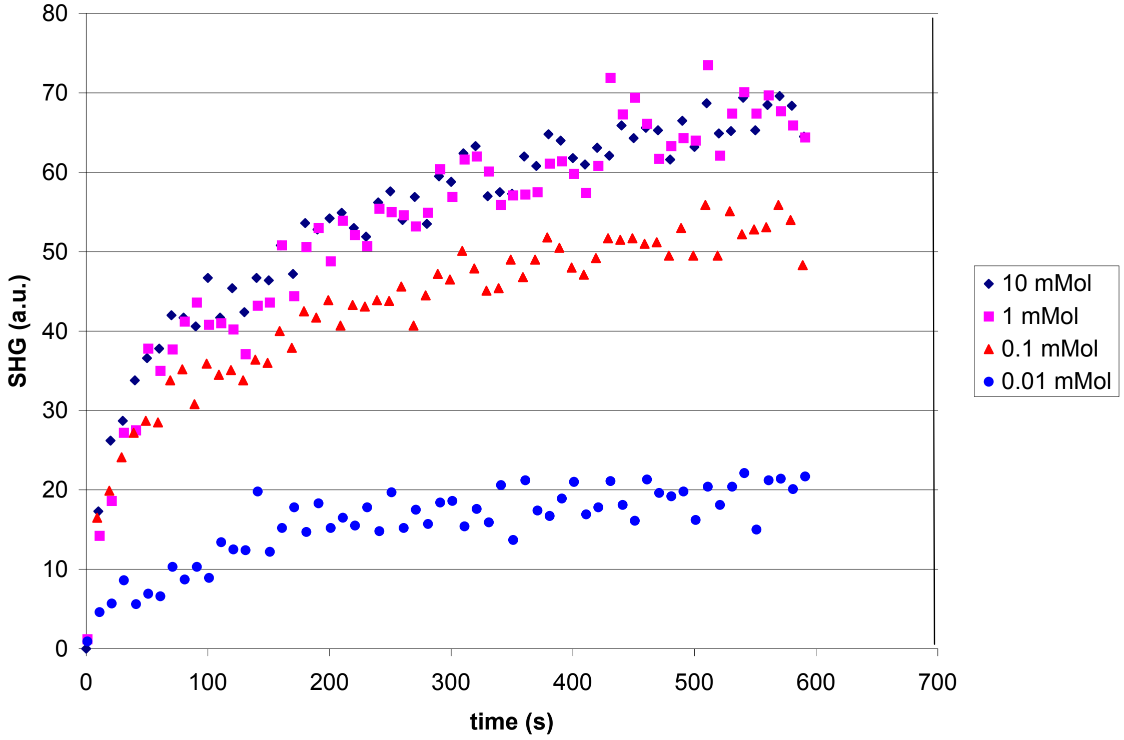

Figure 5.2.1. The SHG signal as function of time for glass / PAH samples immersed in PCBS solution. The deposition rate is constant over a large range of concentrations and there is still significant deposition at 0.001mMol.

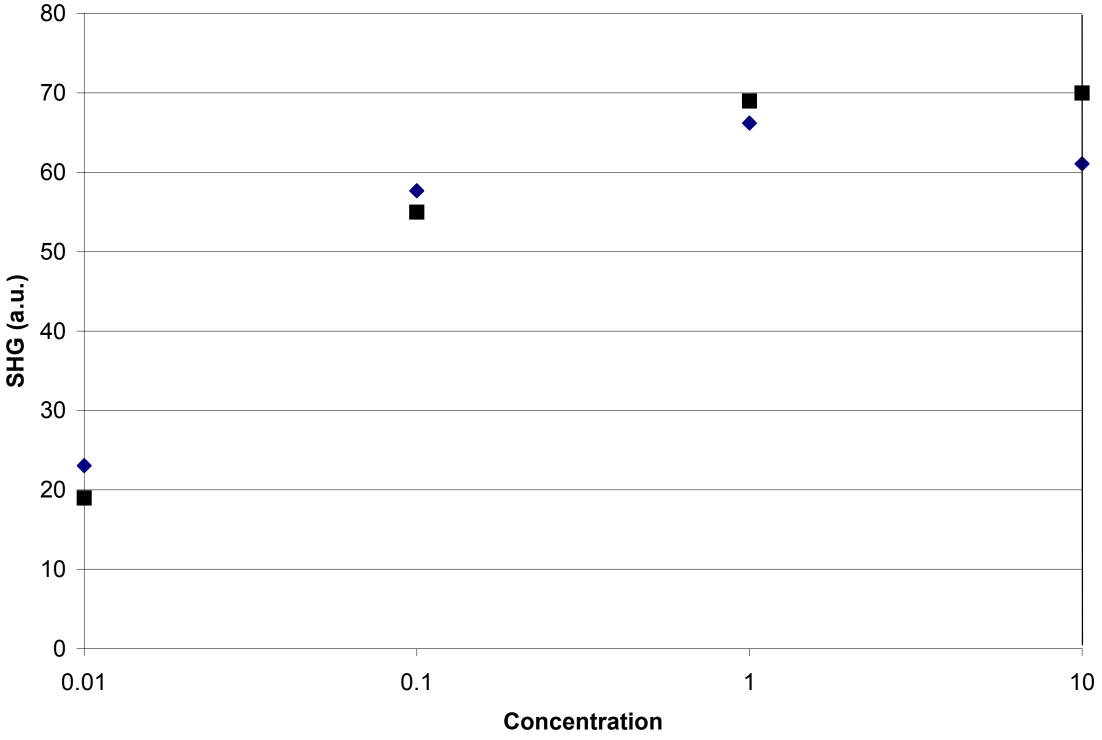

Figure 5.2.2. The final *in situ* SHG values (squares) and *ex situ* SHG values (diamonds) for PAH /PCBS samples as a function of the PCBS concentration in mMol.

Bilayer number

In situ measurements were taken during PCBS deposition for the first five bilayers of a PAH / PCBS sample. In between, *ex situ* measurements were taken after each monolayer. Figures 5.2.3 and 5.2.4 depict the *in situ* and *ex situ* results respectively. As explained in Section 5.1, all measurements were done on the same spot on the sample. The angular positions of the interference peaks are dependent on the index of refraction of the surrounding medium. Therefore, the samples were rotated before each step such that the sample was at the same interference maximum during each step of the measurement. The results of the *in situ* measurements show excellent overlap, indicating that the deposition process as well as orientation is independent of the layer number for the first few bilayers. From the data in Figures 5.2.3 and 5.2.4, it is clear that the SHG of capped and uncapped layers show slow growth for the first 5 bilayers. This is consistent with Figura's work.[18]

Figure 5.2.4 shows the increase in SHG signal during PCBS deposition on a sample that had already ten PAH / PAA buffer bilayers deposited on it. As expected from the interface studies in Chapter Four, the signal was much weaker for a bulk measurement than for an interface measurement. It is important to note that the deposition time of a "bulk" layer is the same as the deposition time for an interface layer.

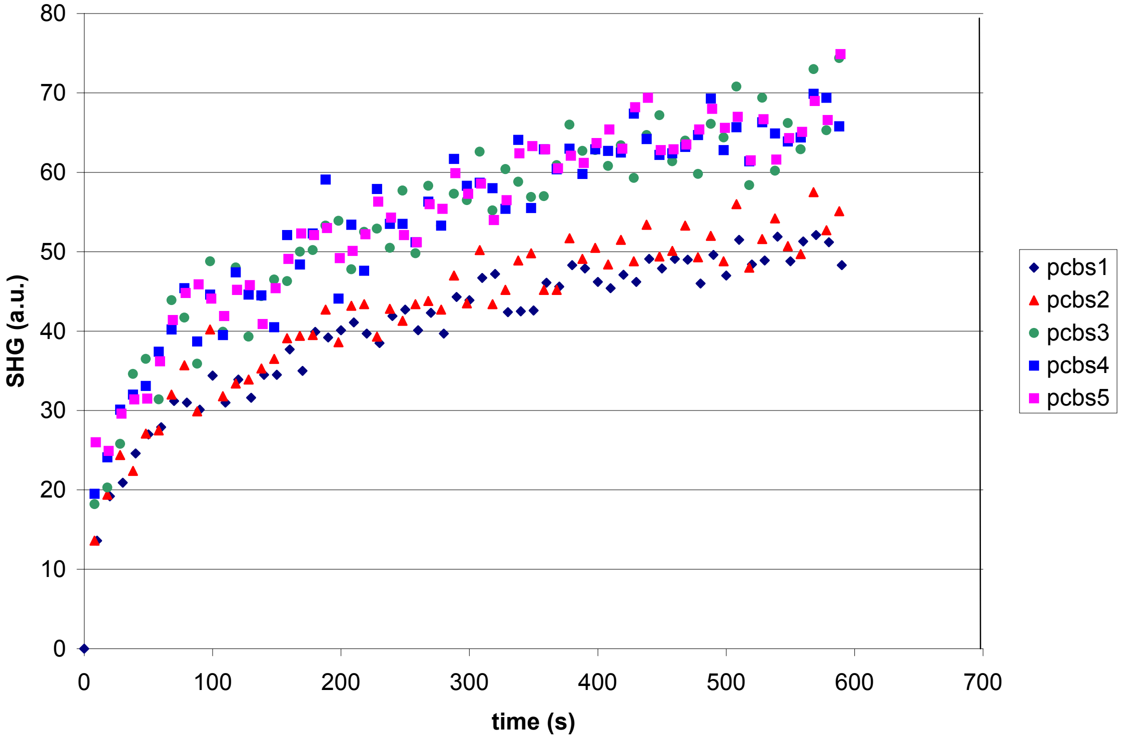

Figure 5.2.3. The SHG signal as a function of time during PCBS deposition for the first five bilayers.

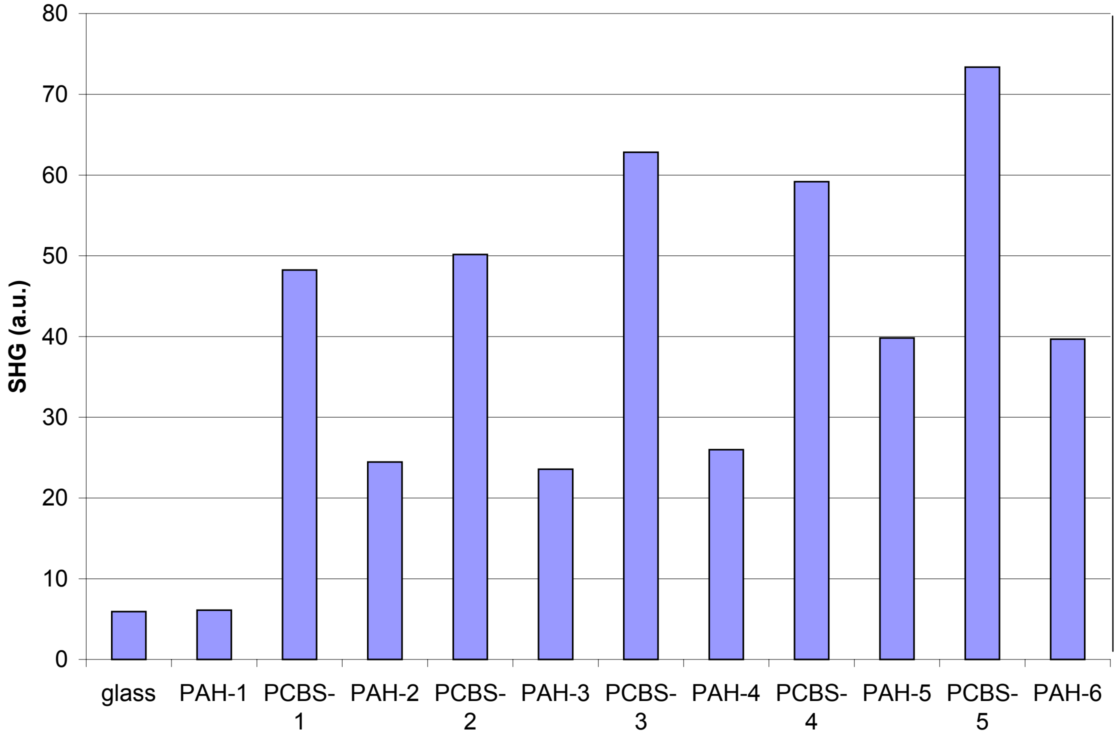

Figure 5.2.4. *Ex situ* measurements of a PAH / PCBS sample. A measurment was taken after every step for the first five bilayers.

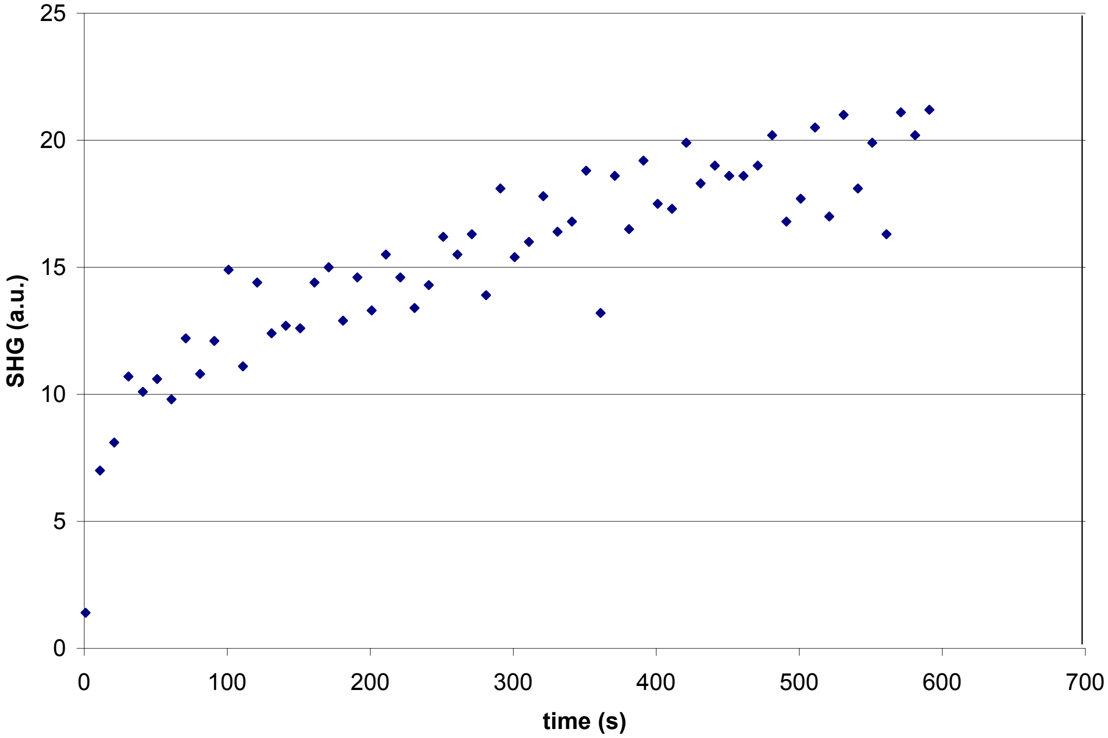

Figure 5.2.5. The SHG signal as a function of time during PCBS deposition for an (PAH / PAA)^{10} / PAH sample.

5.3 Deposition rate of Acid Blue 92

The relationship between deposition rate and concentration was also investigated for Acid Blue 92 (Figure 5.3.1). *In situ* measurements could not be done on concentrations larger than 0.1 mMol due to the strong absorbance of Acid Blue at 532 nm. The data are corrected for absorption in the same way as described in Section 5.2. The data show a rapid increase that plateaus after approximately 400 seconds. Contrary to the graphs representing PCBS deposition, there is no apparent evidence of reorganization in the film after Acid Blue 92 deposition. In addition, there is a marked decrease in the amount of material deposited at 0.01 mMol and 0.001 mMol. The SHG data for 0.001 mMol have been multiplied by a factor of 10 in Figure 5.3.1. Also in the figure are fits to the theoretical curve $SHG = (C_2(1-\exp(-C_1 t)) + C_3)^2$, where C_1 represents a time constant, C_2 represents a multiplication constant, which contains $\chi^{(2)}$, and C_3 is the SHG before the layer is deposited. Table 5.3.1 represents the values of the reaction constants for Acid Blue 92 deposition on PAH.

Concentration (Mol)	C_1 (s^{-1})	C_2	C_3
0.1	0.008	15	5.2
0.01	0.008	14.7	5.2
0.001	0.006	15	2

Table 5.3.1. The reaction constants C_1, C_2, and C_3 for Acid Blue 92 deposition on PAH.

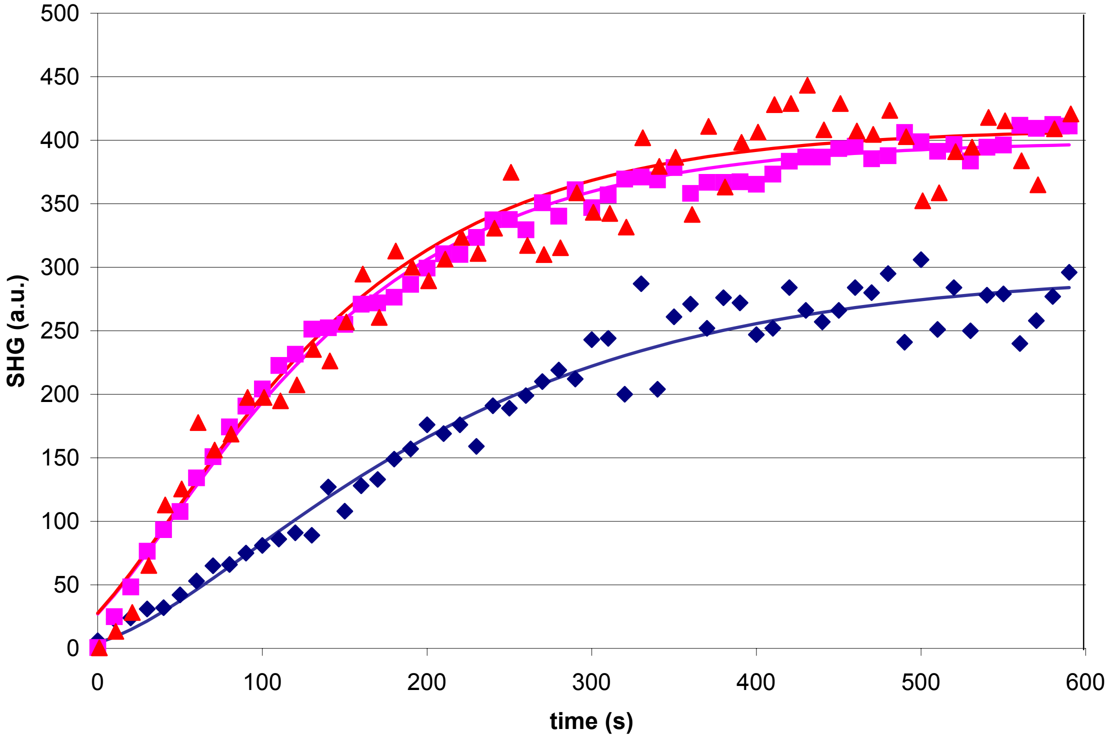

Figure 5.3.1. The increase in SHG signal during Acid Blue 92 deposition as a function of concentration. The concentrations where 0.1 mMol (orange triangles), 0.01 mMol (purple squares), and 0.001 mMol (blue diamonds). The data for the deposition at 0.001 mMol concentration are multiplied by a factor of 10. The curves are fits to the theoretical curve $SHG = (C_2(1-\exp(-C_1 t)) + C_3)^2$.

5.4 Deposition rate of Procion Red

The deposition rate of Procion Red on a PAH sample is depicted in Figures 5.4.1. (pH = 7.0) and 5.4.2. (pH = 10.0). In both cases, the pH of the PAH solution was 7.0. In the pH = 7.0 regime, the Procion Red molecules are charged and the deposition process is expected to be similar to Acid Blue 92. At pH = 10.0, the Procion Red molecules are uncharged and the deposition that takes place is most likely of a covalent nature as explained in Chapter 2. The data are again corrected for absorption at the fundamental and second harmonic wavelengths. Comparison of the graphs of Figures 5.3.1 and 5.4.1 reveals that the deposition of Procion Red (at pH = 7.0) and Acid Blue 92 are indeed similar. Both depositions consist of a rapid increase and level off after a comparable time, ~350 seconds for Procion Red and ~400 for Acid Blue 92. Both deposition processes result in less deposition for concentrations lower than 0.01 mMol, although the drop off is much larger for Acid Blue 92. Figure 5.4.1 also shows fits to the theoretical curve $SHG = (C_2(1 - \exp(-C_1 t)) + C_3)^2$, where C_1 represents a time constant, C_2 represents a multiplication constant, which contains $\chi^{(2)}$, and C_3 is the SHG before the layer is deposited.

Concentration (Mol)	C_1 (s^{-1})	C_2	C_3
1	0.008	7.3	2.5
0.1	0.001	10.1	3.2
0.01	0.001	10.7	3.19

Table 5.3.2. The reaction constants C_1, C_2, and C_3 for Procion Red deposition on PAH at pH 7.0.

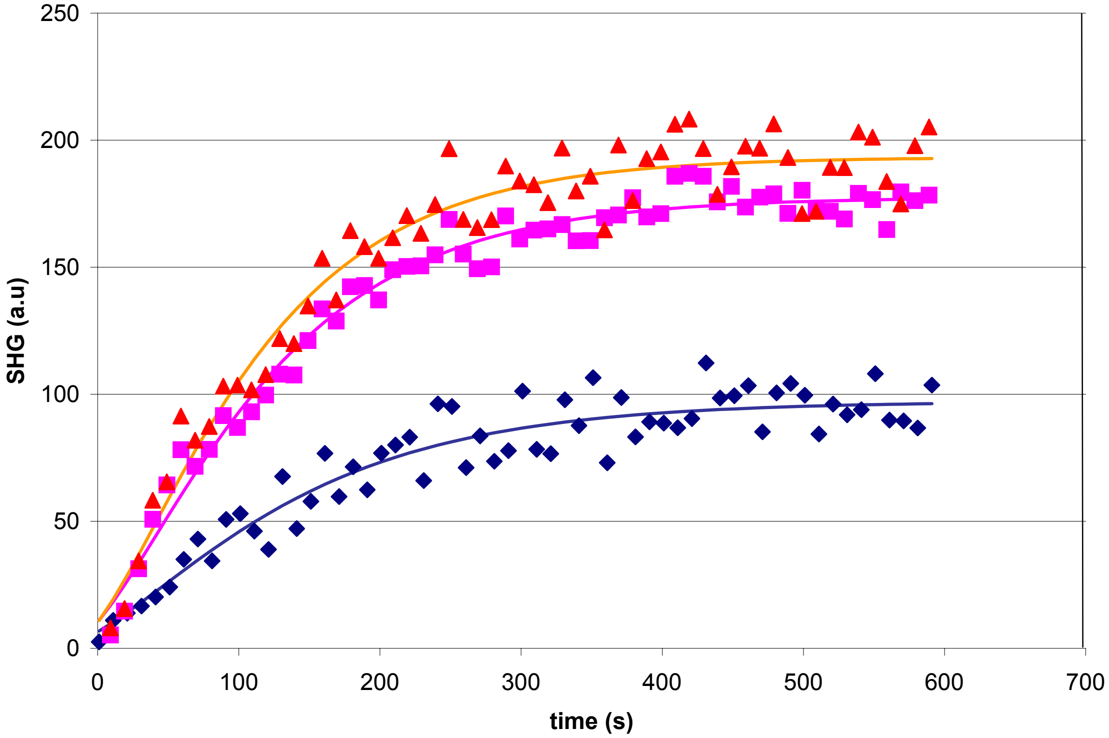

Figure 5.4.1. Deposition rate of Procion Red on a PAH at pH 7.0 sample for different concentrations. The concentrations were 1 mMol (orange triangles), 0.1 mMol (purple squares), and 0.01 mMol (blue diamonds). The curves are fits to the theoretical curve $SHG = (C_2(1-\exp(-C_1 t)) + C_3)^2$.

Figure 5.4.2 shows Procion Red deposition at pH = 10.0. For concentrations above 0.1 mMol, the covalent deposition is faster than ionic deposition of monomers. The initial rise of the SHG signal is very fast and the signal plateaus after ~150 seconds. It is also clear that at low concentration (<0.01 mMol), the covalent deposition process is much slower than the ionic deposition. Figure 5.4.2 also shows fits to the theoretical curve $SHG = (C_2(1-\exp(-C_1 t)) + C_3)^2$. In this figure, the values for the curve representing the

1 Mol deposition, were $C_1 = 0.001\ s^{-1}$, $C_2 = 12.8\ s^{-1}$, and $C_3 = 0.9\ s^{-1}$. For 0.1 Mol the values were $C_1 = 0.01\ s^{-1}$, $C_2 = 6.5\ s^{-1}$, and $C_3 = 6.7\ s^{-1}$. The values for 0.01 Mol were $C_1 = 0.03\ s^{-1}$, $C_2 = 6.7\ s^{-1}$, and $C_3 = 6.7\ s^{-1}$.

Concentration (Mol)	C_1 (s^{-1})	C_2	C_3
1	0.001	12.8	0.9
0.1	0.01	6.5	6.7
0.01	0.03	6.5	6.7

Table 5.3.3. The reaction constants C_1, C_2, and C_3 for Procion Red deposition on PAH at pH 7.0.

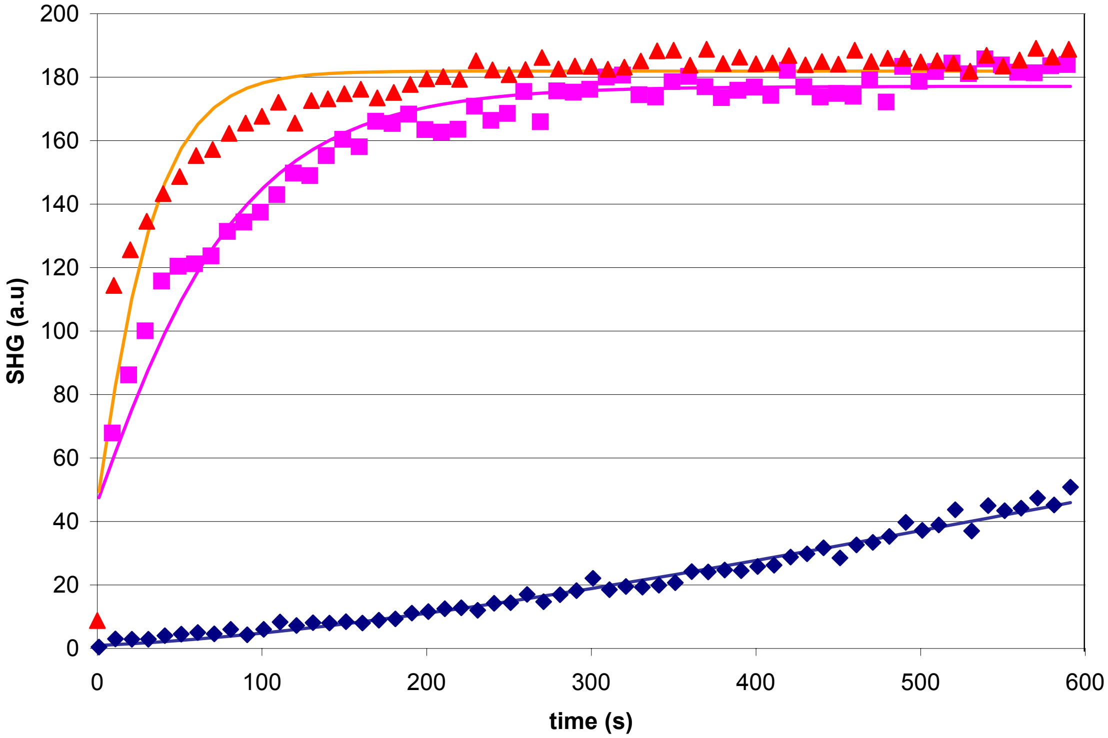

Figure 5.4.2. The SHG signal as a function of time during Procion Red deposition at pH = 10.0. The concentrations were 1 mMol (orange triangles), 0.1 mMol (purple squares), and 0.01 mMol (blue diamonds). The curves are fits to the theoretical curve $SHG = (C_2(1-\exp(-C_1t)) + C_3)^2$.

5.5 Time dependence of the capping effect

Figure 5.5.1 shows the SHG signal during the capping of a PCBS sample in PAH solution. The signal drops from 70 counts to 40 immediately upon immersion in the PAH solution. The data points with zero SHG signal are caused by the brief interruption of the laser beam during the placement of the cell containing the solution. Figure 5.5.2 shows the capping effect of a Procion Red sample in a PAH solution. It too shows an instantaneous decrease. Finally, Figure 5.5.3 also shows the capping effect for a Procion Red sample in PAH, but in this case there were 10 bilayers of PAH/PAA deposited first as a buffer layer. The capping effect is the same for all samples, an immediate drop in SHG signal is observed. Immersion in solution is apparently similar to being capped by a monolayer with a thickness of the cell. This means that the film goes from an environment with a refractive index of 1 (air) to a refractive index of 1.5 (water). This results in an immediate drop in SHG signal. The chromophores that are bound to the previous PAH layer will remain in place, as a change would require a simultaneous release in the ionic and hydrogen bonds that exist between the PCBS and PAH polymers. It does not appear to be possible to observe the adsorption of the PAH capping layer because there is little distinction between the decrease of SHG signal with a single adsorbed capping layer and the decrease caused by surrounding the NLO-active layer with aqueous liquid. It is interesting to note that the instantaneous drop in SHG signal also occurs when the substrate is immersed in water. A nine bilayer PAH / sample was immersed in water. The SHG data showed an immediate drop. The sample remained immersed for 30 minutes. The sample was dried and the *ex situ* SHG response was measured to be 30% lower than before immersion in water. This permanent decrease is believed to be due to reorganization of the layer in the aqueous environment in a manner that decreases the net polar orientation.

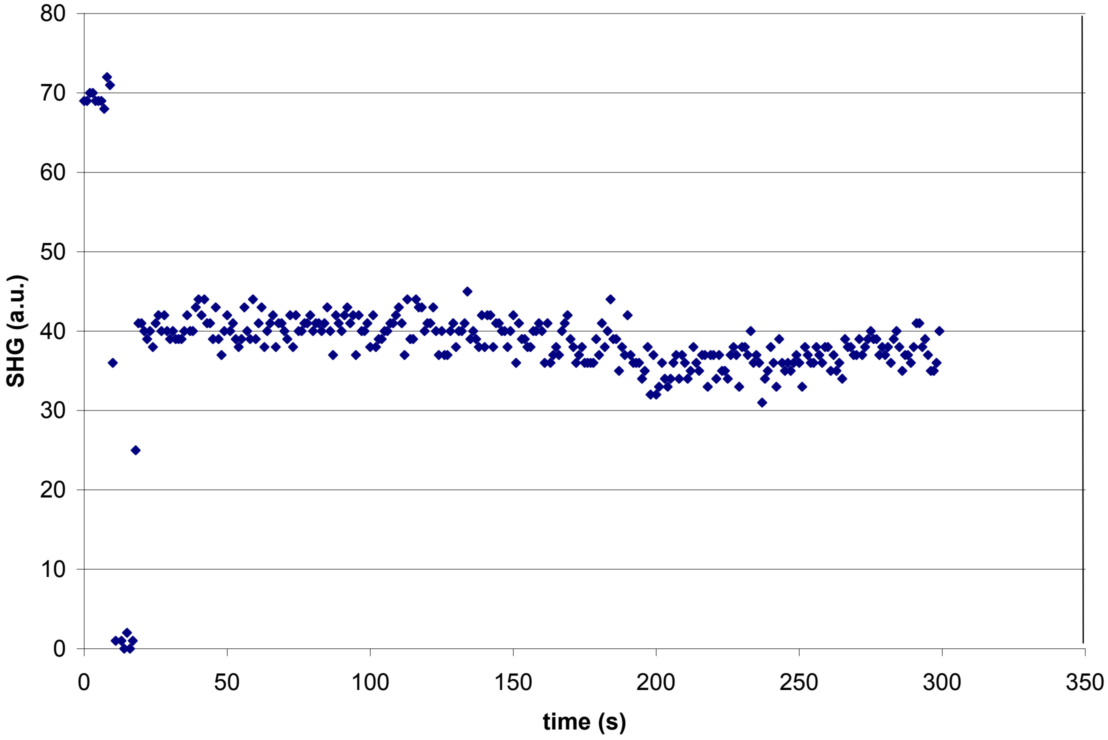

Figure 5.5.1. The capping effect for PCBS. Notice that the reduction in SHG signal is immediate on immersion.

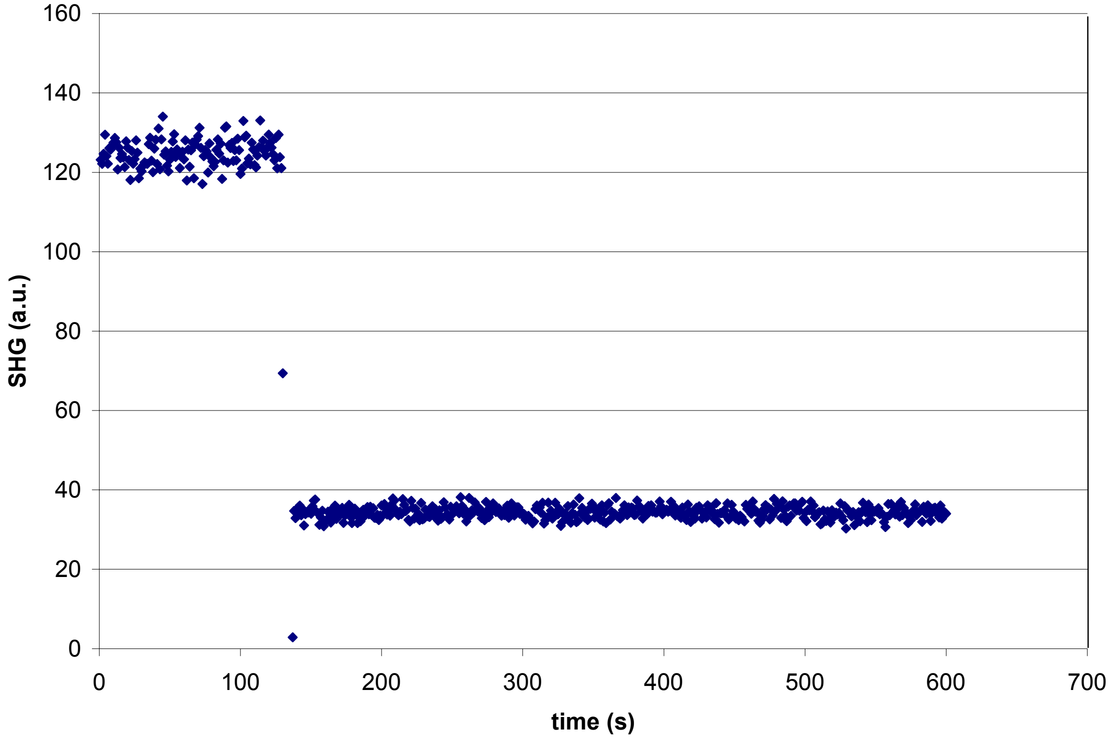

Figure 5.5.2. The capping effect for a Procion Red sample.

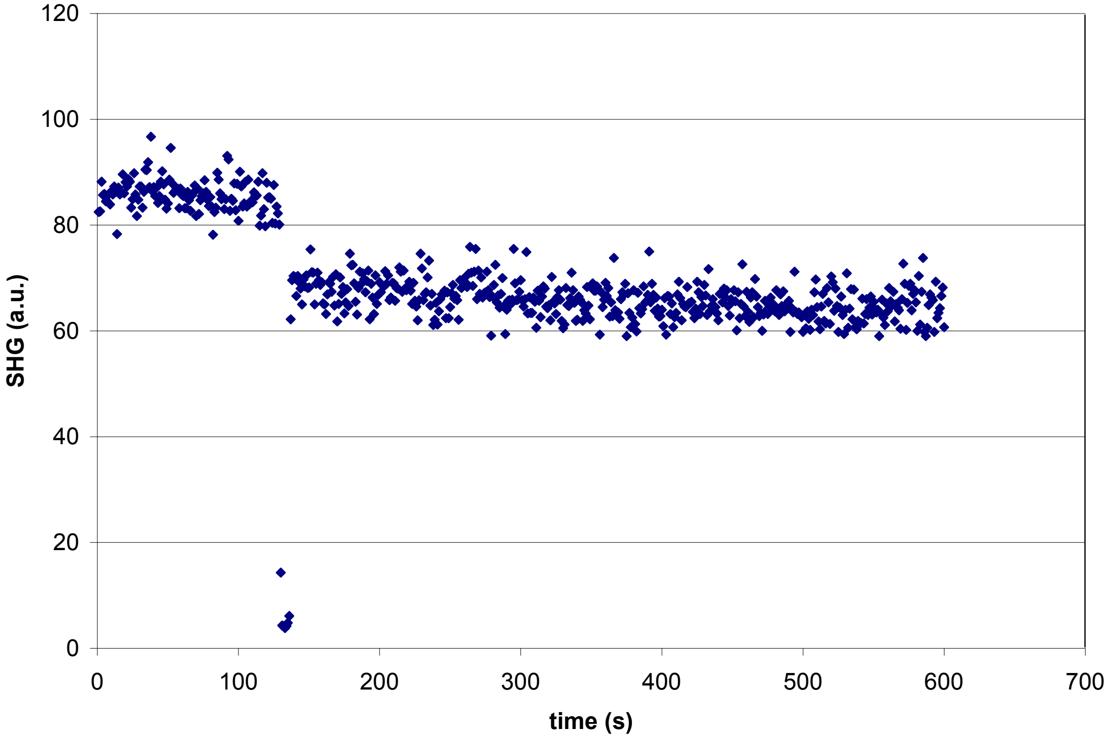

Figure 5.5.3. The capping effect in PAH solution for a $(PAH/PAA)^{10}$/PAH/Procion Red sample.

5.6 Conclusions

Most of the deposition of an ISAM film takes place in less than a minute. The deposition rate as well as the final SHG value is independent of the concentration for PCBS, Acid Blue 92, and Procion Red if the concentration is above a minimum concentration (~0.1 mMol.). While a further slow growth of this SHG signal continues beyond ten minutes for PCBS (presumably due to reorganization of the adsorbed polymer layer), no such slower growth of the SHG signal is observed for the monomers Acid Blue 92 and Procion Red. Finally, the capping effect occurs instantaneously upon immersion of the PAH solution for both Procion Red and PCBS. This is most likely due to the instantaneous change in refractive index of the surrounding material (air versus solution).

References

[1] D.G. Kurth and R. Osterhout, Langmuir **15,** (1999) 4828.

[2] K. Ariga, Y. Lvov, T. Kunitake, J. Am. Chem. Soc. **119** (1997) 2224.

[3] O. Onitsuka, A.C. Fou, M. Ferreira, B.R. Hsieh, and M.F. Rubner, J. Appl. Phys. **80** (1996) 4067.

[4] F. Caruso, H. Möhwald, J. Am. Chem. Soc., **121** (1999) 6039.

[5] Y. Lvov, G. Decher, and G. Sukorukov, Macromolecules, **26** (1993) 5396.

[6] S.W. Keller, H.N. Kim, and T.E. Mallouk, J. Am. Chem. Soc. **116** (1994) 8817.

[7] X. Chattelier and J. Joanny, J. Phys, II **6** (1996) 1696.

[8] R.R. Netz and J. Joanny, Macromolecules **26** (1999) 9013.

[9] V.V. Tsukuruk, V.N. Bliznuyuk, and D. Visser, Macromolecules **30** (1997) 6615.

[10] H.M. Schneider, P. Frantz, and S. Granick, Langmuir **12** (1996) 994.

[11] R.A. McAloney and M.C. Goh, J. Phys. Chem. B **103** (1999) 10729.

[12] C. Brands, P.J. Neyman, M. Guzy, S. Shah, R.M. Davis, K. Van Cott, H. Wang, H.W. Gibson, J.R. Heflin. SPIE 4461, 311 (2001).

[13] R. Advincula, E. Aust, W. Meyer, and W. Knoll, Langmuir **12**, (1996) 3536.

[14] F. Caruso, E. Rodda, D.N. Furlong, K. Niijura, and Y. Okahata, Anal. Chem. **69** (1997) 2043.

[15] A.F. Xie and S. Granick, J. Am. Chem. Soc. **123** (2001) 3175.

[16] H. Wang, T. Troxler, A.G. Yeh, and H.L. Dai, *Langmuir* **16** (2000) 2475.

[17] X. Shang, A.V. Benderskii, K.B. Eisenthal, *J. Phys. Chem. B* **105** (2001) 11578.

[18] C. Figura, *Second Order Nonlinear Optics in Ionically Self Assembled Thin films, Thesis, Virginia Polytechnic Institute and State University* (1999).

Chapter Six: Summaries and Thoughts on Future Work.

6.1 Conclusions

This thesis has presented studies of ionically self-assembled thin films formed from polyelectrolytes, multivalent monomers, and monomers containing both reactive and electrostatic binding sites. It was shown that these films have several advantages as second-order NLO films over films that have been produced in more traditional ways. The self-assembled films are easy and very inexpensive to fabricate. They are exceptionally homogeneous and possess considerable $\chi^{(2)}$ values, up to 1.2×10^{-9} esu. And they have excellent temporal and thermal stability.

In the ISAM film deposition process, a substrate is alternately immersed in oppositely charged aqueous polyelectrolyte solutions. The polyelectrolytes are attracted to the surface through electrostatic attraction. After a monolayer is deposited, the surface charge is reversed and the deposition comes to a halt as other polymer molecules are now repelled. After thorough rinsing, the process is repeated in the other solution. The multivalent monomer deposition process is the similar to the polymeric ISAM process with the exception that the optically active polymer is replaced with an optically active monomer.

The ISAM film structures have been studied with spectrophotometry and *in situ* and *ex situ* SHG measurements. These measurements were executed for a variety of materials and deposition conditions. At present, the $\chi^{(2)}$ values are comparable to up to an order of magnitude larger than that of quartz depending on the parameters of the immersion solutions.

Polymer ISAM films possess noncentrosymmetry because there is a net orientation of the chromophores in the direction of the substrate. As the NLO active polymer is deposited, chromophores bound to the surface (and thus oriented towards the surface) are in larger number than the chromophores that are directed back into the solution. The net orientation gives rise to the nonlinear optical response of the film. However, large numbers of chromophores are oriented away from the surface, thereby reducing the $\chi^{(2)}$ value of the film, as the subsequent oppositely-charged layer is adsorbed. Therefore, other deposition methods have been proposed and attempted, such as multivalent monomer deposition and hybrid covalent/ionic deposition.

Multivalent monomer films are expected to have a larger net orientation than polymer ISAMs as each chromophores, is preferentially oriented by electrostatic means and the orientations of individual chromophores are decoupled from one another. Multivalent monomer films show indeed a large response for small number of bilayers, but show a decrease in SHG with added bilayers for larger number of bilayers. The multivalent monomer films are apparently not as sturdy as ISAM films. Several attempts have been made to increase the net orientation of multivalent monomer films with β-cyclodextrin derivatives, so far with only limited success.

In polymer ISAM, multivalent monomer, and hybrid covalent/ionic deposition processes, it was observed that films with very small number of layers generated much larger SHG signals than is expected based on their number of layers. Apparently, the NLO materials near the glass and air interfaces are more efficient than the same NLO materials in the film bulk. This interface effect has been extensively studied with the use of optically inactive buffer layers. It was found that the glass interface effect extends roughly one bilayer deep for all studied materials. The air interface effect extends only one bilayer deep for multivalent monomer and hybrid covalent/ionic films. In contrast, the air interface effect extends multiple layers deep for polymer ISAM films, with each added monolayer decreasing the SHG response of the film a little bit further up to approximately seven monolayers. When the effects of both interfaces are reduced by sandwiching the NLO materials between two sets of buffer layers, the SHG shows the theoretically expected quadratic dependence on the number of bilayers beginning with the very first NLO bilayer.

Attempts have been made to reproduce the interface effect in the bulk of the film with inclusion of laponite, colloidal silica, and colloidal gold layers. So far, we have not been able to reproduce the interface effect in the bulk layers. This could be due to chemicals included in the solution by the manufacturer to stabilize the solutions or due to the processing conditions thus far attempted.

In situ second harmonic measurements proved to be a valuable tool to investigate the deposition process in real time. Deposition times were on the order of a minute for all materials and parameters studied. Deposition times were concentration independent above a minimum threshold concentration. No difference in deposition time was observed between bulk and interface layers. Polymer ISAM films exhibit a second, slower growth of the SHG signal over ~10 minutes. This is presumably due to reorganization of the adsorbed polymer layer. The monomer films do not exhibit this secondary growth of the SHG signal.

6.2 The road ahead

From here, there are several further studies in ionically self-assembled films that are of interest. Hybrid covalent/ionic deposition has been shown to scale well over a large number of bilayers. The covalent bond between the primary amine of the preceding PAH layer and a triazine ring of Procion Red is very strong. Procion Red has shown a strong second harmonic performance despite having a molecular structure that is far from ideal for SHG. However, the hybrid nature of the deposition process causes a large net orientation, and therefore a large SHG response. A small increase in SHG was reported for Acid Blue 92 by immersing in β-cyclodextrin after every acid Blue 92 layer. The β-cyclodextrin apparently improves the net orientation of the Acid Blue 92. It would be interesting to try this with Procion Red or similar molecule. A repeat unit would be PAH/Procion Red/β-cyclodextrin. The pH for Procion Red must be around 10 to prevent ionic binding to the PAH and thereby force all chromophores to orient in one direction.

Biological materials are also of interest. We have done some preliminary experiments with BSA (Bovine Serum Albumin) and found that Procion Red does bind very well to

BSA. This is of interest in two ways. First, the BSA could potentially be used to improve the net orientation of Procion Red molecules. A second use is in biological sensors. The SHG of a sample with a surface functionalized with a receptor could be monitored in solution using the same setup that was used for *in situ* measurements. A change in the SHG would then be induced by the presence of the target analyte in the solution. These biological lock and key mechanisms can be highly specific in principle, reducing the chance of a false positive to near zero.

A major issue is the reorganization of the chromophores after a layer is deposited. Every time a layer is deposited, the sample is in aqueous solution. During this time, the chromophores in previously deposited layers can reorganize, thereby reducing the net orientation. In a recent experiment, a nine-bilayer PAH/PCBS sample was immersed in water for 30 minutes (equivalent to 5-bilayer deposition time). The SHG response was reduced by 30% (measured after 2 hours drying time). The SHG response of the film did not recover at all. Therefore, with *in situ* measurements, a minimum deposition time for each material and parameter combination should be established to prevent unnecessary reorganization. Alternatively, immersion in a solution of cross-linking agents could be considered after each step involving the NLO active material in order to prevent reorganization.

Index

Charles Brands
Ruimtevaartstraat 40
Dirkshorn
1746 AK
The Netherlands

Education:
Virginia Polytechnic Institute and State University, Blacksburg, VA
Doctorate of Philosophy, Physics, Expected August 2003
Dissertation: Interface Effects and Deposition Process of Ionically Self-Assembled Monolayer Films: In Situ and Ex Situ Second Harmonic Generation Measurements

Physics Department, University of Virginia, Charlottesville, VA, 1997
M.S. Physics, 1997
Thesis: Development and initial application of a 24 GHz EPR Spectrometer
Physics Department, University of Amsterdam, The Netherlands.
B.S. Physics, 1993
Thesis: Chemical Vapor Deposition of W on Si, SiO2, and GaAs with in-situ reflectometry and the 19F(p,ag)16O reaction.

Selected Teaching Experience:
1997-Present Teaching assistant, Department of Physics, Virginia Tech, Blacksburg, Virginia.
1994-1997 Teaching assistant, Department of Physics, University of Virginia, Charlottesville, Virginia.
Outstanding Teaching Assistant Award, Physics Department, University of Virginia 1997
Outstanding Teaching Assistant Award, Physics Department, University of Virginia 1995

Selected Research Experience:
1997-Present Research assistant, Nonlinear Optics Laboratory, Department of Physics, Virginia Tech, Blacksburg, Virginia.
1995-1997 Research assistant, Department of Physics, University of Virginia, Charlottesville, Virginia.
1989-1992 Research assistant, Laboratory for Atomic and Molecular Physics (AMOLF), Amsterdam, The Netherlands.

Selected equipment proficiency:
Nanosecond and picosecond Nd:YAG lasers, optical system design, CAMAC systems, Spectrophotometers,

Computer proficiency:
C, C++, Java, Perl, Python, HTML, UML
Linux, DOS, Windows (3.11, 95, 98, NT, 2000)

Recent Publications:
In-situ second harmonic generation measurements of the formation of ionically self-assembled monolayers. C. Brands, P.J. Neyman, M. Guzy, S. Shah, R.M. Davis, K. Van Cott, H. Wang, H.W. Gibson, J.R. Heflin. SPIE 4461, 311 (2001).
In Situ Measurements of the Growth of the Second Order Nonlinear Optical Susceptibility in Ionically Self-Assembled Monolayers. C. Brands, J.R. Heflin, P.J.Neyman, M.T. Guzy, S. Shah, H.W. Gibson, K.E. Van Cott, R.M. davis, MRS Symp. Proc. 660, JJ8.32.1. (2001).
Enhanced Second Order Nonlinear Optical Susceptibilities in Ionically Self-Assembled Films Incorporating Dianionic Molecules. P.J. Neyman, M.T. Guzy, S. Shah, H. Wang, H.W. Gibson, K.E.Van Cott, R.M. Davis, C. Brands, J.R. Heflin, MRS Symp. Proc. 660, JJ8.30.1(2001).
Second-order nonlinear optical responses of ionically sel-assembled films: polycation variations and dianionic chromophores. P.J. Neyman, M. Guzy, M. Shah, R.M.Davis, K. Van Cott, H. Wang, H.W. Gibson, C.Brands, J.R.Heflin. SPIE 4461, 214 (2001).

Photoluminescence studies on energy migration in multilayer organic photopvoltaic devices based on ionically self-assembled monolayers. R. Schroeder, C. Soman, C. Brands, J.R. Heflin, W. Graupner, H.Wang, H.W. Gibson, D. Marciu, M.B. Miller, SPIE 4108, 85 (2001).

Photovoltaic Cells Based on Ionically Self-Assembled Nanostructures. T. Piok, C. Brands, P.J. Neyman, A. Erlacher, C. Soman, M.A. Murray, R. Schroeder, W. Graupner, J.R. Heflin, D. Marciu, A. Drake, M.B. Miller, H. Wang, H. Gibson, H.C. Dorn, G. Leising, M. Guzy, R.M. Davis, Synth. Meth. 116, 343 (2001).

Photocarrier Generation Quantum Yield For Ionically Self-Assembled Monolayers. T. Piok, R. Schroeder, C. Brands, J.R. Heflin, G. Leising, W. Graupner. Synth. Meth. 121, 1589 (2001).

In situ second harmonic generation measurements of the growth of nonlinear optical ionically self assembled monolayers. C.Brands, P.J. Neyman, M. Guzy, S. Shah, H. Wang, H.W. Gibson, K. Van Cott, R.M. Davis, C. Figura, J.R. Heflin. Polym. Mater. Sci. Eng. 83, 219 (2000).

Photovoltaic Responces in Ionically Self-Assembled Nanostructures Containing Conjugated Polymers and Fullerines. C. Brands, T. Piok, P.J. Neyman, A. Erlacher, C. Soman, M.A. Murray, R. Schroeder, J.R. Heflin, W. Graupner, D. Marciu, A. Drake, M.B. Miller, H. Wang, H. Gibson, H.C. Dorn, G. Leising, M. Guzy, R.M. Davis. SPIE 3937, 51 (2000).

Thermal stability and immersion solution dependence of second-order nonlinear optical ionically self assembled films. C. Figura, P.J. Neyman. D. Marciu, C. Brands, M.A. Murray, S. Hair, R.M. Davis, M.B. Miller, J.R. Heflin. SPIE 3939, 214 (2000).

Control of second-order nonlinear susceptibility in ionically self-assembled films by pH and ionic strength. C. Figura. P.J. Neyman, D. Marciu, C. Brands, M.A. Murray, S. Hair, M.B. Miller, R.M. Davis, J.R. Heflin. MRS 598, BB4.9.1 (2000).